MACROPHAGE POLARIZATION IN LIVER DISEASE

By

Jenna Danielle Strickland

A DISSERTATION

Submitted to
Michigan State University
in partial fulfillment of the requirements
for the degree of

Pharmacology and Toxicology – Environmental Toxicology – Doctor of Philosophy

2021

ABSTRACT

MACROPHAGE POLARIZATION IN LIVER DISEASE

By

Jenna Danielle Strickland

In severe cases of acetaminophen (APAP) overdose, acute liver injury rapidly progresses to acute liver failure (ALF), producing life threatening complications including, hepatic encephalopathy and multi-organ failure. Systemic levels of the proinflammatory cytokine interleukin-6 (IL-6) and the anti-inflammatory cytokine interleukin-10 (IL-10) are highest in ALF patients with the poorest prognosis. However, the mechanistic basis for dysregulation of these cytokines, and their association with outcome in ALF remains poorly defined. Standard experimental settings of APAP hepatotoxicity in mice (i.e., 300 mg/kg) do not recapitulate key features of ALF in critically ill patients, including impaired hepatocyte proliferation, kidney injury, evidence of hepatic encephalopathy (HE), and cytokine dysregulation. Further, in stark contrast to ALF patients, IL-6 and IL-10 limit liver injury, increase hepatocyte proliferation, and reduce mortality under these experimental conditions. Thus, to investigate cytokine dysregulation in true ALF, we used a robust experimental setting of failed liver repair after APAP overdose in which a high dose of APAP is administered. Under these experimental conditions, we detected high serum levels of several pro- and anti-inflammatory cytokines, including IL-6 and IL-10, and observed increased levels of PD-L1 on macrophages mimicking systemic inflammatory response syndrome (SIRS) that occurs in critically ill ALF patients. Further, cerebral blood flow was markedly reduced in these mice, recapitulating a key feature of hepatic encephalopathy in ALF patients. Remarkably, neutralization of IL-6 in this setting restored cerebral blood flow, reduced mortality, and normalized levels of IL-10 and PD-L1. Furthermore, neutralization of IL-6 increased levels of Gas6, the primary ligand for the receptor Axl, which our studies revealed is essential for protection of the hepatic sinusoidal vasculature from injury after APAP overdose. In addition, our studies demonstrated that macrophage-mediated clearance of necrotic cells was

prevented in mice with ALF, but was restored by neutralization of IL-10. Lastly, our studies identified Kupffer cells (KCs), the resident macrophages of the liver, as a primary source of IL-6, IL-10 and PD-L1 in APAP-induced ALF, and demonstrated further that the transcriptional regulator, NFKBIZ, may be responsible for enhanced IL-6 production in ALF. Collectively, our studies reveal that exaggerated levels of IL-6 are detrimental in APAP-induced ALF in mice, and suggest that therapies aimed at reducing IL-6 levels in patients with APAP-induced ALF may be beneficial. Additionally, as a part of this dissertation, we have developed a high-throughput assay that can detect differentiation of proinflammatory macrophages into pro-repair macrophages for use as a drug screening platform to identify chemicals/drugs that stimulate this process. Drugs identified from this screen could ultimately be used to restore macrophage function and liver repair in patients with both acute and chronic forms of liver failure.

TABLE OF CONTENTS

LIST OF TABLES

LIST OF FIGURES

KEY TO ABBREVIATIONS

ALF	Acute Liver Failure
APAP	Acetaminophen
NAC	N-acetyl cystine
SIRS	Systemic Inflammatory Response Syndrome
CARS	Compensatory Anti-inflammatory Response Syndrome
IL	Interleukin
MMP	Matrix metalloproteinase
HE	Hepatic Encephalopathy
KC	Kupffer Cell
MDM	Monocyte Derived Macrophage
MDSC	Myeloid Derived Suppressor Cell
PD-L1	Program Death Ligand 1
ALT	Alanine aminotransferase
Ccl	Chemokine (C-C motif) ligand
TNF-α	Tumor Necrosis Factor alpha
NAPQI	N-acetyl-*p*-benzoquinone imine
MOD	Multi-Organ Dysfunction
sAxl	Soluble Axl
H&E	Hematoxylin and Eosin
PCNA	Proliferating Cell Nuclear Antigen
CCR	C-C chemokine receptor
Clec4f	C-Type Lectin Domain Family 4 Member F
ROI	Regions of Interest

ANOVA	Analysis of Variance Analysis
MARCO	Macrophage receptor with collagenous structure
DAMPs	damage-associated molecular patterns
OTC	over-the-counter
INR	international normalized ratio
PT	prothrombin time
IL-10	Interleukin 10
IL-6	Interleukin 6
RTK	receptor tyrosine kinase
HAV	hepatitis A virus
HEV	hepatitis E virus
HBV	hepatitis B virus
HTS	high-throughput screening
CCL_4	carbon tetrachloride
Gas6	growth arrest–specific gene 6
Clec4e	C-Type Lectin Domain Family 4 Member E
iNOS	Inducible nitric oxide synthase
Arg-1	Arginase 1
Ly6c	lymphocyte antigen 6 c
Cx3cr1	C-X3-C Motif Chemokine Receptor 1
NAPQI	*N*-acetyl-*p*-benzoquinone imine
GSH	glutathione
ALT	alanine transaminase
AST	aspartate transaminase
HMGB1	high-mobility group box 1 protein
TLR	toll like receptor

TGF-β	transforming growth factor beta
PS	phosphatidylserine
IGF-1	insulin-like growth factor

CHAPTER 1

INTRODUCTION

1.1 Acute Liver Failure

1.1.1 Etiologies of Acute Liver Failure. Acute liver failure (ALF) is a rare and life-threatening condition that occurs suddenly (<26 weeks in duration) in patients without pre-existing liver disease. ALF is characterized by severe hepatic dysfunction leading to coagulation abnormalities and hepatic encephalopathy (HE). While approximately half of ALF patients will experience spontaneous recovery with supportive care, ALF patients with the poorest prognosis often develop multi-organ failure and are notoriously challenging to treat. If therapeutic interventions in these patients are unsuccessful, an emergency liver transplant is critical for survival. Unfortunately, transplantation may not be an option for every patient.

ALF has many known etiologies, which vary demographically**.** The most frequent cause of ALF worldwide, particularly in developing nations, is viral hepatitis, including hepatitis A (HAV) and hepatitis E (HEV). However, in the United States and Western Europe, acetaminophen (APAP)-induced liver failure is the most common cause of ALF. Other notable causes of ALF include metabolic diseases, autoimmune hepatitis, sepsis, toxins, cancer, and herbal supplements. However, for approximately 1 out of every 6 adult cases of ALF, no specific cause is ever identified (Lee 2008) (Patton et., 2012).

Progression of ALF can vary depending on the etiology; however, in most cases, a key early feature is hepatocyte death resulting from either necrosis or apoptosis. The two exceptions to this are acute fatty liver of pregnancy and Reye's syndrome (Shah et al., 2020). Progression and severity of ALF symptoms can be divided into three categories: hyperacute, acute, and subacute (Patton et al., 2012). In cases of hyperacute ALF, patients experience severe coagulopathy and rapidly progress to encephalopathy (Patton et., 2012). Typical causes of hyperacute ALF include APAP, HAV, and HEV. Acute ALF is most frequently caused by hepatitis B (HBV) and is characterized by moderately severe coagulopathy and jaundice. Acute ALF patients typically progress from jaundice to encephalopathy in 1-4 weeks and have a moderate chance of survival without a liver transplant (Patton et al., 2012). Both hyperacute

and acute ALF are classified as fulminant forms of hepatic failure. Subacute ALF, a form of sub-fulminant liver failure, usually results from non-APAP induced drug toxicity. These patients experience mild coagulopathy, severe jaundice, and progress from jaundice to encephalopathy in 4-12 weeks. Patients with subacute ALF generally will not survive without a liver transplant (Patton et al., 2012).

In cases where ALF is suspected, patient medical history can help guide determination of the etiology. However, depending on the severity of HE at the time of hospital admittance, this information can be difficult to obtain from the patient. Determination of etiology though, provides the strongest predictor of outcome and informs the best treatment approach (Lee 2012). In addition to etiology, multiple case studies have shown patient sex differences also play a role in ALF progression and severity (Ostapowicz et al., 2002). Regardless of the cause, female patients are at greater risk of developing and succumbing to ALF (Ostapowicz et al., 2002). The reason(s) for this are unclear, and it has yet to be determined if women are innately at higher risk for developing ALF (Ostapowicz et al., 2002). While there are causes of ALF that are specific to women (i.e., ALF in pregnancy), these causes only result in a small number of cases annually, and are thus unlikely to fully explain the observed sex differences (Ostapowicz et al., 2002).

1.2 Acetaminophen-Induced Acute Liver Failure

1.2.1 Acetaminophen. Acetaminophen (APAP) is one of the most common over-the-counter analgesics and antipyretics, with over 25 billion doses of APAP sold annually in the United States (McGill and Jaeschke 2013). It is estimated that more than 60 million Americans ingest APAP on a weekly basis (Yoon et al., 2016). While widely regarded as safe and effective at therapeutic doses (≤ 4 grams/daily), overconsumption of APAP can produce hepatotoxicity that progresses to ALF in severe cases. In some cases, concomitant use of APAP with other drugs, chronic alcohol use, and/or malnutrition may result in APAP toxicity within or slightly

above the therapeutic range (Yoon et al., 2016). The minimum dose of APAP required to cause hepatocellular injury ranges from 4-10 grams (Yoon et al., 2016).

In the United States, APAP overdose is among the leading causes of both intentional and unintentional poisoning and is responsible for approximately half of ALF cases (Yoon et al., 2016). It is estimated that APAP-induced ALF results in approximately 26,000 hospitalizations and 500 deaths each year in the United States (Nourjah et al., 2006) (Lee 2017). Approximately 20% of ALF cases requiring emergency liver transplantation in the United States are the result of APAP overdose (Yoon et al., 2016). If left untreated, severe APAP-induced hepatoxicity may result in death within 4-18 days (Chun et al., 2009).

When overconsumption of APAP occurs, it can have a range of consequences including alterations in liver function, ALF, and death (Chun et al., 2009). Overconsumption of APAP may occur both intentionally and unintentionally, and while symptoms may be similar in both cases, symptom progression and severity can differ. Intentional APAP overdoses, with suicidal intent, account for approximately 52% of cases (Yoon et al., 2016). In the case of an intentional overdose, APAP-induced ALF can occur after a single, large dose of APAP and may occur in combination with other drugs. In contrast to intentional overdoses, accidental overconsumption of APAP generally occurs over a period of several days; thus, in these patients, serum levels of APAP may be low or even undetectable. However, upon admittance to the hospital, these patients typically have more advanced encephalopathy. Regardless of overdose intent, patient outcome following the development of ALF is similar (Lee 2012). Approximately 64% of patients will undergo spontaneous hepatic recovery, while the remaining 36% of patients will develop life-threatening complications (Lee 2011).

Approximately 48% of APAP-induced ALF cases are the result of a non-intentional overdose (Yoon et al., 2016). Unintentional overdoses of APAP may result from taking more than one drug combination containing APAP or from taking a higher than recommended dose for a period of several days. There are several factors that contribute to patients accidently

overdosing on APAP. For example, many adults either misunderstand the instructions on over-the-counter (OTC) medications or underestimate the risk of overconsumption (Wolf et al., 2012) (Fontana 2008). To better understand the prevalence of APAP misuse in the United States, Wolf and colleagues surveyed 500 patients (ages 18-80) seeking primary care regarding their previous APAP use and presented scenarios to determine how well the patients understood APAP product labeling, dosing instructions, and instructions regarding use of two products containing APAP at once (2012). Strikingly, they determined nearly half of patients surveyed would overdose by taking two over-the-counter medications that contained APAP (Wolf et al., 2012). Additionally, approximately 1 in 4 patients surveyed indicated they would overdose on single APAP product by exceeding 4 grams in a 24-hour period (Wolf et al., 2012).

In addition to OTC APAP medications that are formulated in combination with other drugs (i.e., cold medicines and cough syrups), prescription opioids are commonly formulated with APAP (Mitchell et al., 2020). Three out four of the most commonly prescribed opioids in 2017 were formulated in combination with APAP (Mitchell et al., 2020). These included APAP/hydrocodone, APAP-oxycodone, and APAP-codeine (Mitchell et al., 2020). While opioid/APAP prescriptions have decreased in recent years, APAP/hydrocodone remains one of the most commonly prescribed pain medications in the United States (Mitchell et al., 2020). Strikingly, these opioid-APAP formulations account for 63% of unintentional APAP overdoses (Yoon et al., 2016) (Michna et al., 2010) (Lee 2012).

In 2011, in an attempt to reduce the risk of APAP hepatotoxicity in patients using prescribed combination therapies, the Food and Drug Administration (FDA) urged health care providers to no longer prescribe combination therapies that contain more than 325 mg/tablet of APAP (Krenzelok 2009). Furthermore, they required manufacturers to limit the amount of APAP in combination therapies to 325 mg/tablet by 2014 and additionally, required manufacturers to provide clear labeling on OTC APAP products specifically stating maximum daily amounts of APAP (Krenzelok 2009).

1.2.2 Mechanism of Toxicity. At therapeutic doses, APAP is rapidly absorbed, and metabolism primarily occurs in the liver. Three main pathways contribute to APAP metabolism: glucuronidation, sulfation, and CYP450 2E1 oxidation. The glucuronidation and sulfation pathways are responsible for approximately 90% of APAP metabolism, with approximately 2% of APAP being excreted unchanged in the urine. The remaining APAP is metabolized by CYP450 2E1 to *N*-acetyl-*p*-benzoquinone imine (NAPQI). NAPQI is an electrophilic molecule that is highly reactive. Under normal conditions, NAPQI is rapidly inactivated through conjugation with glutathione (GSH) in hepatocytes. However, in cases of APAP overdose, this pathway becomes overwhelmed leading to the rapid depletion of hepatic GSH. This in turn results in the accumulation of NAPQI which can react with protein sulfhydryl groups thereby disrupting key cellular pathways ultimately leading to hepatocyte death (Chun et al., 2009).

Necrosis of hepatocytes leads to the release of damage-associated molecular patterns, or DAMPs, which bind to pattern recognition receptors (e.g., toll-like receptors, or TLRs) on immune cells. The binding of DAMPs, which can include mitochondrial DNA, high-mobility group box 1 (HMGB1) protein, or nuclear DNA fragments, to TLRs serves as a potent stimulator of the immune system by promoting the formation of cytokines, including tumor necrosis factor α (TNF-α). Pro-inflammatory cytokine and chemokine production leads to the rapid expansion of the immune cell population. Immune cells, including proinflammatory monocytes, are recruited to the site of injury (i.e., necrosis) via a Ccl2 chemokine gradient (Graubardt et al., 2017).

1.2.3 Symptoms of Acetaminophen Overdose. The progression of APAP hepatotoxicity is now well established and typically divided into four stages. At onset, ALF patients typically only experience non-specific symptoms, which include vomiting, nausea, and lethargy (Fontana 2008) (Yoon et al., 2015). These symptoms generally last 12-24 hours and severity is often associated with the dose ingested. While these symptoms may appear to

dissipate after the first 24 hours, the next 24-72 hours are characterized by biochemical changes. These include a rise in bilirubin levels resulting in jaundice, prolonged prothrombin time (PT), and elevated levels of alanine transaminase (ALT) and aspartate transaminase (AST). Patients may also begin to experience right-upper quadrant pain and hepatomegaly during this window (Chun et al., 2009) (Yoon et al., 2015). A small percentage of patients (<2%) may also experience renal failure during this phase (Yoon et al., 2015).

Neurological symptoms typically begin to occur 72-96 hours after onset. These symptoms may include confusion, lethargy, or coma. Liver test abnormalities generally peak at this stage as hepatocellular injury and cell death predominate. Resolution of liver injury can occur following this phase and approximately 70% of ALF patients will recover without the need for a liver transplant. ALF patients who experience spontaneous recovery generally improve within 4-14 days with restoration of hepatic architecture occurring within 3 months (Chun et al., 2009). For patients who do not recover during this stage, multi-organ failure may result (Yoon et al., 2015).

1.2.4 Clinical Diagnosis of APAP Induced ALF. APAP-induced ALF patients present with non-specific symptoms at onset including, fatigue, and vomiting. Clinical presentation of non-specific symptoms at onset can complicate ALF diagnosis, and diagnosis is frequently overlooked during initial patient-physician contact if the overdose was unintentional or not witnessed (Lee 2012). This initial phase of injury represents a critical window for identification and treatment of ALF, and if the diagnosis is missed, the opportunity to provide the best course of therapy may be lost. Unfortunately, ALF symptoms can progress rapidly after this phase in patients who do not undergo spontaneous recovery.

The greatest early indicator that a patient may be experiencing ALF is any change in mental status occurring in the absence of pre-existing conditions. Cerebral edema, or swelling of the brain, is a clinical symptom that is frequently found in ALF patients (Lee 2012). In addition to encephalopathy, another hallmark feature of ALF is coagulopathy (Lee 2012). The

international normalized ratio, or INR, is a clinical tool that can be used to determine the coagulation status in patients with ALF (Harrison 2018). INR is determined by calculating the ratio of a patient's prothrombin time (PT), a measure of a patient's ability to form blood clots, compared to a standardized PT control (Harrison 2018).

In patients with suspected APAP overdose, serum APAP levels can be quantified to estimate the risk of developing liver injury and to guide the physician on whether to initiate pharmacological therapy. However, if overdose occurred over the course of several days, serum APAP levels may be undetectable. For these patients, it may be more helpful to quantify serum acetaminophen-protein adducts, which have a much longer half-life (Stravitz et al., 2007) (Patton, Misel, and Gish 2012). Serum alanine aminotransferase (ALT) levels should be determined and monitored (Stravitz et al., 2007) (Patton, Misel, and Gish 2012). Other markers of liver injury may include elevated levels of bilirubin and albumin (Stravitz et al., 2007) (Patton, Misel, and Gish 2012).

1.2.4.1 Complications of ALF. A healthy liver performs critical functions in the body ranging from immune support, production of bile, storage of glucose, production of blood clotting factors and amino acids, transport of oxygen, drug metabolism, and conversion of waste products to urea so that they may be excreted. However, in a setting of acute liver failure, deterioration of liver function occurs rapidly leading to life-threatening hepatic dysfunction. For example, a failing liver cannot make clotting factors, produce bile, or guard against infections. Loss of these critical functions can have significant impacts on the body resulting in cardiovascular failure, pulmonary failure, and kidney failure. In fact, more than 50% of patients who succumb to ALF will die from multi-organ failure (Patton, Misel, and Gish 2012). Thus, strategies aimed at preventing multi-organ failure in this setting are urgently needed.

A change in mental status, or encephalopathy, is a critical defining feature of ALF. APAP-induced ALF patients with the poorest prognosis develop advanced stages hepatic encephalopathy (HE). HE in ALF is associated with high rate of mortality and often leads to

cerebral edema, coma, and brain herniation (Fontana 2008). Cerebral edema is a leading cause of death in ALF (Fontana 2008). Clinically, physicians rely on both the West Haven criteria for encephalopathy and the Glasgow coma score to assess the progression of HE in ALF patients. For patients not requiring intubation, the West Haven criteria is most commonly used to assess the progression of neurological abnormalities. The West Haven criteria is divided into four stages or grades. Patients in grade I may experience subtle personality changes, difficulty concentrating, altered sleep patterns, euphoria, or anxiety. Patients who progress to grade II become lethargic and display obvious personality changes. These patients also experience time disorientation and are unable to recall the current day of the week or day of the month. Furthermore, they may be unable to identify the year or season. Patients are assigned to grade III if they can no longer identify the country, state, city, region, or place they are currently in. In addition to space disorientation, patients in this grade may also exhibit bizarre behavior, drowsiness, confusion, or become incoherent. Patients who enter a prolonged state of unconsciousness, or coma, are assigned to grade IV. The patients may be either minimally responsive or unresponsive to stimuli. Survival dramatically decreases once patients progress to grade III, where rates of mortality can be as high as 80% (Fontana 2008).

1.2.4.2 Treatment Options. The etiology of ALF often guides the course of treatment. In the case of APAP overdose, the only pharmacological therapy available is N-acetyl cysteine, or NAC. NAC works primarily by replenishing glutathione stores, which become depleted under conditions of excessive NAPQI generation. However, NAC has a narrow therapeutic window and is only efficacious within 16 hours of overdose. While many suicidal patients who intentionally overdose on APAP generally receive medical attention within 4 hours of overconsumption, patients who unintentionally overdose of APAP do not seek medical attention until this early critical phase has passed (Lee 2004). Thus, for these patients NAC will not be an effective antidote. However, all patients with suspected APAP toxicity are generally administered NAC, as it has few side effects, and has been shown to improve chances of

transplant-free survival if given in early stages of APAP-induced ALF (Lee et al., 2009). Patients who intentionally overdose on APAP may also receive activated charcoal in conjunction with NAC if medical attention is provided within the first 4 hours following the overdose to help reduce absorption (Lee, Stravitz, and Larson 2011).

Aside from NAC, there are no known pharmacological therapies available for ALF patients. Thus, patients typically receive supportive care aimed at symptom management and treatment of complications (Lee, Stravitz, and Larson 2011). Courses of treatment for HE are dependent upon the severity of symptoms. However, the main goal is to prevent exacerbation of HE to cerebral edema, which can lead to cerebral herniation and death (Lee, Stravitz, and Larson 2011). Supportive care for this involves administration of lactulose to decrease blood ammonia levels and elevating hospital beds at >30° from horizontal (Lee, Stravitz, and Larson 2011). Patients who develop cerebral edema may be administered mannitol, which may temporarily decrease cerebral edema (Lee, Stravitz, and Larson 2011). The patient may also be subjected to hypothermia to slow production of and cerebral uptake of ammonia (Lee, Stravitz, and Larson 2011).

ALF patients also experience coagulation abnormalities. If patient INR is high, plasma infusions can be used to lower it (Lee, Stravitz, and Larson 2011). If this is not successful, higher volume plasma infusions or recombinant activated factor VII can also be used to attempt to rectify coagulopathy (Lee, Stravitz, and Larson 2011). However, these options should be used with caution as they may increase risk of complications. ALF patients experiencing significant bleeding, with low platelet counts, are given platelet transfusions to minimize bleeding (Lee, Stravitz, and Larson 2011).

ALF patients may also experience life threatening infections. Not only does the development of infections worsen HE, but it may also prevent the patient from receiving a liver transplant. Thus, patients with advanced stages of ALF may be given antibiotics prophylactically. APAP-induced ALF patients are also at high risk of developing renal failure,

which necessitates the need to continuously monitor renal function. If renal failure is not prevented, patients may require dialysis (Lee, Stravitz, and Larson 2011). If early attempts at supportive care are not successful and the patient does not undergo spontaneous recovery, a liver transplant may be the only available treatment option for survival. APAP-induced ALF currently accounts for approximately 20% of liver failure cases requiring transplantation in the US (Yoon et al. 2015).

1.2.4.2.1 Liver Transplant. The ability to transplant donor livers has greatly improved the survival rates for ALF patients and it is currently the only lifesaving treatment option for the most critically ill patients. Strikingly, prior to the availability of liver transplants, an ALF diagnosis carried a 90% mortality rate (Akamatsu, Sugawara, and Kokudo 2013). However, 75% of patients are now expected to survive following emergency liver transplantation (O'Grady 2014). While potentially life-saving, patients who receive a donor liver face major risk of complications and a lifetime of taking medications including immunosuppressants (O'Grady 2014). Unfortunately, some patients are unable to receive a transplant due to the severity of ALF complications, such as severe cerebral edema or multi-organ failure. For these patients, non-transplant therapies are urgently needed to increase survival. Recent findings indicate that immune-targeted therapies might be of benefit in ALF patients.

1.3 Immune System Dysfunction in APAP-Induced ALF

1.3.1 The Roles of Systemic Inflammatory Response Syndrome and Compensatory Anti-Inflammatory Response Syndrome in Acute Liver Failure. Immune system dysregulation is a key component of ALF, and studies indicate that the intensity of the innate immune response triggered by the hepatic injury is one of the most important determinants of outcome in ALF patients (Donnelly, Hayes, and Simpson 2016) (Antoniades et al. 2008) (Krenkel, Mossanen, and Tacke 2014). Clinically, ALF patients with the poorest prognosis exhibit high systemic levels of proinflammatory cytokines indicative of systemic inflammatory response syndrome (SIRS). Paradoxically, these patients often exhibit increased levels of anti-

inflammatory cytokines, including IL-10, IL-4 and transforming growth factor beta (TGF-β) reflective of compensatory anti-inflammatory response syndrome (CARS) (Antoniades et al., 2008). Interestingly, studies indicate that development of SIRS in ALF may be etiology specific, occurring more frequently in patients with APAP-induced ALF (Craig et al., 2011) (Leithead et al., 2008).

SIRS, in APAP-induced ALF, frequently occurs simultaneously with CARS, and the presence of these disorders is associated with a greater risk of developing multi-organ failure and death. Although the mechanistic basis for this is not fully known, immune suppression associated with CARS may dramatically increase the risk of developing life-threatening infections. Further, because of the importance of the immune system for repair of the liver after injury, SIRS and CARS may prevent recovery from the severe hepatocellular injury allowing for the progression to multi-organ failure (Donnelly, Hayes, and Simpson 2016). Unfortunately, the presence of these syndromes also decreases patient survival after a liver transplant, making it necessary to stabilize the patient prior to surgery (Donnelly, Hayes, and Simpson 2016). Thus, there is a critical need for novel therapies that will improve survival in these patients. An effective approach would be to correct the immune dysregulation that occurs in this patient population. Before this can be accomplished, however, the mechanistic basis of immune dysregulation needs to be established.

Monocyte dysfunction plays a central role in the pathogenesis of SIRS and CARS in ALF patients, and studies have demonstrated that this is associated with a poor outcome (Antoniades et al., 2008). It has been proposed that DAMPs released from damaged cells in the liver stimulate monocytes to produce high levels of proinflammatory cytokines that spill into the systemic circulation producing SIRS and triggering multiorgan failure. To counter this, monocytes begin to express membrane proteins, such as programmed death-ligand-1 (PD-L1) and produce anti-inflammatory cytokines, such as IL-10, that cause the systemic immune

suppression characteristic of CARS. In support of this, blood monocytes isolated from patients with APAP-induced ALF show impaired secretion of pro-inflammatory cytokines, including TNF-α, after *ex vivo* stimulation with bacterial lipopolysaccharide (de la Mata M et al., 1990) (Wigmore et al., 1998). Instead, these monocytes secrete large quantities of the anti-inflammatory cytokine, IL-10, (Wolk et al., 1999) (Wolk et al., 2000). While the presence of IL-10 is generally regarded as beneficial for wound healing, in the setting of CARS, IL-10 deactivates monocytes causing immune paralysis which impairs the pro-repair activity of monocytes and renders patients highly susceptible to opportunistic infections (Wolk et al., 1999) (Wolk et al., 2000). While the presence of SIRS and CARS in ALF patients has been well established, the impact of these syndromes on APAP-induced liver disease in animal models remains to be investigated. Without these studies, it will be difficult to elucidate the mechanism of immune dysregulation in ALF which is needed to design novel therapeutics to restore immune system regulation in ALF.

1.4 Mouse Model of Acetaminophen-Induced Acute Liver Failure

1.4.1 Features of ALF in Mouse Models. Mice are frequently used as a model organism to study APAP-induced ALF (Bhushan et al., 2014). Unfortunately, a lack of standardization of APAP doses across different laboratories has led to substantial controversy regarding the pathogenesis of APAP-induced ALF. Many laboratories treat mice with a dose of APAP at or near 300 mg/kg. These mice develop liver injury that is largely repaired by 96 hours without the need for therapeutic interventions (Bhushan et al., 2014). Because of the rapid nature of liver repair in these mice, many of the important pathological features of APAP-induced ALF occurring in the sickest patients (e.g., multiorgan failure) are not recapitulated in mice treated with this dose. By contrast, mice treated with 600 mg/kg APAP develop liver injury that fails to repair ultimately resulting in liver failure and often death (Bhushan et al., 2014). Importantly, this dose of APAP produces additional features of ALF observed in humans, including renal toxicity (multi-organ dysfunction) and elevated blood ammonia levels, which

contributes to the development of HE (2014). It remains to be investigated, however, whether SIRS and CARS are causally involved in the development of extrahepatic complications in these mice.

Studies have identified IL-6 and IL-10 as key hepatoprotective cytokines in mice treated with 300 mg/kg APAP. IL-10 is upregulated in the livers of mice treated with this dose of APAP, and studies have revealed that liver injury, proinflammatory cytokine synthesis and mortality are greatly exacerbated in APAP-treated IL-10 knockout mice (Bourdi et al., 2002). Similarly, IL-6 knockout mice treated with 300 mg/kg APAP develop greater liver injury and show reduced hepatocyte proliferation (James et al., 2003). Based upon these findings, it has been proposed that therapeutic elevation of these cytokines may be of benefit to APAP overdose patients. Remarkably, though, high serum levels of IL-6 and IL-10 are independent predictors of a poor outcome in APAP-induced ALF patients. In fact, IL-6 and IL-10 are two of the signature cytokines that are highly expressed in APAP overdose patients with SIRS and CARS. In these patients, high levels of IL-6 are associated with more severe multiorgan dysfunction, worsening of hepatic encephalopathy, and death. Similarly, high levels of IL-10 are associated with an increased risk of death in ALF patients. Collectively, these disparate findings between humans and mice suggest that either the mouse is not an appropriate model organism to investigate APAP-induced ALF or that the experimental paradigm commonly used (e.g., at or near 300 mg/kg APAP) does not accurately model APAP-induced ALF. Several lines of evidence indicate that the latter is the most likely explanation.

As discussed above, liver injury is repaired, and the mouse fully recovers after treatment with 300 mg/kg APAP. Because of this, the severity of APAP-induced ALF that occurs in patients is poorly modeled by this dose of APAP. By contrast, Bhushan and colleagues demonstrated that liver repair fails to occur in mice treated with 600 mg/kg APAP, a finding that has been reported in the most critically ill patients with APAP-induced ALF (2014). Although it is not clear whether SIRS and CARS occur in these mice, Bhushan and colleagues demonstrated

further that blood levels of IL-6 were higher and remained elevated for longer in mice treated with 600 mg/kg APAP when compared to mice treated with 300 mg/kg APAP (2014). This suggests that immune dysregulation may occur in mice treated higher doses of APAP, and that this may better mirror the pathogenesis of ALF occurring in APAP overdose patients. Many questions remain to be answered, however, including the impact of high doses of APAP on the function of monocytes and macrophages during liver repair.

1.5 Monocyte and Macrophage Regulation and Function in the Liver after APAP Overdose

1.5.1 Macrophages. Macrophages are specialized innate immune cells present in every tissue in the body that play a vital role in maintaining homeostasis. In addition to being vital for tissue homeostasis, macrophages play crucial roles in development, tissue repair, and in clearance of invading pathogens, such as bacteria (Hu et al., 2018). Heterogenous populations of macrophages exist and through polarization, these highly adaptable and dynamic cells can switch their phenotype in response to local changes in the microenvironment. Macrophage polarization states have been traditionally categorized into two functionally distinct subsets: classically activated (M1) or alternatively activated (M2) macrophages. In this paradigm, classically activated macrophages, or M1 macrophages, are drivers of the inflammatory response that targets invading pathogens. Unfortunately, these cells can produce collateral tissue damage if they are not properly regulated. On the other hand, M2 macrophages, or alternatively activated macrophages, dampen the inflammatory response and promote resolution of tissue injury. It is clear from a number of recent studies, however, that the traditional M1/M2 classification represents two extremes of a continuum and that macrophages can express features of both M1 and M2 phenotypes simultaneously (Hu et al., 2018).

The origin of tissue macrophage populations has been the subject of much debate; however, it is now widely accepted that these cells originate from yolk sac progenitors and not bone marrow in most tissues (Ginhoux et al., 2010) (Yona et al., 2013) (Hashimoto et al., 2013).

These tissue macrophages undergo differentiation during developmental stages and their lifespan can range from months to years. Under homeostatic conditions, studies have shown that tissue macrophages are replenished through self-renewal. However, if pathological conditions result in excessive loss of tissue macrophages, they can be replaced by monocyte-derived macrophage arising from bone marrow (Watanabe et al., 2019) (Bain and Schridde 2018) (De Schepper et al, 2018) (Li and Barnes 2018) (Shaw et al., 2018).

Macrophages represent a heterogenous population of cells, and most tissues contain more than one macrophage population. The liver, for example, consists not only of self-renewing resident macrophages, termed Kupffer cells (KCs), but also a population of macrophages derived from the bone marrow (Dou et al., 2020). Similarly to other tissues, these two hepatic macrophage populations each differ in their capacity for self-renewal, their rate of replacement, and their roles in maintaining homeostasis, modulating response to injury, and orchestrating tissue repair (Hu et al., 2018). The functions of hepatic macrophage populations in maintaining homeostasis and in APAP-induced liver injury and repair are highlighted in the following sections (section 1.5.1.1-1.5.1.3).

1.5.1.1 Resident Hepatic Macrophages. Kupffer Cells (KCs) are the resident population of macrophages in the liver. Located in the hepatic sinusoids, KCs are of myeloid lineage, and they are the largest population of resident macrophages in the body. KCs play vital roles in protecting the liver against pathogens, restoring liver tissue following injury, and in initiating both innate and adaptive immune responses (van der Heide, Weiskirchen, and Bansal 2019). Additionally, this population of resident macrophages sense and remove foreign materials, including, pathogens and cellular debris, that have entered the liver through the portal circulation (Roth, Strickland, and Copple 2020).

KCs can be identified through their selective expression of the specific KC marker, C-type lectin 4F (Clecf4). These cells are characterized as being $CD45^{+}$ $F4/80^{+}$ $CD11b^{int}$ by flow cytometry (van der Heide, Weiskirchen, and Bansal 2019). More recent studies, however, using

newer technologies, such as mass cytometry and single cell gene expression profiling have identified two distinct subsets of KCs (Beattie et al., 2016). While one of these populations is yolk sac derived, the other is derived from bone marrow. The yolk sac derived KC population migrates to the liver, where they become fully functioning KCs. These cells can be identified by its expression of macrophage receptor with collagenous structure (MARCO) and T-cell immunoglobin and mucin domain containing 4, or Tim 4 (Beattie et al., 2016). This population of KCs is an important regulator of immunity (Beattie et al., 2016). Replenishment of this population of KCs has been shown to occur though local proliferation, and while the stimulus leading to replenishment is not fully known, studies have shown colony stimulating factors may play a role in this process (Yona et al., 2013) (Zigmond et al., 2014). If a substantial loss of KCs occurs, for example following exposure to lethal irradiation, bone marrow progenitors recruited from the circulation can replenish the KC population (Roth, Rockwell, and Copple 2019) (Scott et al., 2016). These bone marrow progenitors take up residence within the hepatic sinusoids and receive local cues which reprograms them to become KCs (Sakai et al., 2019) (Roth, Strickland, and Copple 2020).

1.5.1.2 Contribution of Kupffer Cells to APAP-Induced Liver Injury and Repair. Macrophages play several key roles in the liver following APAP overdose, including production of cytokines, clearance of dead cells and debris, and production of pro-mitogenic growth factors (Ju and Tacke 2016). The importance of KCs in regulating these processes following APAP-induced hepatoxicity, however, has been subject to much debate. Early studies suggested KCs were critical for liver toxicity following APAP overdose (Laskin et al., 1995) (Michael et al., 1999). For instance, treatment of mice with gadolinium chloride, a macrophage inhibitor, was protective against APAP hepatoxicity (Laskin et al., 1995). However, later studies using clodronate-containing liposomes to fully deplete KCs, reported KC depletion leads to enhanced hepatic necrosis 8 and 24 hours following an acutely toxic dose of APAP (Ju et al., 2002).

In this setting, KC depletion was associated with a reduction in the anti-inflammatory cytokine, IL-10 (Ju et al., 2002). Studies in IL-10 knockout mice supported this finding, as IL-10 knockout mice had increased liver toxicity and mortality following APAP overdose (Bourdi et al., 2002). These studies suggested a protective, rather than pathogenic, role for KCs following APAP-induced hepatoxicity. In addition to being an important source of IL-10, other studies in murine models of APAP-induced hepatoxicity have shown that KCs also produce proinflammatory mediators as early as 6 hours following APAP overdose, including IL-1β, TNF-α, IL-6, and Ccl2 (Fisher et al., 2013) (Dambach et al., 2002) (Gao et al., 2020). Importantly, secretion of IL-6 by hepatic macrophages has been shown to be protective against liver toxicity in this setting (Gao et al., 2020). Collectively, these studies suggest KCs play a crucial role in early cytokine induction following APAP overdose, however, by 24 hours, KC populations are substantially reduced (Zigmond et al., 2014) (Dambach et al., 2002). While the reasons for this are unclear, KC numbers return to baseline levels by 72 hours through local proliferation of mature KCs (Zigmond et al., 2014) (Dambach et al., 2002).

1.5.1.3 Function of Monocyte-Derived Macrophages in Liver Repair after APAP-Induced Liver Injury. Studies have shown that a population of monocyte-derived macrophages, distinct from Kupffer cells and other resident macrophages, rapidly infiltrate the liver after APAP overdose (Holt, Cheng, and Ju 2008). Unlike KCs, monocyte-derived macrophage populations do not proliferate or undergo self-renewal (Italiani and Boraschi 2014). These cells are recruited to the liver in a Ccr2- and M-CSF-dependent manner (Zigmond et al., 2014). During the initial phases of injury, these cells are proinflammatory and express high levels of proinflammatory genes, indicating an M1-like phenotype (Zigmond et al., 2014). Studies identifying macrophage subsets in the liver following APAP challenge have shown these cells highly express the cell surface antigen, lymphocyte antigen 6 complex, locus C1, or Ly6C, during the initial phases of injury (Zigmond et al., 2014). Fate tracing studies have revealed that

$Ly6C^{hi}F4/80^{low}$ proinflammatory monocytes ultimately differentiate into pro-repair macrophages which are $Ly6C^{low}F4/80^{hi}$ (Yona et al., 2014) (Girgis et al., 2014) (Sunderkotter et al., 2004) (Zigmond et al., 2014). Importantly, by 72 hours, the dominant macrophage population in the liver was characterized as being $Ly6C^{low}F4/80^{hi}$ (Zigmond et al., 2014). These macrophages were further classified by their high-level expression of the chemokine C-X3-C motif receptor 1, or Cx3cr1, making them distinguishable from KCs, which are $Cx3cr1^{-}$ (Zigmond et al., 2014). The gene expression profile for pro-repair macrophages also differs from KCs, with pro-repair macrophages expressing high levels of pro-restorative and anti-inflammatory genes, indicating an M2-like phenotype (Zigmond et al., 2014).

As noted above, monocyte-derived macrophages are recruited to the liver after injury by the chemokine, chemokine (C-C motif) ligand 2 (Ccl2), also called monocyte chemoattractant protein-1. Several studies have shown that Ccl2 stimulates chemotaxis of monocytes by activating the C-C chemokine receptor type 2 (Ccr2) (Kurihara et al., 1997). Following APAP challenge, expression of Ccl2 is increased in hepatocytes and in KCs as early as 12 hours following administration, leading to the accumulation of $Ccr2^{+}$ monocytes (Dambach et al., 2002). Reduced numbers of monocyte-derived macrophages are present in the livers of Ccr2 knockout mice following APAP overdose (Holt, Cheng, and Ju 2008) (Dambach et al., 2002). Furthermore, despite similar levels of liver injury between wild-type and Ccr2 knockout mice following APAP overdose, impaired clearance of necrotic cells was observed in Ccr2 knockout mice (Dambach et al., 2002). This important finding highlights the role of monocyte-derived macrophages in mediating clearance of necrotic cells and debris in this setting.

Recently it was reported that phagocytosis of neutrophils by macrophages promotes macrophage polarization after APAP overdose (Graubardt et al., 2017). Additionally, we have recently shown that phagocytosis of necrotic hepatocytes by cultured $Ly6C^{hi}F4/80^{low}$ cells decreases proinflammatory cytokine expression, while increasing expression of macrophage pro-repair markers (e.g., Arg-1, Cx3cr1, and Vsig4) (Roth et al., 2019). Following polarization to

a pro-repair phenotype, these cells produced pro-repair growth factors and anti-inflammatory cytokines that trigger the transition from the inflammatory phase of liver injury to the reparative phase (Graubardt et al., 2017). However, the mechanisms controlling the intrahepatic trafficking, phagocytosis and phenotype switching by these cells following APAP challenge remains poorly understood.

Interestingly, clinical studies have revealed monocyte deactivation is a predictor of poor outcome in APAP-Induced ALF patients with the poorest prognosis (Antoniades 2008) (Triantafyllou et. al, 2018). In these patients, monocyte dysregulation causes sustained proinflammatory cytokine release that drives the development of life-threatening complications, including multi-organ failure (Triantafyllou et. al, 2018) (Antoniades 2008). Thus, elucidation of mechanism(s) leading to impaired monocyte differentiation in ALF has the potential to revolutionize treatment of ALF. Identification of receptor(s) responsible for stimulating maturation of proinflammatory monocytes into pro-repair macrophages will be necessary for the development of any pharmacological treatment aimed at stimulating this differentiation. The TAM family of receptor kinases play a vital role in the resolution of inflammation. Additionally, studies have shown TAM receptor signaling is important for promoting macrophage polarization (Myers, Amend, and Pienta 2019). Thus, the role of TAM receptors in promoting liver repair following APAP-induced ALI warrants further investigation.

1.6 TAM Receptors

1.6.1 Introduction to TAM Family of Receptors. Discovered in the 1990s, by Lai and Lemke, TAM (Tryro3, Axl, and Mer) receptors were the last family of receptor tyrosine kinases (RTKs) to be identified. The structure and expression of TAM receptors and their ligands are outlined in Sections 1.6.1.1-1.6.1.2. The TAM receptor family is unique to the RTK family in that these receptors play no role in embryonic development. Importantly, this enabled the generation of viable and fertile single, double, and triple TAM receptor KO mouse models. Generation of these TAM mutants has played a major role our understanding of TAM function in

inflammatory diseases. While indistinguishable from wild-type mice, during their first week of life, triple TAM receptor mutant mice begin to develop a wide range of degenerative diseases (Lemke and Rothlin 2010). Specifically, 4-6 weeks after birth, these mice begin to develop splenomegaly, lymphadenopathy, and lymphocyte infiltration in nearly all tissues. Strikingly, the spleen and lymph nodes of these mice can weigh up to 10 times those from wild-type mice of the same age (Lemke and Rothlin 2010). Immune cell populations, including macrophages, are constitutively active in these mice producing features of autoimmune diseases, including swollen joints, skin lesions, and blood vessel hemorrhages (Lemke and Rothlin 2010). Notably, these mice develop clinical symptoms similar to those observed in patients with either systemic lupus erythematosus (SLE) or rheumatoid arthritis (RA) (Lemke 2017) (Cohen and Shao 2019). Single TAM KO mice exhibit much milder phenotypes, with the primary defect being diminished phagocytic clearance of apoptotic cells (Lemke and Rothlin 2010).

Several studies have shown that the TAM family of receptors are important regulators of phagocytosis in both homeostatic and inflammatory conditions (Lemke and Rothlin 2010) (Rothlin et al., 2015) (Lemke 2017). Specifically, activation of this family of receptors, by phosphatidylserine, exposed on the surface of apoptotic cells, dampens the immune response (Rothlin et al., 2015) (Lemke 2017). In particular, TAM receptor activation skews macrophage polarization towards an M2 phenotype which increases expression of anti-inflammatory cytokines thereby favoring resolution of inflammation and wound healing (Mukherjee et al., 2016) (Rothlin et al., 2015) (Lemke 2017). (Lemke and Rothlin 2010).

1.6.1.1 Expression. TAM receptors are widely expressed throughout the body; however, their highest level of expression is typically found in immune cell populations. Specifically, in addition to macrophage and dendritic cell populations, TAM receptors are also active in natural killer cells. Patterns of TAM receptor expression can vary; however, it is generally the case that multiple TAM receptors are expressed on a given cell (Lemke 2013). For example, all three TAM receptors are expressed on platelets (van der Meer et al., 2014).

High levels of Tyro3 and Mer expression can be found in the kidneys, ovaries, and testes. Additionally, several studies have shown Tryo3 is highly expressed in the central nervous system (Lemke 2013). Axl is expressed on nearly all cells that originate from hematopoietic and mesenchymal stem cells, and epithelial cells (van der Meer et al., 2014). Many cells that express TAM receptors, also express at least one of the TAM receptor ligands (Lemke and Rothlin 2008).

Axl is the most widely expressed TAM receptor in the liver. In addition to immune cell populations, studies have shown Axl expression on hepatocytes, endothelial cells, and stellate cells (Zagórska et al., 2020) (Bárcena et al., 2015). Mer is co-expressed with Axl on hepatic macrophage populations including both KCs and monocyte-derived macrophages, and generally induction of Axl is followed by inhibition of Mer and vice versa (Zagórska et al., 2020). While Axl and Mer are expressed on multiple cell types in the liver, Tyro3 is only expressed in resident macrophages the liver, and in settings other than hepatocellular carcinoma, hepatic expression of Tyro3 is low (Duan et al., 2016).

1.6.1.2 Ligands. The two most well-known TAM receptor ligands are Protein S and growth arrest–specific gene 6, or Gas6. Protein S and Gas6 share structural homology (~42% amino acid identity), including a sex hormone-binding globulin (SHBG) domain, which binds to the TAM Ig-like domains (Lemke and Rothlin 2008). The N-terminus contains a glutamic acid (Gla)-rich domain that is gamma carboxylated in a vitamin K-dependent manner. This domain binds phosphatidylserine (PS) exposed on the surface of apoptotic cells, a reaction that occurs in a calcium-dependent manner (Lemke 2013). In this context, Gas6 and Protein S serve as a "bridging molecule" linking the TAM receptors on immune cells with PS apoptotic cells (Lemke and Rothlin 2008). Importantly, binding of Protein S or Gas6 to PS is a prerequisite for full activation of TAM receptors.

Gas6 and Protein S have different binding affinities for each of the three TAM receptors (Lemke and Rothlin 2008). For example, while Protein S has a high binding affinity for Tyro3

and Mer, it does not bind to Axl (van der Meer et al., 2014). Gas6, however, binds to all three TAM receptors with the highest affinity being for Axl (Axl ≥ Tyro3 >> Mer) (van der Meer et al., 2014) (Lemke and Rothlin 2008). Following ligand binding by either Gas6 or Protein S, the TAM receptor will dimerize, leading to a conformational change that activates the receptor (Lemke and Rothlin 2008).

1.6.2 TAM Receptors in Liver Diseases. TAM receptors have been implicated in a number of acute and chronic liver diseases, including fibrosis, hepatitis C virus infection, and in hepatocellular carcinoma (Bernsmeier et al., 2017) (Barcena et al., 2015) (Duan et al., 2016). While all TAM receptors are expressed in the liver, it is the overexpression of Axl that contributes to the development of many chronic liver diseases. For example, activation of the Gas6/Axl pathway has been shown to promote fibrosis. In fact, in an experimental setting of CCl4 induced fibrosis, targeting of the Gas6/Axl pathway with BGB324 reduced fibrosis through inactivation of hepatic stellate cells (Barcena et al., 2015). The development of liver fibrosis in this model was similarly reduced in Axl KO mice (Barcena et al., 2015). While overexpression of Axl has shown do be a driving factor in some liver diseases, deficiencies in Axl expression have been reported in others. For example, failed upregulation of Axl occurs in patients with acute-on-chronic liver failure, as clinical studies have shown decreased levels of Axl mRNA as compared to healthy individuals (Bernsmeier et al., 2017).

Studies examining the role of TAMs in APAP-induced ALI models have largely been limited to Mer. Mer-mediated phagocytosis in the APAP-induced ALI model only showed modest effects, suggesting it does not play a major role in mediating repair in APAP induced liver injury (Triantafyllou et al., 2018). Additionally, in this setting, the dead cells were ultimately cleared from the liver despite the loss of Mer (Triantafyllou et al., 2018). Given that Mer-mediated phagocytosis predominates in homeostatic environments, and not in inflammatory environments, this result is unsurprising. It leaves open the possibility however, that Axl is a major regulator of inflammatory mediated phagocytosis in APAP-induced ALI. As noted above,

hepatic macrophage populations play crucial role(s) in mediating immune responses and clearance of dead cells following APAP-induced ALI. Axl has been shown to be highly expressed on both KCs and in pro-inflammatory and pro-repair macrophage populations (Graubardt et al., 2017). Furthermore, expression of Axl and its agonist Gas6 are significantly upregulated following proinflammatory monocyte differentiation (Graubardt et al., 2017).

As noted above, loss of TAM receptor function been shown to induce a proinflammatory state characterized by a reduction in clearance of necrotic and apoptotic cellular debris (Rothlin et al., 2015). Impaired efferocytosis and a persistent proinflammatory environment are clinical features of ALF patients with the worst prognosis. Thus, given the role of hepatic macrophage populations in immune system dysfunction in the pathogenesis of ALF, the role of Axl in liver repair following APAP induced hepatoxicity warrants further investigation.

1.7 Macrophage Targeted Therapies in Treatment of Liver Diseases

1.7.1 Urgent Need for Novel Therapeutics. The role of macrophage polarization in stimulating hepatic repair is not limited to acute liver injury. Several studies have shown this process is also vital to liver repair in settings of chronic liver diseases including fibrosis (Ramachandran et al., 2012). In fibrosis, proinflammatory monocyte populations stimulate hepatic stellate cell differentiation into myofibroblasts, leading to the production of extracellular matrix. Over time, this leads to the development of fibrosis and can eventually progress to cirrhosis. Fibrosis, and even cirrhosis, have been shown to be reversible in both patients and in animal models following the cessation of liver injury (Ismail and Pinzani 2009). Linage tracing studies have revealed that macrophage polarization plays a fundamental role in fibrosis reversal. Proinflammatory monocyte differentiation to pro-repair macrophages in this setting leads to the generation of active-matrix metalloproteinases (MMPs), which remove excess extracellular matrix. Additionally, these pro-repair macrophages produce insulin-like growth factor-1 (IGF-1), which promotes apoptosis and senescence of myofibroblasts. Furthermore, recent studies provide compelling evidence that modulation of macrophage phenotype may

directly stimulate fibrosis reversal. For example, while depletion of pro-resolving macrophages prevents reversal of liver fibrosis in experimental settings, manipulations that stimulate formation of pro-resolving macrophages accelerates the reversal of liver fibrosis in mice (Ramachandran et al., 2012). Thus, the ability to pharmacologically induce pro-inflammatory monocyte polarization would significantly impact clinical treatment of liver diseases, including liver fibrosis and cirrhosis. Additionally, identification of compounds capable of stimulating macrophage polarization could provide therapeutic benefit to patients with ALF, as failed macrophage differentiation also occurs in this setting.

Despite the wide prevalence of fibrosis and cirrhosis, at present, no antifibrotic therapies are available. Current therapeutic approaches for reversing fibrosis primarily involve treating the underlying etiology, such as antivirals to eradicate hepatitis virus or cessation of alcohol consumption in ALD. While this treatment strategy has proved beneficial for some patients, in others they have been largely unsuccessful, and in the case of genetic disorders and abnormalities, they are not feasible. For these patients, supportive medical care and liver transplantation are the only remaining options. While liver transplantation is widely regarded as improving long-term outcomes for patients with advanced liver disease, it carries tremendous clinical and economic burden. Furthermore, the demand for transplantable livers far exceeds the available supply, with fewer than half of patients needing a donor liver receiving one (Habka et al., 2015). Unfortunately, donor shortages are only expected to increase due to the impending epidemic of nonalcoholic steatohepatitis (NASH). In addition to currently representing the 2nd leading etiology requiring liver transplantation, the presence of hepatic steatosis has become increasingly common in donor livers making them high risk for organ transplantation (Wong et al., 2015) (Busuttil and Tanaka, 2003). Given the limitations associated with liver transplantation, development novel therapeutics and treatment strategies that stimulate the reversal of fibrosis will be necessary for successful treatment of the growing number of patients with chronic liver diseases.

Utilization of high-throughput screening techniques offers a novel approach for identifying compounds that may drive macrophage polarization towards a pro-reparative state. Although this is a high-risk approach, it offers a rapid and inexpensive method to identify new candidates for anti-fibrotic drug therapies; thus, it has the potential to tremendously impact clinical treatment of liver fibrosis. High-throughput screening assays aimed at detecting changes in macrophage polarization hold great promise as several studies have shown distinct and easily detectable differences exist between the proinflammatory monocytes and pro-repair macrophages (Ramachandran et al., 2012).

1.7.2 High-throughput Screening. High-throughput drug screening is a drug discovery platform used to screen thousands of compounds for drug activity in a relatively short period of time. For years, this approach was largely limited to drug companies because of the high cost and the lack of commercially available compound libraries. In recent years, however, compound libraries have become increasingly accessible allowing academia and private institutions the opportunity to establish high-throughput screening facilities. During high-throughput screening, automated equipment (e.g., robotics) is used to screen hundreds of thousands of chemicals and/or biological compounds for a specific activity (i.e., biological effect). To accomplish this, a screening assay is first developed that allows for the detection of compounds with a particular pharmacological or biological activity (e.g., inhibition of enzyme activity, increase cellular influx of calcium, inhibition of cell proliferation). The screening assay is typically amenable to microtiter plates (i.e., 96-, 384-, or 1536-well formats); is easy to perform (e.g., minimal steps and reagents) and inexpensive; and must provide a read-out that is rapid and robust. Once an assay is developed, compound libraries can be rapidly screened for drug activity.

1.8 Purpose. Acetaminophen overdose is the leading cause of ALF in the United States. Immune system dysfunction is a central player in the pathogenesis of ALF in APAP-induced ALF patients with the poorest prognosis. It is highly probable that in these patients their own innate immune response to the hepatic injury largely determines patient outcome. The

mechanisms underlying immune system dysfunction in these patients remain unknown. However, patients with the poorest prognosis display symptoms consistent with SIRS and CARS. Development of SIRS and CARS in these patients is associated with a high rate of mortality. Uncovering the mechanisms that underly development of SIRS and CARS in these patients, has the potential to revolutionize the treatment of ALF. The goals of the present studies were to determine mechanisms contributing to immune dysfunction in ALF patients.

Hepatic macrophage populations, including proinflammatory monocytes, have been shown to play a central role in the development of SIRS and CARS and monocyte dysfunction is associated with a poor outcome in ALF. Macrophage polarization has been shown to play a vital role in hepatic repair following APAP-induced ALI. Thus, identification of receptors that stimulate macrophage polarization towards a reparative phenotype will aid in the development of pharmacological treatments. The TAM receptor, Axl, has been shown to be highly expressed on both KCs and in pro-inflammatory and pro-repair macrophage populations. Activation of this receptor has been shown to mediate clearance of dead cells, stimulate macrophage polarization, and suppress inflammation. Thus, we have investigated the role of Axl in mediating dead cell clearance and in regulating inflammation in APAP-induced hepatoxicity.

The role of macrophage polarization in stimulating hepatic repair extends beyond acute liver injury. Importantly, failed macrophage differentiation is also a defining feature of chronic liver diseases, including fibrosis. Current therapeutic approaches for reversing fibrosis are limited. However, there is evidence to suggest modulation of macrophage phenotype may lead to fibrosis reversal. Thus, the identification and development of novel therapeutics to stimulate macrophage polarization is urgently needed as it may benefit patients with both acute and chronic liver diseases. High-throughput screening represents a novel approach for identifying compounds that may drive macrophage polarization towards a pro-reparative state and could lead to the identification of compounds capable of stimulating this process in patients.

Thus, we have developed a phenotypic high-throughput screening assay capable of detecting changes in macrophage polarization. Additionally, we have utilized this assay to identify compounds capable of simulating macrophage differentiation.

BIBLIOGRAPHY

Akamatsu N, Sugawara Y, Kokudo N. Acute liver failure and liver transplantation. Intractable Rare Dis Res. 2013 Aug;2(3):77-87. doi: 10.5582/irdr.2013.v2.3.77. PMID: 25343108; PMCID: PMC4204547.

Antoniades CG, Berry PA, Wendon JA, Vergani D. The importance of immune dysfunction in determining outcome in acute liver failure. J Hepatol. 2008 Nov;49(5):845-61. doi: 10.1016/j.jhep.2008.08.009. Epub 2008 Aug 21. PMID: 18801592.

Bárcena C, Stefanovic M, Tutusaus A, Joannas L, Menéndez A, García-Ruiz C, Sancho-Bru P, Marí M, Caballeria J, Rothlin CV, Fernández-Checa JC, de Frutos PG, Morales A. Gas6/Axl pathway is activated in chronic liver disease and its targeting reduces fibrosis via hepatic stellate cell inactivation. J Hepatol. 2015 Sep;63(3):670-8. doi: 10.1016/j.jhep.2015.04.013. Epub 2015 Apr 20. PMID: 25908269; PMCID: PMC4543529.

Bain CC, Schridde A. Origin, Differentiation, and Function of Intestinal Macrophages. Front Immunol. 2018 Nov 27;9:2733. doi: 10.3389/fimmu.2018.02733. PMID: 30538701; PMCID: PMC6277706.

Beattie L, Sawtell A, Mann J, Frame TCM, Teal B, de Labastida Rivera F, Brown N, Walwyn-Brown K, Moore JWJ, MacDonald S, Lim EK, Dalton JE, Engwerda CR, MacDonald KP, Kaye PM. Bone marrow-derived and resident liver macrophages display unique transcriptomic signatures but similar biological functions. J Hepatol. 2016 Oct;65(4):758-768. doi: 10.1016/j.jhep.2016.05.037. Epub 2016 Jun 1. PMID: 27262757; PMCID: PMC5028381.

Bernsmeier C, Triantafyllou E, Brenig R, Lebosse FJ, Singanayagam A, Patel VC, Pop OT, Khamri W, Nathwani R, Tidswell R, Weston CJ, Adams DH, Thursz MR, Wendon JA, Antoniades CG. CD14+ CD15- HLA-DR- myeloid-derived suppressor cells impair antimicrobial responses in patients with acute-on-chronic liver failure. Gut. 2018 Jun;67(6):1155-1167. doi: 10.1136/gutjnl-2017-314184. Epub 2017 Jun 7. PMID: 28592438; PMCID: PMC5969362.

Bhushan B, Walesky C, Manley M, Gallagher T, Borude P, Edwards G, Monga SP, Apte U. Pro-regenerative signaling after acetaminophen-induced acute liver injury in mice identified using a novel incremental dose model. Am J Pathol. 2014 Nov;184(11):3013-25. doi: 10.1016/j.ajpath.2014.07.019. Epub 2014 Sep 2. PMID: 25193591; PMCID: PMC4215032.

Bourdi M, Masubuchi Y, Reilly TP, Amouzadeh HR, Martin JL, George JW, Shah AG, Pohl LR. Protection against acetaminophen-induced liver injury and lethality by interleukin 10: role of inducible nitric oxide synthase. Hepatology. 2002 Feb;35(2):289-98. doi: 10.1053/jhep.2002.30956. PMID: 11826401.

Busuttil RW, Tanaka K. The utility of marginal donors in liver transplantation. Liver Transpl. 2003 Jul;9(7):651-63. doi: 10.1053/jlts.2003.50105. PMID: 12827549.

Chun LJ, Tong MJ, Busuttil RW, Hiatt JR. Acetaminophen hepatotoxicity and acute liver failure. J Clin Gastroenterol. 2009 Apr;43(4):342-9. doi: 10.1097/MCG.0b013e31818a3854. PMID: 19169150.

Craig DG, Reid TW, Martin KG, Davidson JS, Hayes PC, Simpson KJ. The systemic inflammatory response syndrome and sequential organ failure assessment scores are effective triage markers following paracetamol (acetaminophen) overdose. Aliment Pharmacol Ther. 2011 Jul;34(2):219-28. doi: 10.1111/j.1365-2036.2011.04687.x. Epub 2011 May 10. PMID: 21554357.

Dambach DM, Watson LM, Gray KR, Durham SK, Laskin DL. Role of CCR2 in macrophage migration into the liver during acetaminophen-induced hepatotoxicity in the mouse. Hepatology. 2002 May;35(5):1093-103. doi: 10.1053/jhep.2002.33162. PMID: 11981759.

de la Mata M, Meager A, Rolando N, Daniels HM, Nouri-Aria KT, Goka AK, Eddleston AL, Alexander GJ, Williams R. Tumour necrosis factor production in fulminant hepatic failure: relation to aetiology and superimposed microbial infection. Clin Exp Immunol. 1990 Dec;82(3):479-84. doi: 10.1111/j.1365-2249.1990.tb05475.x. PMID: 2124956; PMCID: PMC1535494.

De Schepper S, Verheijden S, Aguilera-Lizarraga J, Viola MF, Boesmans W, Stakenborg N, Voytyuk I, Schmidt I, Boeckx B, Dierckx de Casterlé I, Baekelandt V, Gonzalez Dominguez E, Mack M, Depoortere I, De Strooper B, Sprangers B, Himmelreich U, Soenen S, Guilliams M, Vanden Berghe P, Jones E, Lambrechts D, Boeckxstaens G. Self-Maintaining Gut Macrophages Are Essential for Intestinal Homeostasis. Cell. 2018 Oct 4;175(2):400-415.e13. doi: 10.1016/j.cell.2018.07.048. Epub 2018 Aug 30. Erratum in: Cell. 2019 Jan 24;176(3):676. PMID: 30173915.

Donnelly MC, Hayes PC, Simpson KJ. Role of inflammation and infection in the pathogenesis of human acute liver failure: Clinical implications for monitoring and therapy. World J Gastroenterol. 2016 Jul 14;22(26):5958-70. doi: 10.3748/wjg.v22.i26.5958. PMID: 27468190; PMCID: PMC4948263.

Dou L, Shi X, He X, Gao Y. Macrophage Phenotype and Function in Liver Disorder. Front Immunol. 2020 Jan 28;10:3112. doi: 10.3389/fimmu.2019.03112. PMID: 32047496; PMCID: PMC6997484.

Duan Y, Wong W, Chua SC, Wee HL, Lim SG, Chua BT, Ho HK. Overexpression of Tyro3 and its implications on hepatocellular carcinoma progression. Int J Oncol. 2016 Jan;48(1):358-66. doi: 10.3892/ijo.2015.3244. Epub 2015 Nov 13. PMID: 26573872.

Fisher JE, McKenzie TJ, Lillegard JB, Yu Y, Juskewitch JE, Nedredal GI, Brunn GJ, Yi ES, Malhi H, Smyrk TC, Nyberg SL. Role of Kupffer cells and toll-like receptor 4 in acetaminophen-induced acute liver failure. J Surg Res. 2013 Mar;180(1):147-55. doi: 10.1016/j.jss.2012.11.051. Epub 2012 Dec 20. PMID: 23260383; PMCID: PMC3578072.

Fontana RJ. Acute liver failure including acetaminophen overdose. Med Clin North Am. 2008 Jul;92(4):761-94, viii. doi: 10.1016/j.mcna.2008.03.005. PMID: 18570942; PMCID: PMC2504411.

Gao S, Silasi-Mansat R, Behar AR, Lupu F, Griffin CT. Excessive Plasmin Compromises Hepatic Sinusoidal Vascular Integrity After Acetaminophen Overdose. Hepatology. 2018 Nov;68(5):1991-2003. doi: 10.1002/hep.30070. Epub 2018 Sep 20. PMID: 29729197; PMCID: PMC6204085.

Graubardt N, Vugman M, Mouhadeb O, Caliari G, Pasmanik-Chor M, Reuveni D, Zigmond E, Brazowski E, David E, Chappell-Maor L, Jung S, Varol C. Ly6Chi Monocytes and Their Macrophage Descendants Regulate Neutrophil Function and Clearance in Acetaminophen-Induced Liver Injury. Front Immunol. 2017 Jun 1;8:626. doi: 10.3389/fimmu.2017.00626. PMID: 28620383; PMCID: PMC5451509.

Ginhoux F, Greter M, Leboeuf M, Nandi S, See P, Gokhan S, Mehler MF, Conway SJ, Ng LG, Stanley ER, Samokhvalov IM, Merad M. Fate mapping analysis reveals that adult microglia derive from primitive macrophages. Science. 2010 Nov 5;330(6005):841-5. doi: 10.1126/science.1194637. Epub 2010 Oct 21. PMID: 20966214; PMCID: PMC3719181.

Girgis NM, Gundra UM, Ward LN, Cabrera M, Frevert U, Loke P. Ly6C(high) monocytes become alternatively activated macrophages in schistosome granulomas with help from CD4+ cells. PLoS Pathog. 2014 Jun 26;10(6):e1004080. doi: 10.1371/journal.ppat.1004080. PMID: 24967715; PMCID: PMC4072804.

Habka D, Mann D, Landes R, Soto-Gutierrez A. Future Economics of Liver Transplantation: A 20-Year Cost Modeling Forecast and the Prospect of Bioengineering Autologous Liver Grafts. PLoS One. 2015 Jul 15;10(7):e0131764. doi: 10.1371/journal.pone.0131764. PMID: 26177505; PMCID: PMC4503760.

Harrison MF. The Misunderstood Coagulopathy of Liver Disease: A Review for the Acute Setting. West J Emerg Med. 2018 Sep;19(5):863-871. doi: 10.5811/westjem.2018.7.37893. Epub 2018 Aug 8. PMID: 30202500; PMCID: PMC6123093.

Hashimoto D, Chow A, Noizat C, Teo P, Beasley MB, Leboeuf M, Becker CD, See P, Price J, Lucas D, Greter M, Mortha A, Boyer SW, Forsberg EC, Tanaka M, van Rooijen N, García-Sastre A, Stanley ER, Ginhoux F, Frenette PS, Merad M. Tissue-resident macrophages self-maintain locally throughout adult life with minimal contribution from circulating monocytes. Immunity. 2013 Apr 18;38(4):792-804. doi: 10.1016/j.immuni.2013.04.004. PMID: 23601688; PMCID: PMC3853406.

Holt MP, Cheng L, Ju C. Identification and characterization of infiltrating macrophages in acetaminophen-induced liver injury. J Leukoc Biol. 2008 Dec;84(6):1410-21. doi: 10.1189/jlb.0308173. Epub 2008 Aug 19. PMID: 18713872; PMCID: PMC2614594.

Hu K, Jin Y, Chroneos Z, Han X, Liu H, Lin L. Macrophage Functions and Regulation: Roles in Diseases and Implications in Therapeutics. J Immunol Res. 2018 Jun 5;2018:7590350. doi: 10.1155/2018/7590350. PMID: 29967802; PMCID: PMC6008777.

Ismail MH, Pinzani M. Reversal of liver fibrosis. Saudi J Gastroenterol. 2009 Jan;15(1):72-9. doi: 10.4103/1319-3767.45072. PMID: 19568569; PMCID: PMC2702953.

Italiani P, Boraschi D. From Monocytes to M1/M2 Macrophages: Phenotypical vs. Functional Differentiation. Front Immunol. 2014 Oct 17;5:514. doi: 10.3389/fimmu.2014.00514. PMID: 25368618; PMCID: PMC4201108.

James LP, Lamps LW, McCullough S, Hinson JA. Interleukin 6 and hepatocyte regeneration in acetaminophen toxicity in the mouse. Biochem Biophys Res Commun. 2003 Oct 3;309(4):857-63. doi: 10.1016/j.bbrc.2003.08.085. PMID: 13679052.

Ju C, Reilly TP, Bourdi M, Radonovich MF, Brady JN, George JW, Pohl LR. Protective role of Kupffer cells in acetaminophen-induced hepatic injury in mice. Chem Res Toxicol. 2002 Dec;15(12):1504-13. doi: 10.1021/tx0255976. PMID: 12482232.

Ju C, Tacke F. Hepatic macrophages in homeostasis and liver diseases: from pathogenesis to novel therapeutic strategies. Cell Mol Immunol. 2016 May;13(3):316-27. doi: 10.1038/cmi.2015.104. Epub 2016 Feb 24. PMID: 26908374; PMCID: PMC4856798.

Krenkel O, Mossanen JC, Tacke F. Immune mechanisms in acetaminophen-induced acute liver failure. Hepatobiliary Surg Nutr. 2014;3(6):331-343. doi:10.3978/j.issn.2304-3881.2014.11.01

Krenkel O, Mossanen JC, Tacke F. Immune mechanisms in acetaminophen-induced acute liver failure. Hepatobiliary Surg Nutr. 2014 Dec;3(6):331-43. doi: 10.3978/j.issn.2304-3881.2014.11.01. PMID: 25568858; PMCID: PMC4273118.

Kurihara T, Warr G, Loy J, Bravo R. Defects in macrophage recruitment and host defense in mice lacking the CCR2 chemokine receptor. J Exp Med. 1997 Nov 17;186(10):1757-62. doi: 10.1084/jem.186.10.1757. PMID: 9362535; PMCID: PMC2199145.

Laskin DL, Gardner CR, Price VF, Jollow DJ. Modulation of macrophage functioning abrogates the acute hepatotoxicity of acetaminophen. Hepatology. 1995 Apr;21(4):1045-50. PMID: 7705777.

Lee WM. Acetaminophen and the U.S. Acute Liver Failure Study Group: lowering the risks of hepatic failure. Hepatology. 2004 Jul;40(1):6-9. doi: 10.1002/hep.20293. PMID: 15239078.

Lee WM. Acetaminophen-related acute liver failure in the United States. Hepatol Res. 2008 Nov;38 Suppl 1:S3-8. doi: 10.1111/j.1872-034X.2008.00419.x. PMID: 19125949.

Lee WM, Stravitz RT, Larson AM. Introduction to the revised American Association for the Study of Liver Diseases Position Paper on acute liver failure 2011. Hepatology. 2012;55(3):965-967. doi:10.1002/hep.25551

Lee WM. Acute liver failure. Semin Respir Crit Care Med. 2012 Feb;33(1):36-45. doi: 10.1055/s-0032-1301733. Epub 2012 Mar 23. PMID: 22447259.

Lee WM. Acetaminophen (APAP) hepatotoxicity-Isn't it time for APAP to go away? J Hepatol. 2017 Dec;67(6):1324-1331. doi: 10.1016/j.jhep.2017.07.005. Epub 2017 Jul 20. PMID: 28734939; PMCID: PMC5696016.

Lemke G, Rothlin CV. Immunobiology of the TAM receptors. Nat Rev Immunol. 2008 May;8(5):327-36. doi: 10.1038/nri2303. PMID: 18421305; PMCID: PMC2856445.

Lemke G. Biology of the TAM receptors. Cold Spring Harb Perspect Biol. 2013 Nov 1;5(11):a009076. doi: 10.1101/cshperspect.a009076. PMID: 24186067; PMCID: PMC3809585.

Lemke G. Phosphatidylserine Is the Signal for TAM Receptors and Their Ligands. Trends Biochem Sci. 2017 Sep;42(9):738-748. doi: 10.1016/j.tibs.2017.06.004. Epub 2017 Jul 19. PMID: 28734578; PMCID: PMC5600686.

Li Q, Barres BA. Microglia and macrophages in brain homeostasis and disease. Nat Rev Immunol. 2018 Apr;18(4):225-242. doi: 10.1038/nri.2017.125. Epub 2017 Nov 20. PMID: 29151590.

Leithead JA, Ferguson JW, Bates CM, Davidson JS, Lee A, Bathgate AJ, Hayes PC, Simpson KJ. The systemic inflammatory response syndrome is predictive of renal dysfunction in patients with non-paracetamol-induced acute liver failure. Gut. 2009 Mar;58(3):443-9. doi: 10.1136/gut.2008.154120. Epub 2008 Nov 10. PMID: 19001057.

McGill MR, Jaeschke H. Metabolism and disposition of acetaminophen: recent advances in relation to hepatotoxicity and diagnosis. Pharm Res. 2013 Sep;30(9):2174-87. doi: 10.1007/s11095-013-1007-6. Epub 2013 Mar 6. PMID: 23462933; PMCID: PMC3709007.

Michael SL, Pumford NR, Mayeux PR, Niesman MR, Hinson JA. Pretreatment of mice with macrophage inactivators decreases acetaminophen hepatotoxicity and the formation of reactive oxygen and nitrogen species. Hepatology. 1999 Jul;30(1):186-95. doi: 10.1002/hep.510300104. PMID: 10385655.

Michna E, Duh MS, Korves C, Dahl JL. Removal of opioid/acetaminophen combination prescription pain medications: assessing the evidence for hepatotoxicity and consequences of removal of these medications. Pain Med. 2010 Mar;11(3):369-78. doi: 10.1111/j.1526-4637.2010.00811.x. PMID: 20447306.

Mitchell RA, Rathi S, Dahiya M, Zhu J, Hussaini T, Yoshida EM. Public awareness of acetaminophen and risks of drug induced liver injury: Results of a large outpatient clinic survey. PLoS One. 2020 Mar 4;15(3):e0229070. doi: 10.1371/journal.pone.0229070. PMID: 32130228; PMCID: PMC7055817.

Myers KV, Amend SR, Pienta KJ. Targeting Tyro3, Axl and MerTK (TAM receptors): implications for macrophages in the tumor microenvironment. Mol Cancer. 2019 May 14;18(1):94. doi: 10.1186/s12943-019-1022-2. PMID: 31088471; PMCID: PMC6515593.

Mukherjee SK, Wilhelm A, Antoniades CG. TAM receptor tyrosine kinase function and the immunopathology of liver disease. Am J Physiol Gastrointest Liver Physiol. 2016 Jun 1;310(11):G899-905. doi: 10.1152/ajpgi.00382.2015. Epub 2016 Feb 11. PMID: 26867565; PMCID: PMC4935487.

Nourjah P, Ahmad SR, Karwoski C, Willy M. Estimates of acetaminophen (Paracetomal)-associated overdoses in the United States. Pharmacoepidemiol Drug Saf. 2006 Jun;15(6):398-405. doi: 10.1002/pds.1191. PMID: 16294364.

O'Grady J. Timing and benefit of liver transplantation in acute liver failure. J Hepatol. 2014 Mar;60(3):663-70. doi: 10.1016/j.jhep.2013.10.024. Epub 2013 Nov 6. PMID: 24211740.

Ostapowicz G, Fontana RJ, Schiødt FV, Larson A, Davern TJ, Han SH, McCashland TM, Shakil AO, Hay JE, Hynan L, Crippin JS, Blei AT, Samuel G, Reisch J, Lee WM; U.S. Acute Liver Failure Study Group. Results of a prospective study of acute liver failure at 17 tertiary care centers in the United States. Ann Intern Med. 2002 Dec 17;137(12):947-54. doi: 10.7326/0003-4819-137-12-200212170-00007. PMID: 12484709.

Patton H, Misel M, Gish RG. Acute liver failure in adults: an evidence-based management protocol for clinicians. Gastroenterol Hepatol (N Y). 2012 Mar;8(3):161-212. PMID: 22675278; PMCID: PMC3365519.

Ramachandran P, Pellicoro A, Vernon MA, Boulter L, Aucott RL, Ali A, Hartland SN, Snowdon VK, Cappon A, Gordon-Walker TT, Williams MJ, Dunbar DR, Manning JR, van Rooijen N, Fallowfield JA, Forbes SJ, Iredale JP. Differential Ly-6C expression identifies the recruited macrophage phenotype, which orchestrates the regression of murine liver fibrosis. Proc Natl Acad Sci U S A. 2012 Nov 13;109(46):E3186-95. doi: 10.1073/pnas.1119964109. Epub 2012 Oct 24. PMID: 23100531; PMCID: PMC3503234.

Roth K, Rockwell CE, Copple BL. Differential Sensitivity of Kupffer Cells and Hepatic Monocyte-Derived Macrophages to Bacterial Lipopolysaccharide. Clin Exp Gastroenterol Hepatol. 2019 Jan-May;1(1):106. doi: 10.31531/edwiser.jcegh.1000106. Epub 2019 Sep 3. PMID: 31555773; PMCID: PMC6759814.

Roth K, Strickland J, Copple BL. Regulation of macrophage activation in the liver after acute injury: Role of the fibrinolytic system. World J Gastroenterol. 2020 Apr 28;26(16):1879-1887. doi: 10.3748/wjg.v26.i16.1879. PMID: 32390699; PMCID: PMC7201151.

Rothlin CV, Ghosh S, Zuniga EI, Oldstone MB, Lemke G. TAM receptors are pleiotropic inhibitors of the innate immune response. Cell. 2007 Dec 14;131(6):1124-36. doi: 10.1016/j.cell.2007.10.034. PMID: 18083102.

Sakai M, Troutman TD, Seidman JS, Ouyang Z, Spann NJ, Abe Y, Ego KM, Bruni CM, Deng Z, Schlachetzki JCM, Nott A, Bennett H, Chang J, Vu BT, Pasillas MP, Link VM, Texari L, Heinz S, Thompson BM, McDonald JG, Geissmann F, Glass CK. Liver-Derived Signals Sequentially Reprogram Myeloid Enhancers to Initiate and Maintain Kupffer Cell Identity. Immunity. 2019 Oct 15;51(4):655-670.e8. doi: 10.1016/j.immuni.2019.09.002. Epub 2019 Oct 3. PMID: 31587991; PMCID: PMC6800814.

Shah NJ, Royer A, John S. Acute Liver Failure. 2020 Nov 20. In: StatPearls [Internet]. Treasure Island (FL): StatPearls Publishing; 2021 Jan–. PMID: 29493996.

Shaw TN, Houston SA, Wemyss K, Bridgeman HM, Barbera TA, Zangerle-Murray T, Strangward P, Ridley AJL, Wang P, Tamoutounour S, Allen JE, Konkel JE, Grainger JR. Tissue-resident macrophages in the intestine are long lived and defined by Tim-4 and CD4 expression. J Exp Med. 2018 Jun 4;215(6):1507-1518. doi: 10.1084/jem.20180019. Epub 2018 May 22. PMID: 29789388; PMCID: PMC5987925.

Stravitz RT, Kramer AH, Davern T, Shaikh AO, Caldwell SH, Mehta RL, Blei AT, Fontana RJ, McGuire BM, Rossaro L, Smith AD, Lee WM; Acute Liver Failure Study Group. Intensive care of patients with acute liver failure: recommendations of the U.S. Acute Liver Failure Study Group. Crit Care Med. 2007 Nov;35(11):2498-508. doi: 10.1097/01.CCM.0000287592.94554.5F. PMID: 17901832.

Sunderkötter C, Nikolic T, Dillon MJ, Van Rooijen N, Stehling M, Drevets DA, Leenen PJ. Subpopulations of mouse blood monocytes differ in maturation stage and inflammatory response. J Immunol. 2004 Apr 1;172(7):4410-7. doi: 10.4049/jimmunol.172.7.4410. PMID: 15034056.

Triantafyllou E, Pop OT, Possamai LA, Wilhelm A, Liaskou E, Singanayagam A, Bernsmeier C, Khamri W, Petts G, Dargue R, Davies SP, Tickle J, Yuksel M, Patel VC, Abeles RD, Stamataki Z, Curbishley SM, Ma Y, Wilson ID, Coen M, Woollard KJ, Quaglia A, Wendon J, Thursz MR, Adams DH, Weston CJ, Antoniades CG. MerTK expressing hepatic macrophages promote the resolution of inflammation in acute liver failure. Gut. 2018 Feb;67(2):333-347. doi: 10.1136/gutjnl-2016-313615. Epub 2017 Apr 27. PMID: 28450389; PMCID: PMC5868289.

van der Heide D, Weiskirchen R, Bansal R. Therapeutic Targeting of Hepatic Macrophages for the Treatment of Liver Diseases. Front Immunol. 2019 Dec 3;10:2852. doi: 10.3389/fimmu.2019.02852. PMID: 31849997; PMCID: PMC6901832.

van der Meer JH, van der Poll T, van 't Veer C. TAM receptors, Gas6, and protein S: roles in inflammation and hemostasis. Blood. 2014 Apr 17;123(16):2460-9. doi: 10.1182/blood-2013-09-528752. Epub 2014 Mar 4. PMID: 24596417.

Watanabe S, Alexander M, Misharin AV, Budinger GRS. The role of macrophages in the resolution of inflammation. J Clin Invest. 2019 May 20;129(7):2619-2628. doi: 10.1172/JCI124615. PMID: 31107246; PMCID: PMC6597225.

Wigmore SJ, Walsh TS, Lee A, Ross JA. Pro-inflammatory cytokine release and mediation of the acute phase protein response in fulminant hepatic failure. Intensive Care Med. 1998 Mar;24(3):224-9. doi: 10.1007/s001340050554. PMID: 9565803.

Wolf MS, King J, Jacobson K, Di Francesco L, Bailey SC, Mullen R, McCarthy D, Serper M, Davis TC, Parker RM. Risk of unintentional overdose with non-prescription acetaminophen products. J Gen Intern Med. 2012 Dec;27(12):1587-93. doi: 10.1007/s11606-012-2096-3. Epub 2012 May 26. PMID: 22638604; PMCID: PMC3509295

Wolk K, Döcke WD, von Baehr V, Volk HD, Sabat R. Impaired antigen presentation by human monocytes during endotoxin tolerance. Blood. 2000 Jul 1;96(1):218-23. PMID: 10891454.

Wolk K, Döcke W, von Baehr V, Volk H, Sabat R. Comparison of monocyte functions after LPS- or IL-10-induced reorientation: importance in clinical immunoparalysis. Pathobiology. 1999;67(5-6):253-6. doi: 10.1159/000028104. PMID: 10725796.

Wong RJ, Aguilar M, Cheung R, Perumpail RB, Harrison SA, Younossi ZM, Ahmed A. Nonalcoholic steatohepatitis is the second leading etiology of liver disease among adults awaiting liver transplantation in the United States. Gastroenterology. 2015 Mar;148(3):547-55. doi: 10.1053/j.gastro.2014.11.039. Epub 2014 Nov 25. PMID: 25461851.

Yona S, Kim KW, Wolf Y, Mildner A, Varol D, Breker M, Strauss-Ayali D, Viukov S, Guilliams M, Misharin A, Hume DA, Perlman H, Malissen B, Zelzer E, Jung S. Fate mapping reveals origins and dynamics of monocytes and tissue macrophages under homeostasis. Immunity. 2013 Jan 24;38(1):79-91. doi: 10.1016/j.immuni.2012.12.001. Epub 2012 Dec 27. Erratum in: Immunity. 2013 May 23;38(5):1073-9. PMID: 23273845; PMCID: PMC3908543.

Yoon E, Babar A, Choudhary M, Kutner M, Pyrsopoulos N. Acetaminophen-Induced Hepatotoxicity: a Comprehensive Update. J Clin Transl Hepatol. 2016 Jun 28;4(2):131-42. doi: 10.14218/JCTH.2015.00052. Epub 2016 Jun 15. PMID: 27350943; PMCID: PMC4913076.

Zagórska A, Través PG, Jiménez-García L, Strickland JD, Oh J, Tapia FJ, Mayoral R, Burrola P, Copple BL, Lemke G. Differential regulation of hepatic physiology and injury by the TAM receptors Axl and Mer. Life Sci Alliance. 2020 Jun 22;3(8):e202000694. doi: 10.26508/lsa.202000694. PMID: 32571802; PMCID: PMC7335405.
Zigmond E, Samia-Grinberg S, Pasmanik-Chor M, Brazowski E, Shibolet O, Halpern Z, Varol C. Infiltrating monocyte-derived macrophages and resident kupffer cells display different ontogeny and functions in acute liver injury. J Immunol. 2014 Jul 1;193(1):344-53. doi: 10.4049/jimmunol.1400574. Epub 2014 Jun 2. PMID: 24890723.

CHAPTER 2

EXAGGERATED INTERLEUKIN-6 LEVELS IN ACETAMINOPHEN-INDUCED ACUTE LIVER FAILURE REDUCES CEREBRAL BLOOD FLOW AND TRIGGERS COMPENSATORY ANTI-INFLAMMATORY RESPONSE SYNDROME THAT INHIBITS MACROPHAGE-DEPENDENT LIVER REPAIR

2.1 Abstract

In severe cases of acetaminophen (APAP) overdose, acute liver injury rapidly progresses to acute liver failure (ALF), producing life threatening complications including, hepatic encephalopathy and multi-organ failure. Systemic levels of the proinflammatory cytokine interleukin-6 (IL-6) and the anti-inflammatory cytokine interleukin-10 (IL-10) are highest in ALF patients with the poorest prognosis. However, the mechanistic basis for dysregulation of IL-6 and IL-10, and their association with outcome in ALF remains poorly defined. Standard experimental settings of APAP hepatotoxicity in mice (i.e., 300 mg/kg) do not recapitulate key features of ALF in critically ill patients, including impaired hepatocyte proliferation, kidney injury, evidence of hepatic encephalopathy (HE), and cytokine dysregulation. Thus, to investigate this in true ALF, we used a robust experimental setting of failed liver repair after APAP overdose in which a high dose of APAP is administered (i.e., 500-600 mg/kg to wild-type mice). High levels of several proinflammatory cytokines, including IL-6, were present in the serum of mice treated with 600 mg/kg at 72 hours, resembling SIRS. Strikingly, neutralization of IL-6 in this setting restored cerebral blood flow in ALF mice, indicating elevated levels of IL-6 may contribute to the development of this complication in ALF. High levels of IL-10 and PD-L1, a feature of CARS in ALF patients, occurred coincident with high levels of proinflammatory cytokines in ALF mice, recapitulating a paradoxical feature of ALF in patients. Furthermore, our studies indicate that Kupffer cells (KCs) may be the primary source of both IL-6 and IL-10 in APAP-induced ALF. Intriguingly, KCs isolated from mice treated with 600 mg/kg APAP expressed several markers of myeloid-derived suppressor cells, including high-level expression of IL-10, PD-L1, CD11b, Axl and Cx3cr1. Our studies further indicate that high levels of IL-10 negatively impact the ability of MDMs to migrate into injured regions of liver where they phagocytose dead cell debris. Remarkably, in mice treated with 600 mg/kg APAP, neutralization of IL-10 completely restored macrophage trafficking into the necrotic foci resulting in a decrease in dead cells. Collectively,

these studies document a mechanistic basis for the link between high levels of IL-6 and IL-10 poor outcome in patients with ALF.

2.2 Introduction

Acetaminophen (APAP) overdose remains the number one cause of acute liver failure (ALF) in the United States (Stravitz and Lee, 2019). In severe cases, acute liver injury rapidly progresses to acute liver failure (ALF), producing life threatening cardiac instability, hepatic encephalopathy, and multi-organ failure (Lee et al., 2008) (Bernal and Wendon, 2013). First line therapy for APAP overdose is N-acetyl cysteine (NAC), which is most efficacious when administered during the active phase of injury (Smilkstein et al., 1988) (Saito et al., 2010). Because of this, the efficacy of NAC quickly declines for patients that seek medical attention beyond 8 hours. For this group of patients, supportive medical care and liver transplantation are the only remaining therapeutic options (Rolando et al., 2000) (Butterworth, 2015). Unfortunately, despite significant improvements in clinical care and emergency liver transplantation, mortality associated with ALF remains high, underscoring the importance of developing new therapeutic approaches (Bernal and Wendon, 2013).

ALF patients with the poorest prognosis develop systemic inflammatory response syndrome (SIRS), a condition characterized by high systemic levels of proinflammatory cytokines, including tumor necrosis factor-α (TNF-α), Ccl2 and interleukin-6 (IL-6) (Rolando et al., 2000). High levels of these cytokines, in particular IL-6, are associated with a worsening of hepatic encephalopathy, development of multiorgan dysfunction syndrome (MODS) and death (Antoniades et al., 2008) (Butterworth, 2015). To counter the severe systemic inflammation produced by SIRS, immune cells in these patients begin to express immunoregulatory ligands (e.g., PD-L1) and anti-inflammatory cytokines (e.g., IL-10) that produce severe immune suppression (Antoniades et al., 2008). This condition, referred to as compensatory anti-inflammatory response syndrome (CARS), increases the risk of developing life-threatening infections and may disrupt key pro-repair activities of immune cells, including monocytes and macrophages, thereby preventing recovery from liver injury. In fact, studies have documented a clear association between components of CARS (i.e., high systemic levels of IL-10 and PD-L1)

and increased mortality in ALF patients (Berry et al., 2010). While it is well established that SIRS and CARS, and their associated cytokines, are increased in ALF patients, the mechanisms triggering these conditions leading to cytokine dysregulation remain largely unknown.

In mouse models of APAP overdose, high systemic levels of key cytokines associated with SIRS and CARS (i.e., IL-6 and IL-10) have been reported. In stark contrast to ALF patients, however, increased expression of these cytokines in APAP-treated mice is associated with protection from liver injury and reduced mortality. For example, compared to wild-type mice, IL-10 knockout mice treated with hepatotoxic doses of APAP ranging from 150 to 300 mg/kg develop greater liver injury and have reduced survival (Bourdi et al., 2002). Similarly, liver injury is increased and hepatocyte proliferation is reduced in IL-6 knockout mice treated with 300 mg/kg APAP. Considering the contrasting findings reported in mice and ALF patients suggests that either the mouse is not a suitable model organism to investigate APAP-induced ALF or that the experimental paradigm used in mice does not accurately reflect the pathogenesis of ALF, and its associated complications, in patients. Several studies indicate that the latter is the most likely explanation.

By using a comparative dosing strategy, Bhushan and colleagues demonstrated that liver repair fails to occur in mice treated with a high dose of APAP (i.e., 600 mg/kg) mirroring findings reported in APAP-induced ALF patients with the poorest outcome. Failed liver repair in these mice was associated with increased mortality and occurred despite plasma levels of IL-6 that were markedly higher than those in mice treated with a nonlethal dose of APAP (i.e., 300 mg/kg). Further, myeloid cell-dependent clearance of necrotic cells from the injured liver also failed to occur suggesting a functional impairment of myeloid cell populations. Remarkably, despite the striking differences in liver repair, the severity of liver injury was not different between mice treated with 300 mg/kg or 600 mg/kg APAP, mirroring the lack of association between the severity of liver injury and outcome in ALF patients. Collectively, the high levels of

IL-6 coupled with impaired myeloid cell activity and high mortality suggest that SIRS and CARS may develop in mice treated with 600 mg/kg APAP. Based upon these findings, we used a similar comparative dosing strategy to determine whether SIRS and CARS develop in mice treated with a high dose of APAP, thereby recapitulating the pathogenesis of ALF occurring in the most critically ill patients.

2.3 Materials and Methods

2.3.1 Animal Treatments 6-12-week-old male C57BL/6J mice and IL-10 reporter mice ($IL10^{tm1.1Karp}$) (Jackson Laboratories) were used for all studies. Mice were housed in a 12-hour light/dark cycle under controlled temperature (18-21°C) and humidity. Food (Rodent Chow; Harlan-Teklad) and tap water were allowed *ad libitum*.

Mice were fasted for approximately 16 hours prior to administration of 300 mg/kg APAP (Sigma-Aldrich) or sterile saline by intraperitoneal injection. For treatment with 600 mg/kg APAP, mice were fasted for approximately 12 hours prior to APAP injection, as described previously (Bhushan et al., 2014). In all studies, rodent chow was returned immediately after APAP challenge

For IL-10 neutralization studies, mice were injected with 0.5 mg *InVivo*MAb anti-mouse IL-10 antibody (Bio X Cell, clone JES5-2A5) or 0.5 mg isotype control antibody (Innovative Research, Rat IgG) at 24 hours after APAP treatment. Liver and blood were collected at 72 hours after APAP treatment. For recombinant IL-10 studies, mice were injected with 5 μg recombinant mouse IL-10 (Biolegend, San Diego, CA) or sterile saline 24 hours after APAP challenge. Liver and blood were collected at 48 hours after APAP challenge. For IL-6 neutralization studies, mice were injected with 200 μg *InVivo*MAb anti-mouse IL-6 antibody (Bio X Cell, clone MP5-20F3) or *InVivo*MAb rat IgG1 isotype control (Bio X Cell, clone HRPN) at 2 hours after APAP treatment. Liver and blood were collected and cerebral blood flow was measured 24 hours later. All studies were approved by the Michigan State University Institutional Animal Care and Use Committee.

2.3.2 Sample Collection. Mice were anesthetized using Fatal-Plus Solution (Vortech Pharmaceuticals) or isoflurane. Blood was collected from the inferior vena cava and the livers were removed. A portion of each liver was fixed in 10% neutral-buffered formalin. The livers were embedded in paraffin, sectioned, and stained with hematoxylin and eosin. The area of necrosis was quantified as described by us previously (Mochizuki et al., 2014). Additional

portions of the liver were homogenized in TRIzol Reagent (Thermo-Fisher Scientific) for RNA isolation or were snap-frozen in liquid nitrogen for sectioning and immunofluorescence staining.

2.3.3 Immunostaining. Immunofluorescence was used to detect F4/80 and CD68 as described previously (Mochizuki et al., 2014). Briefly, 8 μm sections were cut from frozen livers and fixed for 10 minutes in 4% formalin. The sections were then incubated in blocking buffer (10% goat serum) followed by incubation with either rat anti-F4/80 antibody (Bio-Rad) diluted 1:500 or rat anti-CD68 antibody (Bio-Rad) diluted 1:500. After washing, the sections were incubated with goat anti-rat secondary antibody conjugated to Alexa Fluor 594 (diluted 1:500, Thermo Fisher Scientific). Proliferating cell nuclear antigen (PCNA) was detected as described previously (Mochizuki et al., 2014).

Brains were removed and fixed in 4% paraformaldehyde for 48 hours, then washed and stored in 20% sucrose-PBS until sectioning. 40μm thick cryosections of the cortex were obtained. To quantify the microglia, free-floating brain sections were blocked and permeabilized in 0.1% Triton-X with 10% donkey serum PBS, then incubated in 1:200 rabbit Anti-IBA1 (catalog number 019-19741, Wako, Richmond, VA) overnight at 4°C. After washing in 1X PBS, sections were incubated in secondary AlexaFluor 488 donkey anti-rabbit antibody (catalog number ab150073, Abcam, Cambrige, UK) for one hour. Sections were then washed 4x in 1x PBS (10 min per wash) and coverslips were mounted using Prolong antifade reagent (Invitrogen, Carlsbad, CA).

2.3.4 Luminex Immunoassay. Cytokine levels were measured in blood serum samples by using the Bio-Plex Pro assay kit (Bio-Rad) according to manufacturer's instructions. Bead fluorescent readings were obtained using a Luminex 200 system.

2.3.5 Flow Cytometry. To isolate non-parenchymal cells, mouse livers were perfused and digested with collagenase (Collagenase H, Sigma Chemical Company) as described previously (Allen et al., 2011). Hepatocytes were removed by centrifugation and non-parenchymal cells were collected after centrifugation at 300 *g* for 10 minutes. Non-parenchymal

cells were washed and resuspended in FACs buffer (phosphate-buffered saline, 1% fetal bovine serum). The cells were then incubated with Fc blocking buffer (BD Biosciences; diluted 1:20) for 10 minutes at 4 °C, rinsed, and then pelleted by centrifugation at 300 *g* for 5 minutes. The cells were incubated with anti-F4/80 conjugated to Alexa-488 and anti-Ly6C conjugated to phycoerythrin (PE) for 30 minutes at 4°C. All antibodies were purchased from Biolegend. For studies with IL-10 GFP reporter mice, the following antibodies were used for flow cytometry: anti-Axl (PE), anti-CD45.1 (PE/Cy7), anti-F4/80 (AF594), anti-Cx3cr1 (AF700), anti-Ly6C (APC/Cy7), anti-Cd11b (BV605), anti-Marco (APC), anti-Ccr2 (BV650), anti-PD-L1 (PerCp/Cy5.5). All antibodies were purchased from Biolegend, except anti-Marco and anti-Axl, which were purchased from Invitrogen. The fixable dye, Zombie Aqua, was used to determine cell viability. Following incubation, cells were washed twice and fixed in formalin (Sigma) for 15 minutes at 4°C. The fixed cells were washed twice and resuspended in FACs buffer. An Attune NxT flow cytometer (Life Technologies) was used to measure fluorescence and signal was quantified using Attune NxT software. The gating strategy for flow cytometry is shown in Figure 2.2.

2.3.6 Real-Time PCR. RNA was isolated from liver samples using TRIzol Reagent (Thermo-Fisher Scientific) or from cell culture samples by using the E.Z.N.A Total RNA Kit I (Omega Bio-Tek) according to manufacturer's instructions. Real-time PCR was performed as described by us previously (Kim, 2006). The following primer sequences were used: Tnf-α: Forward- 5'-AGGGTCTGGGCCATAGAACT-3', Reverse- 5'-CCACCACGCTCTTCTGTCTAC-3'; Ccl2: Forward- 5'-CCTGCTGTTCACAGTTGCC-3', Reverse- 5'-ATTGGGATCATCTTGCTGGT-3'; Il-10: Forward- 5'-TGTCAAATTCATTCATGGCCT-3', Reverse- 5'-ATCGATTTCTCCCCTGTGAA-3': Rpl13a: Forward- 5'-GACCTCCTCCTTTCCCAGGC-3', Reverse- 5'-AAGTACCTGCTTGGCCACAA-3'; PD-L1: Forward-5'-CACGCTGAAAGTCAATGCCC-3',

Reverse-5'-AAACATCATTCGCTGTGGCG-3'; IL-6: Forward-5'-CCCAGTGCAAGAATCCTCGT-3', Reverse-5'-GTCATAAGGGCTCTGTGCGT-3'.

2.3.7 Laser Speckle Contrast Imaging. Mice were anaesthetized with 3.5% isoflurane in oxygen. The scalp was removed and the skull was cleared of connective tissue. A thin coat of clear shiny nail polish followed by a thin coat of matte nail polish was used to reduce glare. After reducing the isoflurane to 1.5% for three minutes, the cerebral perfusion was measured over a minute using a Perimed PeriCam PSI Zoom System and PIMSoft software (Perimed Inc, Las Vegas, NV). Regions of interest (ROI) were drawn after locating the midpoint of the sagittal suture between bregma and sigma as described by Polycarpou et. al (2016). The mean perfusion of each ROI was recorded. The average between left and right frontal, parietal and occipital lobe perfusion was calculated. Total cerebral perfusion was defined as the average of frontal, parietal, occipital and pial anastomoses regions combined.

2.3.8 ALT Assay. ALT (TR71121) assay was from Thermo Fisher Scientific and was performed according to the manufacturer's instruction.

2.3.9 Statistical Analysis. Results are presented as the mean + SEM. Data were analyzed by a one-way or two-way Analysis of Variance (ANOVA) where appropriate. Data expressed as a percentage were transformed by arcsine square root prior to analysis. Comparisons among group means were made using the Student-Newman-Keuls test. The criterion for significance was $p < 0.05$ for all studies.

2.4 Results

2.4.1 APAP-Induced ALF is Coupled to Failed Clearance of Necrotic Cell Debris from the Injured Liver. In mice challenged with 300 mg/kg APAP, liver necrosis peaked at approximately 24 hours after treatment (Figure 2.1A and 2.1B). By 48 hours, extensive inflammatory infiltrates were noted within the necrotic lesions (Figure 2.1C). The inflammatory cells, along with the necrotic cell debris, were largely cleared from the liver by 72 hours (Figure 2.1C). In agreement with prior studies by Bhushan and colleagues (Bhushan et al., 2014), administration of 600 mg/kg APAP produced a comparable initial hepatotoxic response (Figs. 2.1A and 2.1B). At this larger dose of APAP, however, necrotic cells persisted at 72 hours suggesting a failure of monocyte-derived macrophages (MDM) to clear dead cell debris (Figure 2.1B). Consistent with this finding, the necrotic lesions in these mice were largely devoid of inflammatory cells, suggesting a potential defect in monocyte recruitment (Figure 2.1D).

2.4.2 Failed Trafficking of MDMS into Necrotic Lesions in Mice with ALF. Because myeloid cells are largely responsible for clearing dead cell debris, we quantified these cells by flow cytometry. Gating for flow cytometry is shown in Figure 2.2. As shown in Figures 2.3A and 2.3B, the numbers of Ly6G+ cells (i.e., neutrophils) in the liver were unaffected by APAP dose. By contrast, the numbers of Ly6C+ cells (i.e., recruited MDMs) were substantially lower in mice treated with 600 mg/kg APAP, whereas, the numbers of F4/80+ cells (i.e., Kupffer cells) were greater (Figure 2.3A and 2.3B).

Next, we quantified $CD68^+$ macrophages in the liver by immunofluorescence labeling. Prior studies revealed that $CD68^+$ macrophages accumulate in the livers of patients with APAP-induced ALF, and our prior studies indicate that these cells are the same as Ly6C+ MDMs (Antoniades et al., 2012) (Mossanen et al., 2016). In mice treated with 300 mg/kg APAP, $CD68^+$ macrophages began to accumulate in the liver and traffic into the necrotic lesions by 24 hours (Figure 2.3C and 2.3D, necrotic lesions demarcated by white dotted lines). By 48 hours, the necrotic lesions were filled with $CD68^+$ macrophages (Figure 2.3C). Interestingly, while $CD68^+$

macrophages accumulated in the livers of mice treated with 600 mg/kg APAP, there was no trafficking into the necrotic lesions at any time point examined (Figure 2.3C). We recently showed that in mice treated with 300 mg/kg APAP that macrophages within the necrotic lesions begin to express the mature tissue macrophage marker, F4/80, coincident with clearance of necrotic cells (Roth et al., 2019). In mice treated with 300 mg/kg APAP, F4/80$^+$ macrophages were largely present outside of the necrotic lesions at 24 and 48 hours after treatment (Figure 2.4A). By 72 hours, however, F4/80$^+$ macrophages filled the necrotic lesions (Figure 2.4A), in agreement with our prior studies (Roth et al., 2019). By contrast, F4/80$^+$ macrophages were rarely observed in the lesions of mice treated with 600 mg/kg APAP (Figure 2.4A).

Prior lineage tracing studies showed that Ly6C$^+$ proinflammatory macrophages, which also express CD68, accumulate in the liver after APAP overdose and begin to express F4/80 as necrotic cells are cleared from the liver (Zigmond et al., 2014). This was associated with a shift in macrophage phenotype from proinflammatory to pro-repair typified by increased F4/80 expression and reduced Ly6C expression (Zigmond et al., 2014). As shown in Figure 2.4B, macrophages in the livers of vehicle-treated mice were largely F4/80$^+$ Ly6C$^-$ (red square). By 24 hours after treatment with 300 mg/kg APAP, however, a population of Ly6C$^+$ F4/80$^-$ macrophages appeared in the liver (Figure 2.4C, green circle). By 72 hours, this population of macrophages was reduced, indicating a transition to Ly6C$^-$ F4/80$^+$ macrophages (Figure 2.4D) in agreement with prior studies (Zigmond et al., 2014). Ly6C$^+$ F4/80$^-$ macrophages also appeared in the liver 24 hours after treatment with 600 mg/kg APAP (Figure 2.4E, green circle). Interestingly, however, this population persisted 72 hours after treatment with 600 mg/kg APAP (Figure 2.4F, green circle). Quantification revealed a similar percentage of Ly6C$^+$ macrophages in the liver at 24 hours after treatment (Figure 2.4G). By 72 hours, however, this population of macrophages was decreased in mice treated with 300 mg/kg APAP, whereas, this population of macrophages continued to increase in mice treated with 600 mg/kg APAP (Figure 2.4G).

Collectively, these results suggest that Ly6C$^+$ proinflammatory macrophages fail to shift phenotype in mice treated with 600 mg/kg APAP.

2.4.3 Sustained Cytokine Production in Mice with APAP-Induced ALF. The transition of macrophages from a proinflammatory to a pro-reparative phenotype in the APAP-injured liver is associated with a decrease in proinflammatory cytokine expression (Zigmond et al., 2014) (Roth et al., 2019). Consistent with this, in mice treated with 300 mg/kg APAP, hepatic mRNA levels of the proinflammatory cytokines, Ccl2 and tumor necrosis factor-α (Tnf-α), peaked at 24 hours and returned to baseline by 72 hours (Figure 2.5A and 2.5B). By contrast, in mice treated with 600 mg/kg APAP, mRNA levels of these cytokines were increased by 24 hours and remained elevated at 72 hours (Figure 2.5A and 2.5B). In addition, compared to mice treated with 300 mg/kg APAP, serum levels of CCL2, TNF-α, interleukin-1β (IL-1β), interferon-γ (IFN-γ), and IL-4 protein were greater in mice treated with 600 mg/kg APAP at 72 hours similar to what has been reported in ALF patients with SIRS (Figure 2.5C-2.5G).

In ALF patients with SIRS that progresses to CARS, high systemic levels of proinflammatory cytokines frequently co-exist with high levels of anti-inflammatory cytokines, such as IL-10 (Berry et al., 2010). Similar to these clinical findings, hepatic mRNA levels of IL-10 were rapidly increased in mice treated with 600 mg/kg APAP and remained elevated at 72 hours (Figure 2.6A). Importantly, elevated mRNA levels were matched by increased IL-10 protein in serum (Figure 2.6A and 2.6B). By contrast, in mice treated with 300 mg/kg APAP, IL-10 mRNA levels did not increase until 72 hours after treatment (Figure 2.6A and 2.6B). Analysis of purified populations of F4/80$^+$ and Ly6C$^+$ (i.e., MDMs) macrophages revealed elevated expression of IL-10 mRNA in F4/80$^+$ cells but not Ly6C$^+$ cells in mice treated with 600 mg/kg APAP (Fig 2.6C). Consistent with these findings, greater numbers of GFP-expressing F4/80$^+$ cells were detected in the livers of IL-10 reporter mice treated with 600 mg/kg APAP (Figure 2.6D and 2.6E). Collectively, these findings demonstrate the presence of both pro- and anti-

inflammatory cytokines in mice treated with 600 mg/kg APAP similar to observations in ALF patients with SIRS and CARS.

2.4.4 Immunophenotyping of IL-10$^+$ F4/80$^+$ Cells Reveals A Myeloid-Derived Suppressor Cell-Like Phenotype. IL-10 GFP reporter mice were treated with 600 mg/kg APAP for 24 hours. Flow cytometry was used to detect IL-10-expressing F4/80$^+$ cells in the liver (Figure 2.7A). Immunophenotyping of these cells revealed that they expressed CD11b, PD-L1, Cx3Cr1 and Axl consistent with a myeloid-derived suppressor cell-like phenotype (Figure 2.7B and 2.7C). These cells did not express MARCO, Ly6C, Ccr2 or Ly6G, however (Figure 2.7B and 2.7C).

2.4.5 IL-10 Prevents Trafficking of Macrophages into Necrotic Lesions In Mice With APAP-Induced ALF. The mechanistic basis for a worse outcome in ALF patients with high systemic levels of IL-10 is not fully understood. Our earlier findings demonstrated that monocyte recruitment and trafficking were disrupted in the livers of mice treated with 600 mg/kg APAP, resulting in a failure to clear dead cell debris (Figure 2.1-2.3). Because of the potent immune inhibitory properties of IL-10, we tested the hypothesis that IL-10 contributes to this defect. To examine this, we used both loss and gain of function approaches. In mice treated with 600 mg/kg APAP, injection of IL-10 neutralizing antibody, 24 hours after APAP, increased inflammatory cell infiltration into necrotic foci by 72 hours (Figure 2.8A-B). By contrast, in mice treated with 300 mg/kg APAP, pharmacological elevation of IL-10 twenty-four hours after APAP, decreased inflammatory cell infiltration into necrotic lesions (Figure 2.8C-D).

In further confirmation of these findings, CD68$^+$ macrophages accumulated at the periphery of necrotic lesions in mice treated with 600 mg/kg APAP and isotype control antibody (Figure 2.8E, necrotic lesions demarcated by a dotted white line). By contrast, neutralization of IL-10 markedly increased the number of CD68$^+$ cells within the necrotic foci (Figure 2.8F). Pharmacological elevation of IL-10 in 300 mg/kg APAP mice prevented accumulation of CD68+ cells within the necrotic lesions (Figure 2.8H-I). Remarkably, the pattern of CD68+ cells in

these mice was strikingly similar to that observed in mice treated with 600 mg/kg APAP. Importantly, restoration of MDM trafficking in 600 mg/kg APAP treated with IL-10 neutralizing antibody was associated with a reduction in the area of necrosis by 72 hours (Figure 2.8G), whereas impairment of MDM trafficking in 300 mg/kg mice increased the area of necrosis (Figure 2.8J). Surprisingly, despite the effect on MDM recruitment and trafficking, modulation of IL-10 levels in mice treated with either 300 mg/kg APAP or 600 mg/kg APAP had minimal impact on the expression of proinflammatory cytokines (Figure 2.9).

Bhushan and colleagues demonstrated that hepatocytes fail to proliferate in mice treated with 600 mg/kg APAP (Bhushan et al., 2014). To determine whether IL-10 is causally involved in this defect, we quantified PCNA positive hepatocytes. As shown in Figure 2.9, modulation of IL-10 levels had no impact on hepatocyte PCNA staining.

2.4.6 Neutralization of IL-6 Decreased Expression of IL-10 in Mice With APAP-Induced ALF. Immunophenotyping of F4/80+ IL-10+ cells indicated a MDSC-like phenotype (Figure 2.7). Studies have identified IL-6 as an important stimulus of MDSC formation in the tumor microenvironment (Yaseen et al., 2020). Therefore, we next determined whether IL-6 levels are increased in mice treated with 600 mg/kg APAP, and determined whether this is important for generation of F4/80+ IL-10+ cells. Hepatic IL-6 mRNA levels were increased to a greater extent in mice treated with 600 mg/kg APAP when compared to mice treated with 300 mg/kg APAP at all time-points (Figure 2.10A). The increase in IL-6 mRNA was matched by increased IL-6 protein in serum. IL-6 mRNA levels were greater in F4/80+ macrophages purified from the livers of mice treated with 600 mg/kg APAP, whereas IL-6 mRNA levels were not different in purified Ly6C+ cells (Figure 2.10C). Next, mice were treated with IL-6 neutralizing antibody to determine whether IL-6 contributed to the early induction of IL-10. As shown in Figure 2.10, neutralization of IL-6 partially reduced IL-10 mRNA levels by approximately 70% (Figure 2.10D). Further, neutralization IL-6 reduced PD-L1 mRNA levels by greater than 90% (Figure 2.10E). Previous studies demonstrated that liver injury is increased IL-

6 knockout mice treated with 300 mg/kg APAP (Gao et al., 2020). In mice treated with 600 mg/kg APAP, however, neutralization of IL-6 beginning at 2 hours after APAP had no impact on liver injury (Figure 2.10F). While conducting these studies, we noticed a striking difference in the behavior of the mice. Mice treated with 600 mg/kg APAP and control IgG experienced general paresis with significant gait abnormalities and demonstrated an apparent loss of balance when prompted to move. Surprisingly, 600 mg/kg APAP mice co-treated with IL-6 neutralizing antibody were more active and alert; were more responsive to stimuli; and did not display gait abnormalities when moving. Consistent with these behavioral observations, mortality was reduced in mice treated with IL-6 antibody (Figure 2.10G).

Rao and colleagues previously reported that mice treated with 500 mg/kg APAP displayed symptoms of hepatic encephalopathy, including lethargy and difficulty in retaining a normal gait, similar to what we observed in mice treated with 600 mg/kg APAP above. They also showed that ammonia, a proposed causative factor of hepatic encephalopathy, was increased in the serum, and brain water content, indicative of brain edema, was increased in these mice. Because IL-6 neutralization appeared to reduce symptoms of hepatic encephalopathy in our study, we examined whether IL-6 neutralization impacted cerebral blood flow in these mice. Prior studies reported that cerebral blood flow is reduced at early stages of hepatic encephalopathy in ALF patients. For this study, we used 500 mg/kg APAP because Rao and colleagues had already measured several end-points related to hepatic encephalopathy in mice treated with this dose of APAP. Similar to mice treated with 600 mg/kg APAP, neutralization of IL-6 improved survival without affecting liver injury or hepatocyte proliferation in mice treated with 500 mg/kg APAP (Figure 2.11). In mice treated with 300 mg/kg APAP, cerebral blood flow was not significantly impacted (Figure 2.12). Consistent with findings of hepatic encephalopathy, however, total frontal blood flow was reduced in mice treated with 600 mg/kg APAP and control IgG (Figure 2.12). Remarkably, neutralization of IL-6 fully restored

cerebral blood flow in mice treated with 600 mg/kg APAP, consistent with the marked differences in behavior in these mice (Figure 2.12).

2.5 Discussion

High systemic levels of IL-6 and IL-10 are frequently observed in ALF patients (Antoniades et al., 2006; Antoniades et al., 2008; Berry et al., 2010). Further, a strong association has been noted between high levels of these cytokines and risk of multi-organ failure and death in these patients (Berry et al., 2010). While this has long been recognized in clinical settings, the mechanistic basis for dysregulation of IL-6 and IL-10 and their association with outcome in ALF remains poorly defined. We propose that standard experimental settings of APAP hepatotoxicity in mice (i.e., doses at or near 300 mg/kg) produce liver injury that is predictably repaired thereby restoring hepatic function and triggering normalization of cytokine levels, including IL-6 and IL-10. While these studies provide important insight into the mechanisms controlling cytokine synthesis and release during normal liver repair, they do not provide insight into the cause of IL-6 and IL-10 dysregulation in ALF. To investigate this in true ALF, we used a robust experimental setting of failed liver repair after APAP overdose in which high dose of APAP is administered (i.e., 500-600 mg/kg to wild-type mice). This experimental approach, characterized in detail by Bhushan and colleagues, recapitulates many of the key features of ALF in critically ill patients, including impaired hepatocyte proliferation, kidney injury, and evidence of hepatic encephalopathy (Bhushan et al., 2014) (Rama Rao et al., 2014) (Akakpo et al., 2020). By using this approach, our studies reveal that cytokine dysregulation is a key feature of APAP-induced ALF in mice, recapitulating findings in ALF patients. In support of this, high levels of several proinflammatory cytokines, resembling SIRS, were present in the serum of mice treated with 600 mg/kg at a time (i.e., 72 hours) where these cytokines were markedly lower in mice receiving 300 mg/kg APAP (Figure 2.5). Further, high levels of IL-10 and PD-L1, a feature of CARS in ALF patients, also occurred coincident with high levels of proinflammatory cytokines, recapitulating a paradoxical feature of ALF in patients (Figure 2.6 and 2.7) (Antoniades et al., 2008; Berry et al., 2010). Thus, this pragmatic experimental approach elegantly replicates cytokine dysregulation that occurs in ALF patients.

Clinical studies have demonstrated a clear association between high systemic levels of IL-6 and severity of hepatic encephalopathy in ALF patients (Antoniades et al., 2008) (Butterworth, 2015). Our studies provide mechanistic support for this association by demonstrating that neutralization of IL-6 restores cerebral blood flow in mice with ALF (Figure 2.12). Several clinical studies have reported reductions in cerebral blood flow in ALF patients with hepatic encephalopathy; however, the importance of this to the pathogenesis of this disorder remains to be defined (Wendon et al., 1994) (Bjerring et al., 2018). Our studies have identified an experimental setting that could be used to mechanistically interrogate this phenomenon in mice. Importantly, cerebral blood flow was not impacted in mice treated with 300 mg/kg APAP providing further evidence that this dosing regimen does not recapitulate features of severe ALF occurring in patients.

Our studies indicate further that Kupffer cells, the resident macrophages of the liver, may be the primary source of IL-6 and IL-10 in APAP-induced ALF. Remarkably, in mice treated with 600 mg/kg APAP, these cells expressed several markers of myeloid-derived suppressor cells (MDSCs), including high-level expression of IL-10, PD-L1, CD11b, Axl and Cx3Cr1 (Figure 2.6 and 2.7) (Yaseen et al., 2020). MDSCs are highly immunosuppressive and are typically generated under pathological conditions (Yaseen et al., 2020). Although MDSCs have not been reported previously in ALF, studies indicate that these cells are increased in acute-on-chronic liver failure and associated with disease severity (Zeng et al., 2019). Our studies indicate further that high levels of IL-6 occurring under conditions of APAP-induced ALF stimulate formation of these cells, as neutralization of IL-6 reduced levels of both IL-10 and PD-L1 (Figure 2.10). Studies have shown that IL-6 contributes to MDSC formation in tumor biology (Jiang et al., 2017). As discussed, high levels of IL-6 are associated with a poor outcome in ALF patients, similar to IL-10 and PD-L1, and our studies linking IL-6 to these immune suppressive pathways provide additional insight into the mechanism by which IL-6 negatively impacts

recovery in ALF patients (Bonkovsky et al., 2019). In fact, it was recently reported that high levels of PD-L1 are expressed on circulating myeloid cells in ALF patients (Triantafyllou et al., 2021). It was proposed that this may contribute to the high incidence of infections seen in ALF patients. Accordingly, therapeutic targeting of IL-6 in ALF patients may improve hepatic encephalopathy and also moderate the immune suppressive environment that occurs in these patients. Because studies have documented increased liver injury and reduced hepatocyte proliferation in IL-6 knockout mice treated with 300 mg/kg APAP, there may be reluctance to target IL-6 in ALF patients. Remarkably, though, our studies in mice treated with 600 mg/kg APAP demonstrated that neutralization of IL-6 not only had no effect on liver injury or hepatocyte proliferation, it actually increased survival.

IL-10 is a potent anti-inflammatory cytokine that is hepatoprotective in several models of liver injury and disease. In fact, liver injury and mortality are greatly enhanced in IL-10 knockout mice treated with doses of APAP ranging from 120 to 300 mg/kg (Bourdi et al., 2002). This long-standing study has driven current dogma that the primary role of IL-10 in experimental liver damage is to inhibit inflammatory liver injury. Yet, these results do not recapitulate what is observed in patients, where high levels of IL-10 are an independent predictor of a poor outcome in ALF patients (Berry et al., 2010). Because IL-10 is well known to suppress immunity against invading pathogens, it is possible that high levels of IL-10 in ALF increase susceptibility to secondary infections that progress to sepsis. Interestingly, though, Berry and colleagues showed no association between high levels of IL-10 and incidence of sepsis in ALF patients (Berry et al., 2010), indicating that IL-10 impacts other processes that are critical for recovery from ALF. Our studies provide an alternative explanation for the connection between high IL-10 levels and poor outcome in ALF. Specifically, IL-10 negatively impacts the ability of MDMs to migrate within the liver. In mice treated with 300 mg/kg APAP, $CD68^+$ macrophages filled the necrotic lesions by 48 hours (Figure 2.2). By contrast, in mice challenged with 600 mg/kg APAP, recruited $CD68^+$ macrophages were seemingly incapable of entering areas of necrosis, a

phenomenon that has been noted in ALF patient livers (Figure 2.2) (Antoniades et al., 2008) (Antoniades et al., 2012). Remarkably, in mice treated with 600 mg/kg APAP, neutralization of IL-10 completely restored macrophage trafficking into the necrotic foci (Figure 2.8). Conversely, treatment of mice with recombinant IL-10, beginning at 24 hours after 300 mg/kg APAP, prevented intrahepatic macrophage trafficking into the necrotic lesions (Figure 2.8). Collectively, these findings offer a mechanistic underpinning for the connection between high IL-10 levels and poor outcome in ALF.

The mechanistic basis for high IL-6 levels in mice treated with 600 mg/kg APAP is not fully clear, however, it is possible that severe hepatocellular hypoxia may be a contributing factor. Gao and colleagues recently showed that the hypoxia-regulated transcription factor, hypoxia-inducible factor-2α (HIF-2α), is activated in hepatic macrophages after treatment of mice with 300 mg/kg APAP (Gao et al., 2020). They demonstrated further that activation of HIF-2α in myeloid cells contributes to IL-6 upregulation (Gao et al., 2020). We and others have reported substantial sinusoidal congestion and hemorrhage in mice treated with 600 mg/kg APAP, a phenotype that is less severe in mice treated with 300 mg/kg APAP (Bhushan et al., 2014). It is possible that the severe sinusoidal congestion occurring in mice treated with 600 mg/kg APAP impairs hepatic blood flow resulting in greater hypoxia. This effect may lead to enhancement of HIF-2α activation resulting in greater IL-6 upregulation. Additional studies are needed, however, to fully evaluate this.

Collectively, our findings demonstrate that myeloid cell dysfunction and cytokine dysregulation are effectively recapitulated in mice treated with a high dose APAP. As such, this experimental setting provides a novel platform to interrogate mechanisms of immune dysregulation in ALF and to identify new therapeutic interventions. Further, by using this approach, our studies identified IL-6 as a central player in macrophage dysregulation in ALF, challenging the long-held belief that IL-6 is hepatoprotective in APAP-induced ALF and

providing a mechanism to explain the paradoxical association between high levels of IL-6 and poor outcome in ALF patients.

ACKNOWLEDGEMENTS

We thank Dr. Katherine Roth, Dr. Anne Dorrance, Jessica Yen, Dr. James Luyendyk, Dr. Asmita Pant, Dr. Cheryl Rockwell, Dr. Robert Freeborn, and Alison Boss for their contributions to this manuscript.

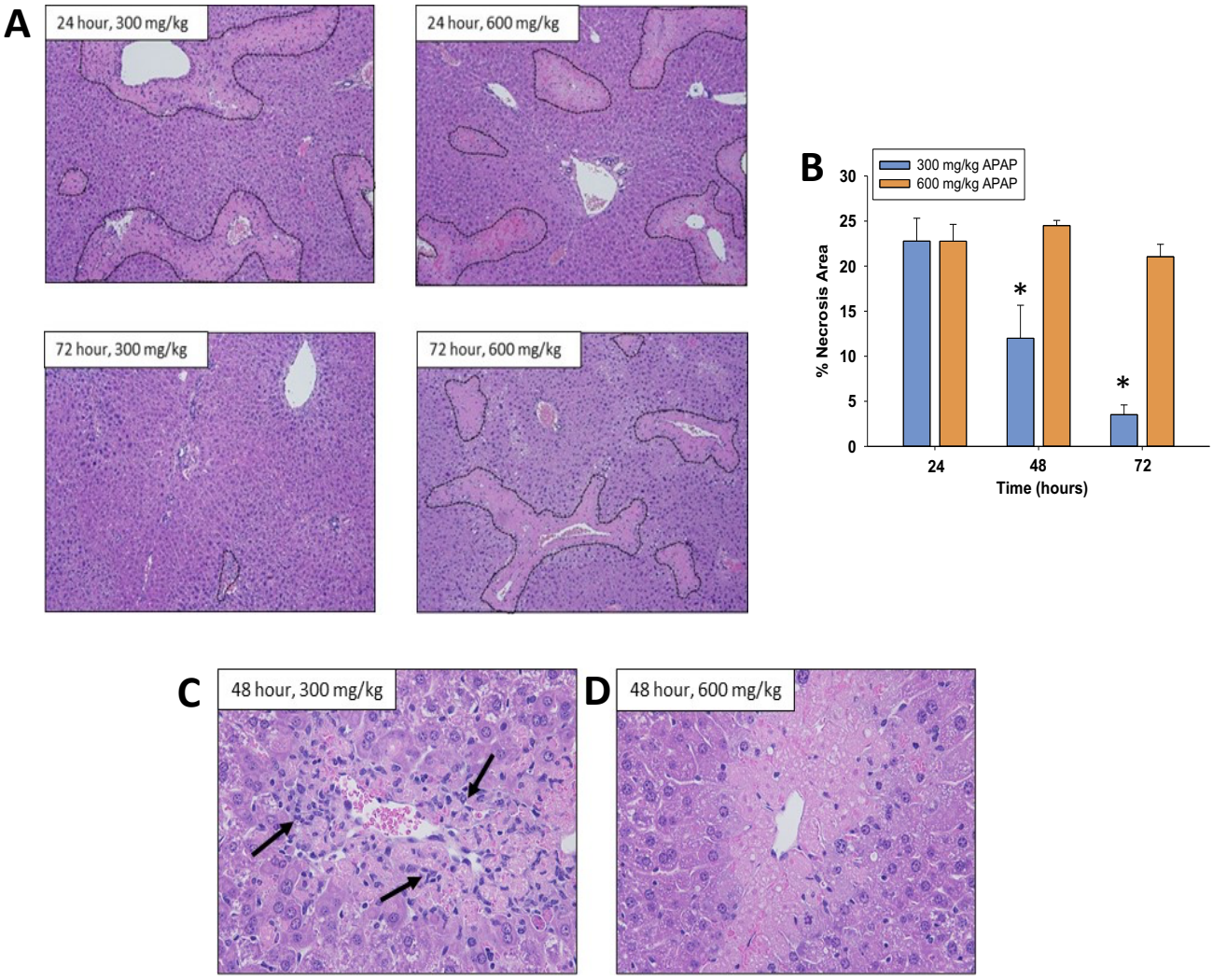

Figure 2.1: Liver injury and inflammation in mice treated with either 300 mg/kg or 600 mg/kg APAP. Mice were treated with either 300 mg/kg APAP or 600 mg/kg APAP as detailed in the methods. (A) Photomicrographs of H&E stained liver sections. Necrotic lesions are demarcated by a dashed line. (B) Area of necrosis was quantified in sections of liver. *Significantly different from mice treated with 300 mg/kg APAP. Data are expressed as mean ± SEM; n = 5-10 mice per group. (C,D) Photomicrographs of H&E stained liver sections. Arrows indicate inflammatory cells within the necrotic lesions.

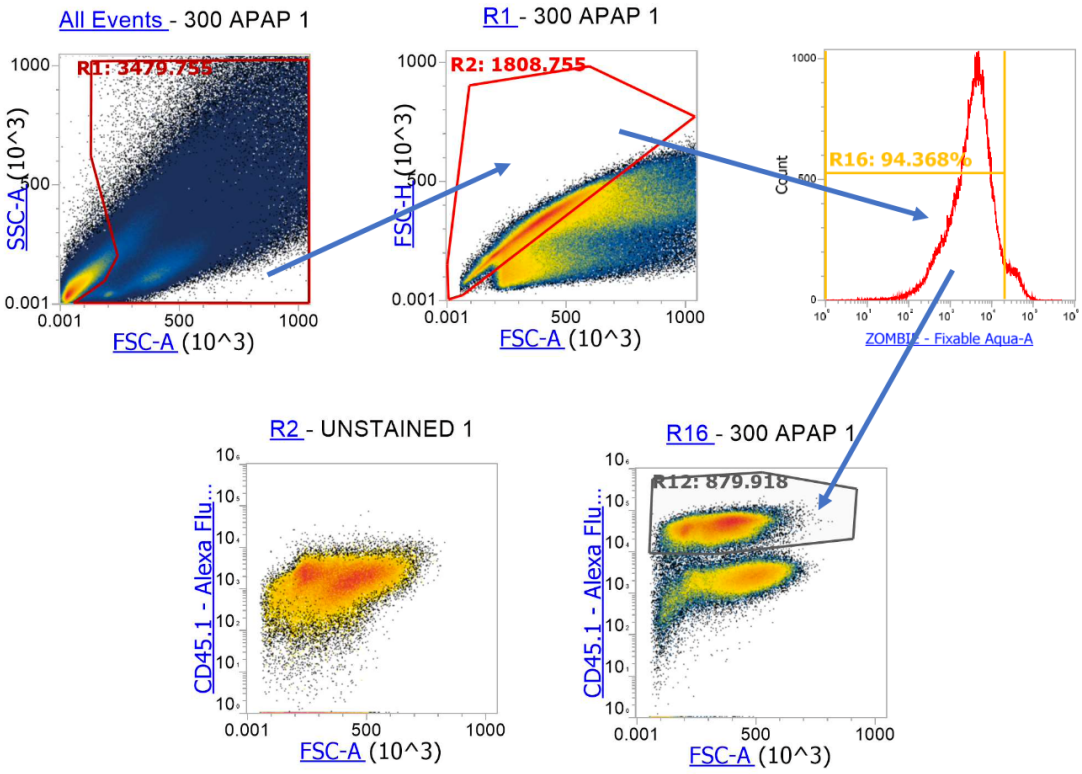

Figure 2.2: Gating strategy for flow cytometry.

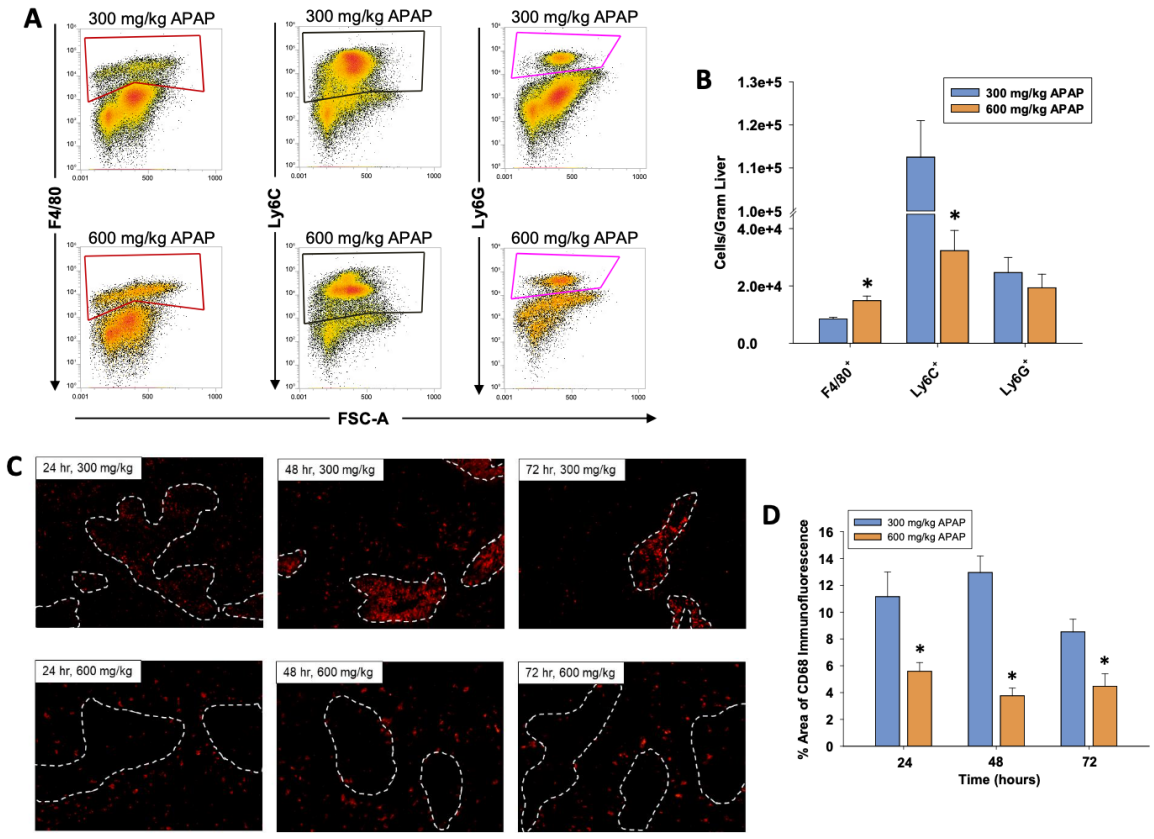

Figure 2.3: Accumulation of myeloid cells in the livers of mice treated with APAP. Mice were treated with either 300 mg/kg APAP or 600 mg/kg APAP. (A) At 24 hours after treatment, flow cytometry was used to detect F4/80+, Ly6C+, and Ly6G+ cells in the liver. Boxes indicate the positive gate. (B) Quantification of absolute cell counts from the flow cytometry. (C) Mice were treated with APAP for the indicated time. Photomicrographs of CD68 immunofluorescent staining in liver sections. Positive staining appears red. Necrotic lesions are demarcated by a dashed white line. (B) The area of CD68 immunofluorescent staining was quantified in sections of liver. *Significantly different from mice treated with 300 mg/kg APAP. Data are expressed as mean ± SEM; n = 5 mice per group.

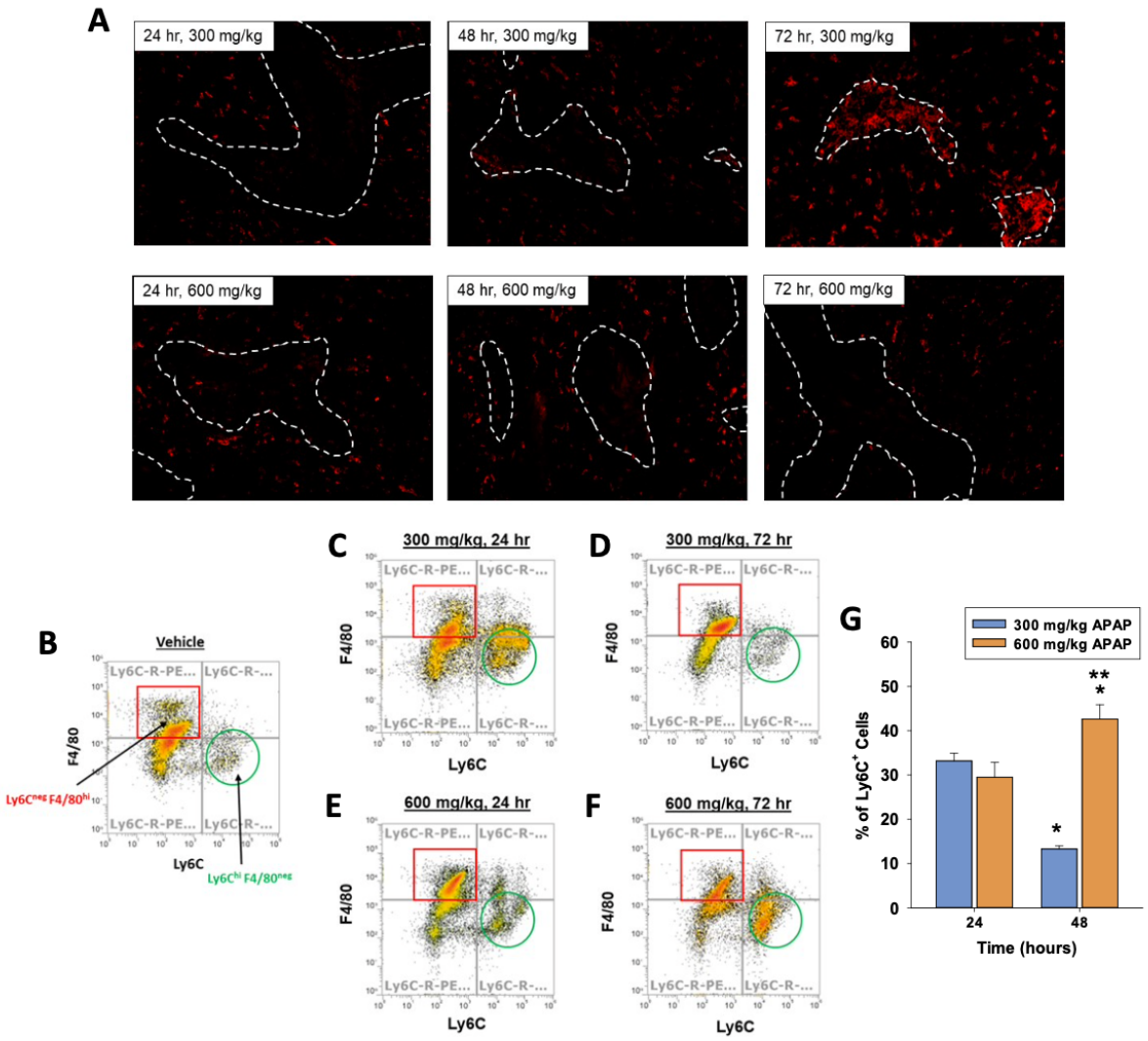

Figure 2.4: Populations of myeloid cells in the livers of mice treated with APAP. Mice were treated with either vehicle control, 300 mg/kg APAP, or 600 mg/kg APAP. (A) After 24 hours, livers were digested and Ly6C+ and F4/80+ cells were detected by flow cytometry in vehicle-treated mice. After 24 (B) and 72 hours (C) Ly6C+ and F4/80+ were detected in the livers of mice treated with 300 mg/kg. After 24 (D) and 72 hours (E) Ly6C+ and F4/80+ were detected in the livers of mice treated with 600 mg/kg. (F) The percentage of Ly6C+ cells was quantified by flow cytometry. *Significantly different from 24 hours. **Significantly different from mice treated with 300 mg/kg APAP 48 hours earlier. Data are expressed as mean ± SEM; n = 3.

Figure 2.4 (cont'd) (G) F4/80 was detected by immunofluorescence in liver sections. Treatment and time point are indicated on the photomicrograph. The necrotic lesions are demarcated by a white dashed line. F4/80+ macrophages appear red in the photomicrographs. Representative from an n = 5-10 mice per group.

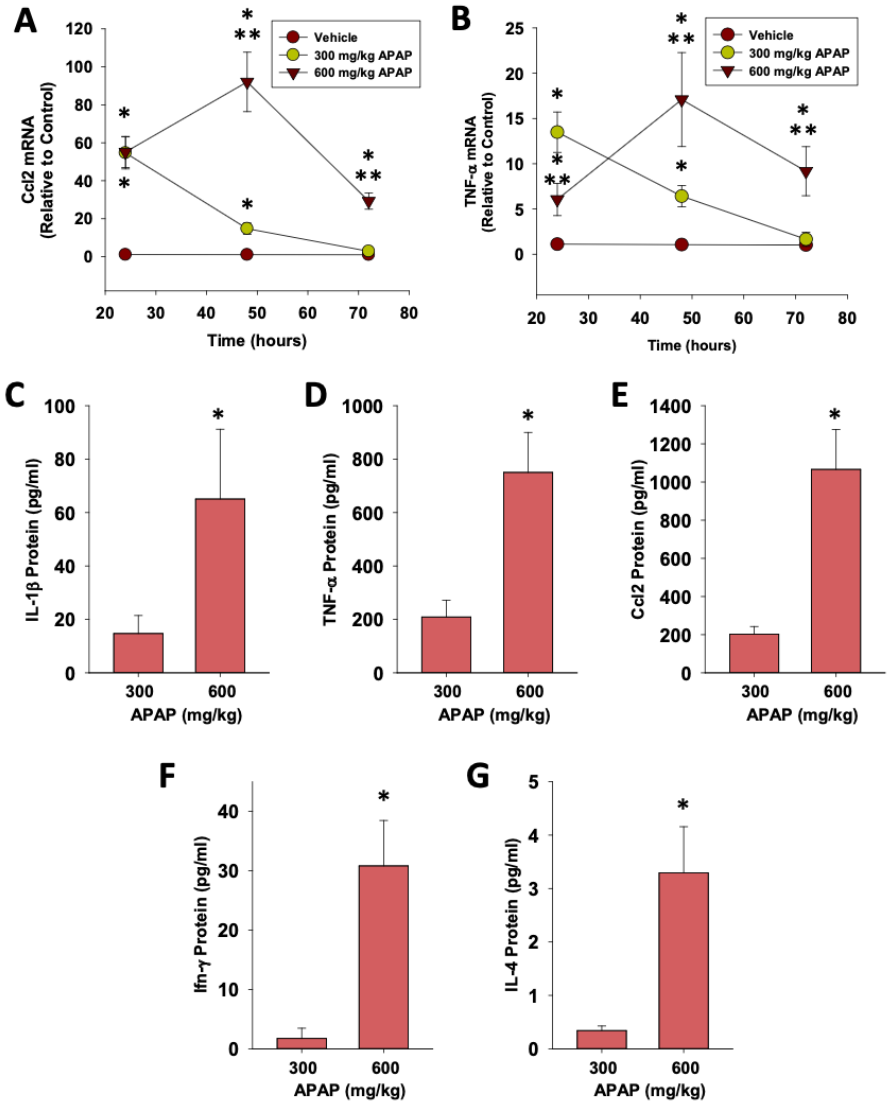

Figure 2.5: Quantification of cytokines in the livers and serum of mice treated with APAP. (A) Ccl2 and TNF-a mRNA levels were measured at 24, 48, and 72 hours after APAP treatment. *Significantly different from vehicle-treated mice. **Significantly different from mice treated with 300 mg/kg at the same time point. Data are expressed as mean ± SEM; *n* = 5-10 mice per group. (C-G) Serum levels of the indicated cytokine were measured at 72 hours after APAP treatment. *Significantly different from mice treated with 300 mg/kg APAP. Data are expressed as mean ± SEM; *n* = 5-10 mice per group.

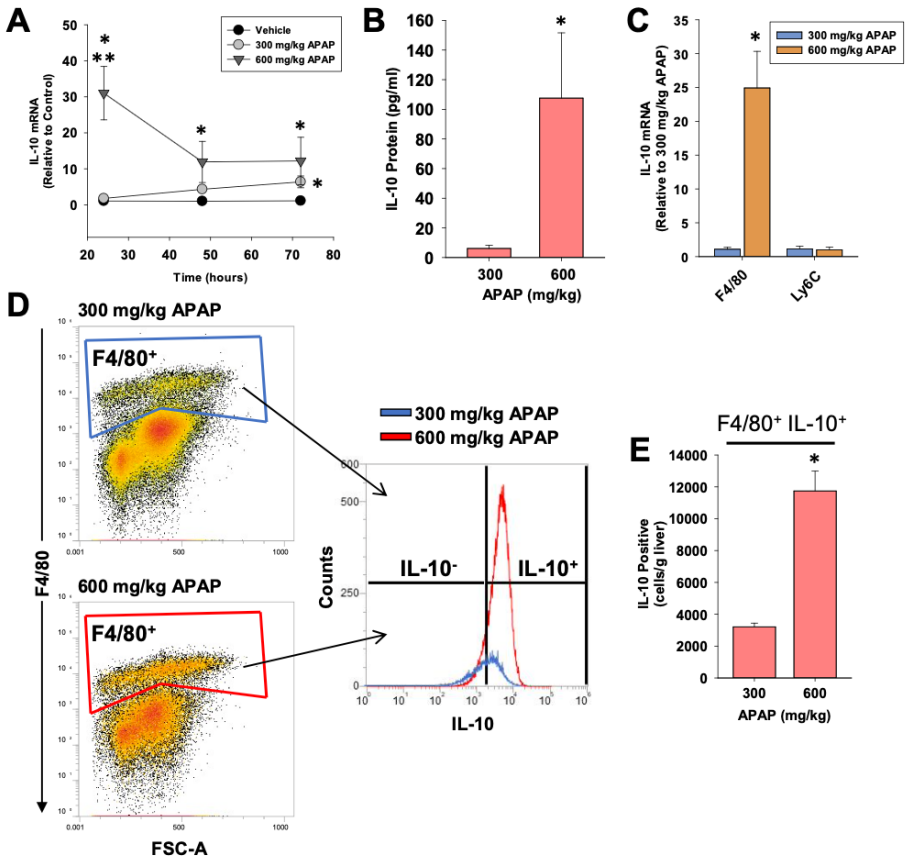

Figure 2.6: Hepatic and systemic levels of IL-10 in APAP-treated mice. Mice were treated with either 300 or 600 mg/kg APAP. (A) At the indicated time, IL-10 mRNA levels were measured in the liver. (B) IL-10 protein was measured in serum at 72 hours after APAP treatment. (C) F4/80+ and Ly6C+ myeloid cells were isolated from the liver at 24 hours after APAP, and IL-10 mRNA levels were measured. (D) Nonparenchymal cells were isolated from the livers of IL-10 reporter mice treated 24 hours earlier with 300 or 600 mg/kg APAP. Flow cytometry was used to identify IL-10 expressing F4/80 cells. Gate for F4/80+ cells indicated in the density plots. Representative histogram of IL-10 expression in F4/80+ cells. (E) Quantification of the number of F4/80+ cells expressing IL-10 in the liver. *Significantly different from mice treated with 300 mg/kg APAP. Data are expressed as mean ± SEM; n = 4-5 mice per group.

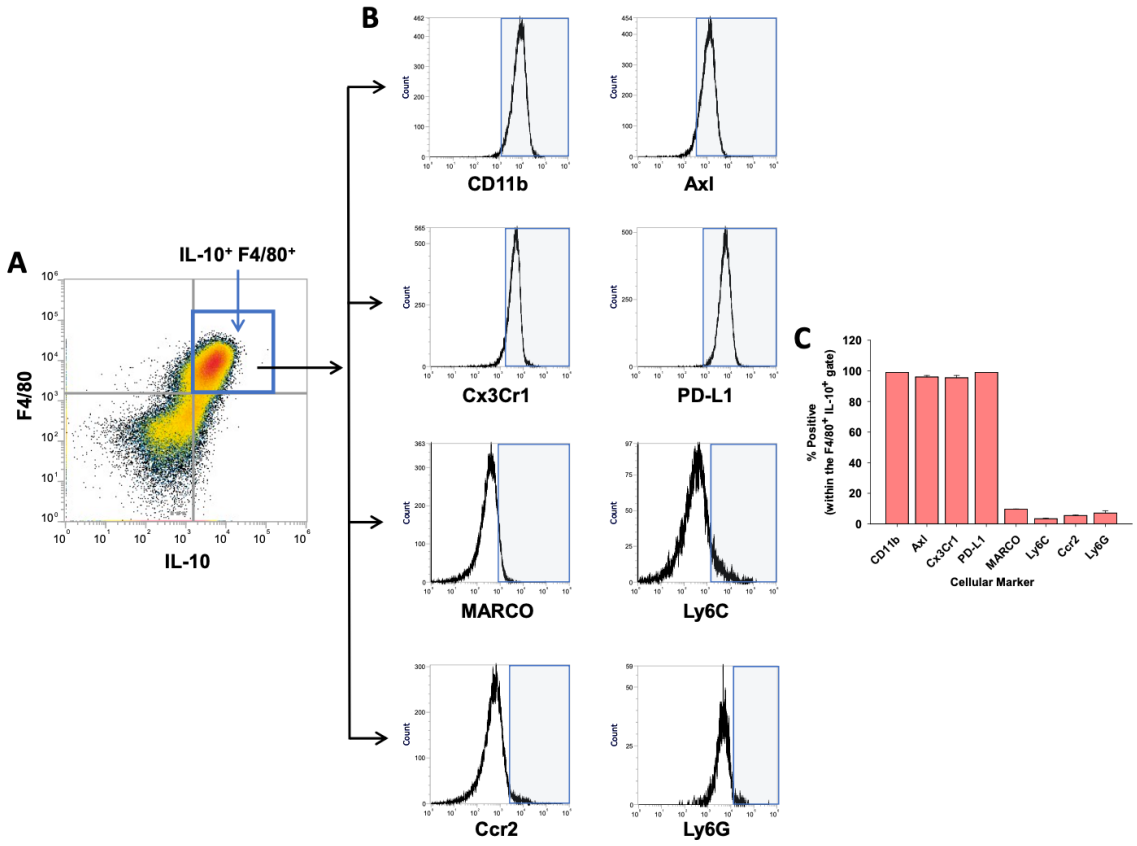

Figure 2.7: Immunophenotyping of IL-10+ F4/80+ cells. Mice were treated with 600 mg/kg APAP. (A) 24 hours later, flow cytometry was used to detect IL-10 expressing F4/80+ cells, indicated by the blue box. (B) Representative histograms of IL-10+ F4/80+ cells expressing the indicated marker (x-axis). Positive staining indicated by the blue shaded box. (C) Quantification of the flow cytometry in B. Data are expressed as mean ± SEM; n = 4 mice per group.

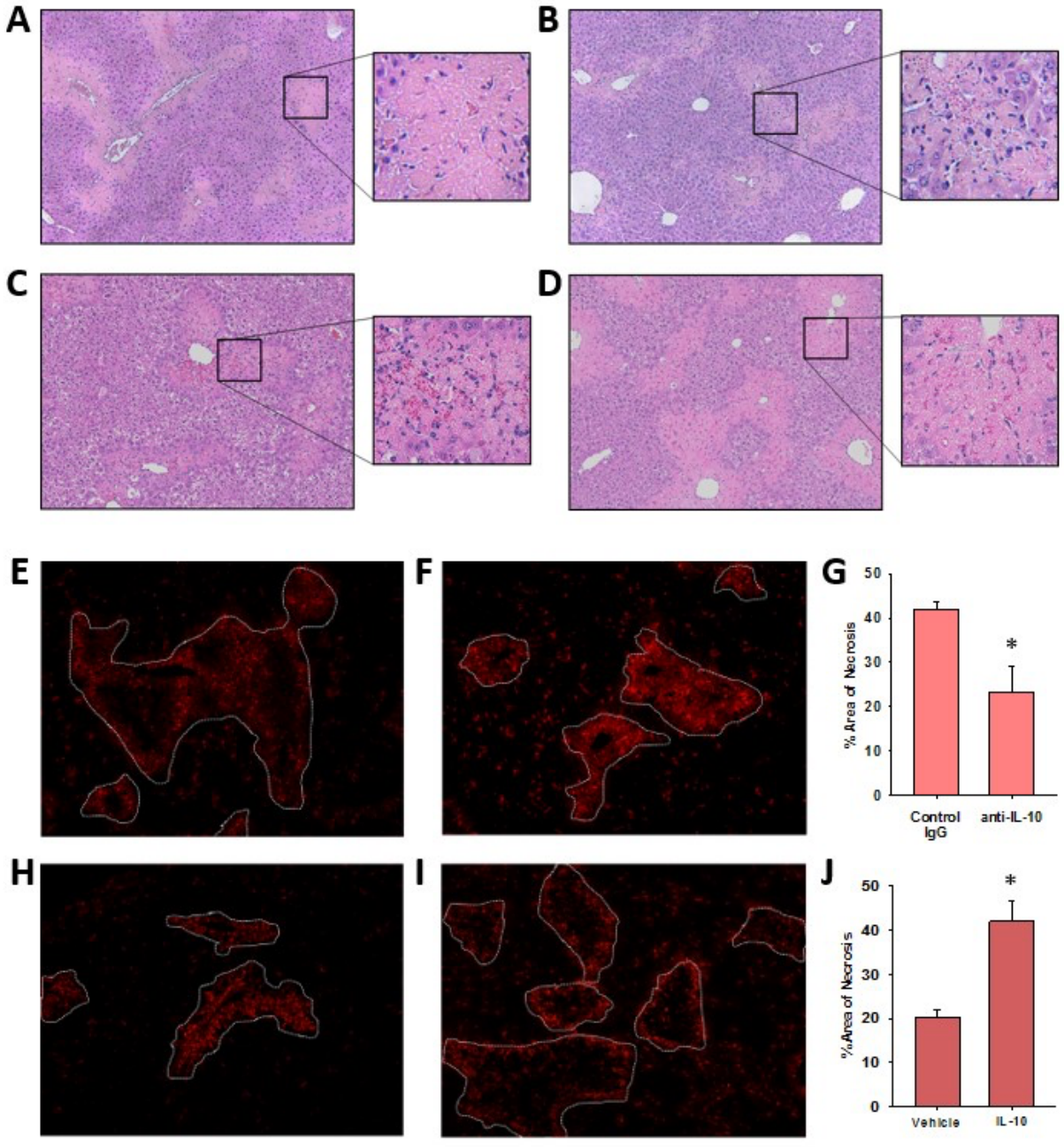

Figure 2.8: **Impact of IL-10 on histopathology and inflammation in mice treated with APAP.** (A-B and E-G) Mice were treated with 600 mg/kg APAP followed by treatment with control IgG or anti-IL-10 antibody 24 hours later. Livers were collected 72 hours after APAP treatment. (C-D and H-J) Mice were treated with 300 mg/kg APAP followed by treatment with vehicle or 5 mg recombinant IL-10 24 hours later. Livers were collected 48 hours after APAP

Figure 2.8 (cont'd) treatment. (A-D) Representative photomicrographs of hematoxylin and eosin stained liver sections. Box highlights a region of interest that is shown at a higher magnification. CD68 was detected by immunofluorescence in sections of liver from mice treated with (E) 600 mg/kg APAP and control IgG, (F) 600 mg/kg APAP and anti-IL-10 antibody, (H) 300 mg/kg APAP and vehicle or (I) 300 mg/kg APAP and recombinant IL-10and anti-IL-10 antibody. The necrotic lesions are demarcated by a dashed line. Representative photomicrographs from an n = 5 mice per group. (G and J) The area of necrosis was quantified. n = 5 mice per group. *Significantly different at $p<0.05$.

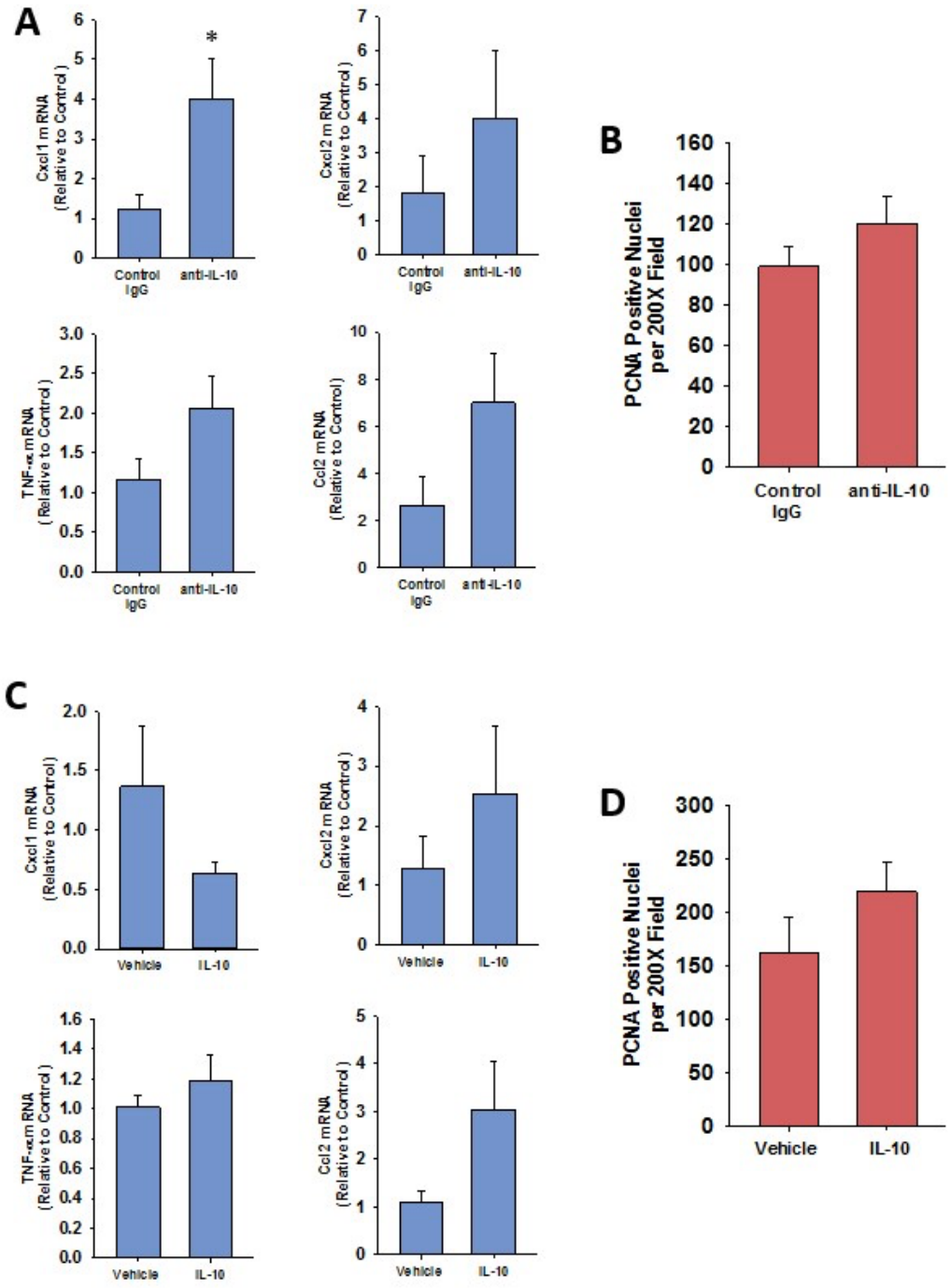

Figure 2.9: Impact of IL-10 on histopathology and inflammation in mice treated with APAP. (A-B) Mice were treated with 600 mg/kg APAP followed by treatment with control IgG or anti-IL-10 antibody 24 hours later. Livers were collected 72 hours after APAP treatment. (C-D) Mice were treated with 300 mg/kg APAP followed by treatment with vehicle or 5 mg

Figure 2.9 (cont'd) recombinant IL-10 24 hours later. Livers were collected 48 hours after APAP treatment. (A and C) mRNA levels of selected cytokines in the liver. n=5. *Significantly different at $p<0.05$. (B and D) PCNA positive nuclei were quantified. n=5.

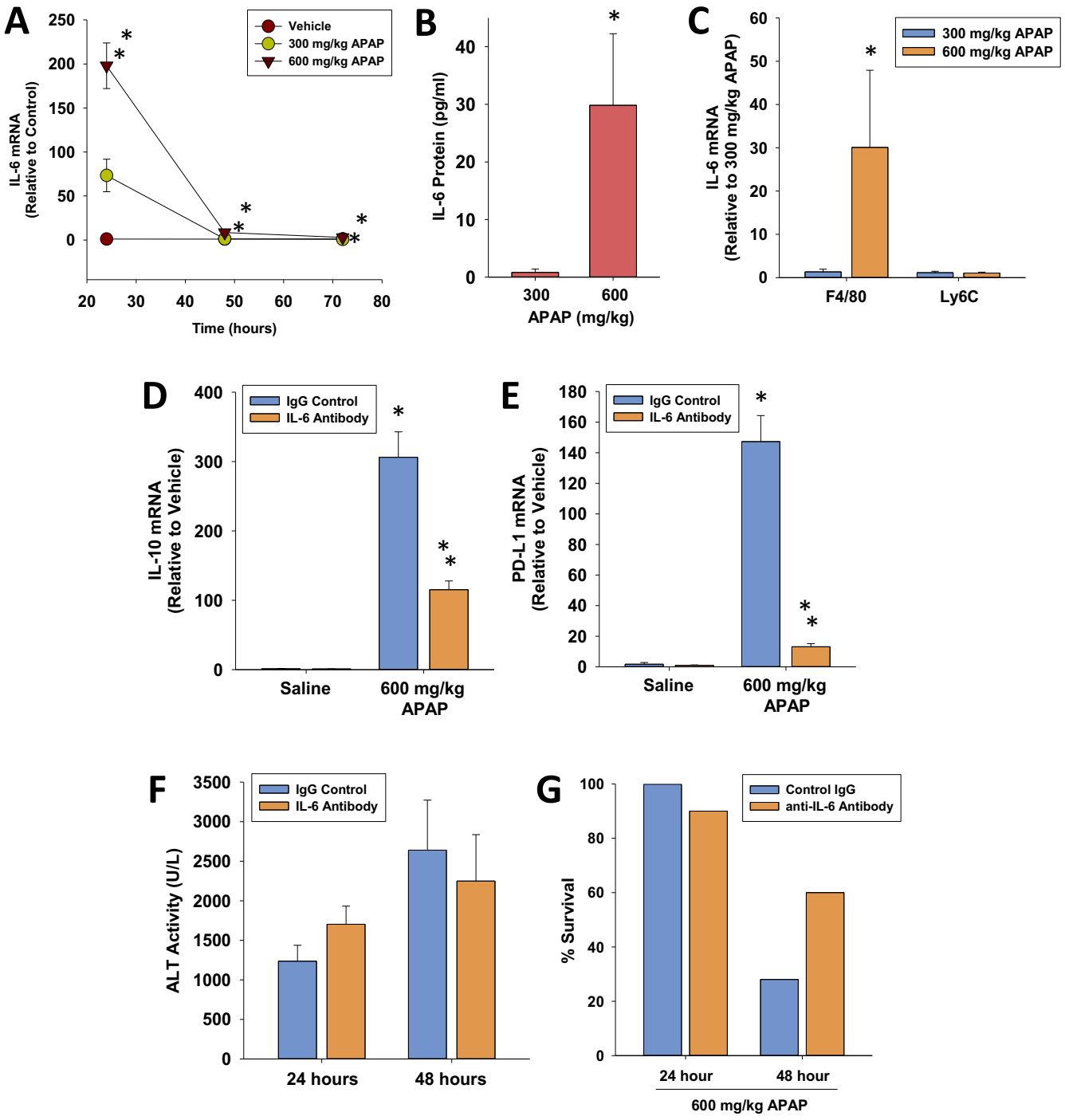

Figure 2.10: Role of IL-6 in regulation of IL-10 after APAP. (A) IL-6 mRNA levels were measured at 24, 48, and 72 hours after APAP treatment. *Significantly different from vehicle-treated mice. **Significantly different from mice treated with 300 mg/kg at the same time point.

Figure 2.10 (cont'd) (B) Serum levels of IL-6 were measured at 72 hours after APAP treatment. (C) IL-6 mRNA levels were measured in F4/80+ and Ly6C+ cells purified from the liver. *Significantly different from mice treated with 300 mg/kg APAP. Data are expressed as mean ± SEM; n = 5-10 mice per group. Mice were treated with 600 mg/kg APAP followed by IgG control or IL-6 neutralizing antibody 2 hours later. mRNA levels of (D) IL-10 and (E) PD-L1 were measured at 24 hours after APAP. (F) ALT activity at 24 and 48 hours. *Significantly different from vehicle-treated mice. **Significantly different from mice treated with 600 mg/kg and IgG control. Data are expressed as mean ± SEM; n = 3 mice per group for saline treated mice. n = 9 mice per group for mice treated with APAP and IgG control or IL-6 antibody. (G) Survival at the indicated time-point.

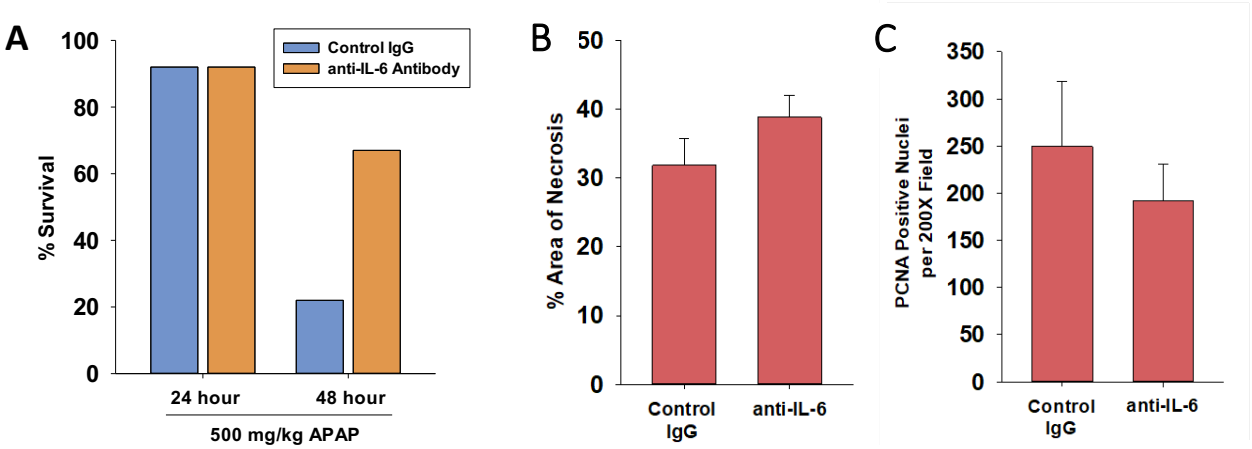

Figure 2.11: Role of IL-6 in liver pathology after APAP. (A) Mice were treated with 500 or 600 mg/kg APAP followed by IgG control or IL-6 neutralizing antibody 2 hours later. Survival at 24 and 48 hours after APAP. n=10 Mice were treated with 500 mg/kg APAP followed by IgG control or IL-6 neutralizing antibody 2 hours later. (B) Area of Necrosis and (C) PCNA positive cells were quantified at 24 hours after APAP.

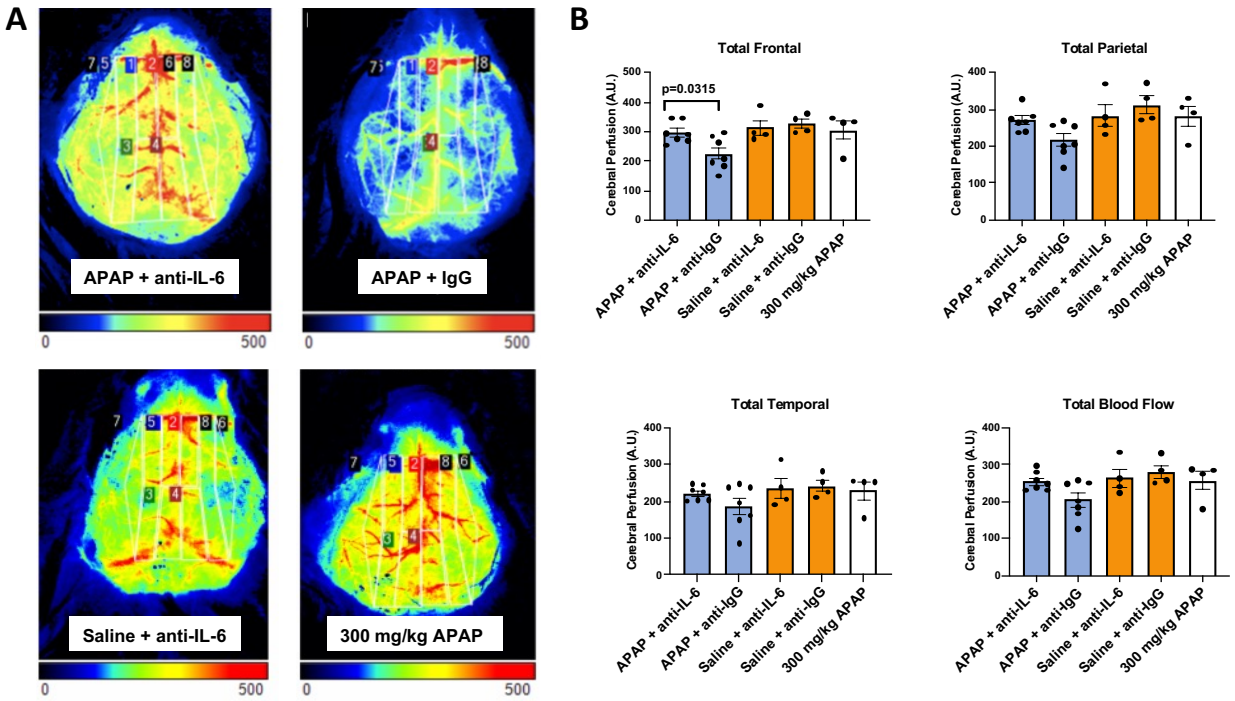

Figure 2.12: Impact of IL-6 on cerebral blood flow after APAP. Mice were treated with 500 mg/kg APAP followed by IgG control or IL-6 neutralizing antibody 2 hours later. Additional mice were treated with saline followed by IgG control or IL-6 neutralizing antibody 2 hours later. A separate cohort of mice were treated with 300 mg/kg APAP for comparison. Laser speckle imaging was used to quantify cerebral blood flow 24 hours after APAP. (A) Representative brain images from laser speckle imaging. (B) Total cerebral blood flow and blood flow within the indicated brain region was quantified. n=7 for 500 mg/kg APAP treated mice. n=3 for other groups.

BIBLIOGRAPHY

Akakpo JY, Ramachandran A, Orhan H, Curry SC, Rumack BH, Jaeschke H. 4-methylpyrazole protects against acetaminophen-induced acute kidney injury. Toxicol Appl Pharmacol. 2020 Dec 15;409:115317. doi: 10.1016/j.taap.2020.115317. Epub 2020 Nov 4. PMID: 33157119; PMCID: PMC7888547.

Allen K, Jaeschke H, Copple BL. Bile acids induce inflammatory genes in hepatocytes: a novel mechanism of inflammation during obstructive cholestasis. Am J Pathol. 2011 Jan;178(1):175-86. doi: 10.1016/j.ajpath.2010.11.026. Epub 2010 Dec 23. PMID: 21224055; PMCID: PMC3070591.

Antoniades CG, Berry PA, Davies ET, Hussain M, Bernal W, Vergani D, Wendon J. Reduced monocyte HLA-DR expression: a novel biomarker of disease severity and outcome in acetaminophen-induced acute liver failure. Hepatology. 2006 Jul;44(1):34-43. doi: 10.1002/hep.21240. PMID: 16799971.

Antoniades CG, Berry PA, Wendon JA, Vergani D. The importance of immune dysfunction in determining outcome in acute liver failure. J Hepatol. 2008 Nov;49(5):845-61. doi: 10.1016/j.jhep.2008.08.009. Epub 2008 Aug 21. PMID: 18801592.

Antoniades CG, Quaglia A, Taams LS, Mitry RR, Hussain M, Abeles R, Possamai LA, Bruce M, McPhail M, Starling C, Wagner B, Barnardo A, Pomplun S, Auzinger G, Bernal W, Heaton N, Vergani D, Thursz MR, Wendon J. Source and characterization of hepatic macrophages in acetaminophen-induced acute liver failure in humans. Hepatology. 2012 Aug;56(2):735-46. doi: 10.1002/hep.25657. Epub 2012 Jul 6. PMID: 22334567.

Berry PA, Antoniades CG, Hussain MJ, McPhail MJ, Bernal W, Vergani D, Wendon JA. Admission levels and early changes in serum interleukin-10 are predictive of poor outcome in acute liver failure and decompensated cirrhosis. Liver Int. 2010 May;30(5):733-40. doi: 10.1111/j.1478-3231.2010.02219.x. PMID: 20456041.

Bhushan B, Walesky C, Manley M, Gallagher T, Borude P, Edwards G, Monga SP, Apte U. Pro-regenerative signaling after acetaminophen-induced acute liver injury in mice identified using a novel incremental dose model. Am J Pathol. 2014 Nov;184(11):3013-25. doi: 10.1016/j.ajpath.2014.07.019. Epub 2014 Sep 2. PMID: 25193591; PMCID: PMC4215032.

Bjerring PN, Gluud LL, Larsen FS. Cerebral Blood Flow and Metabolism in Hepatic Encephalopathy-A Meta-Analysis. J Clin Exp Hepatol. 2018 Sep;8(3):286-293. doi: 10.1016/j.jceh.2018.06.002. Epub 2018 Jun 20. PMID: 30302046; PMCID: PMC6175738.

Bonkovsky HL, Barnhart HX, Foureau DM, Steuerwald N, Lee WM, Gu J, Fontana RJ, Hayashi PH, Chalasani N, Navarro VM, Odin J, Stolz A, Watkins PB, Serrano J; US Drug-Induced Liver Injury Network and the Acute Liver Failure Study Group. Correction: Cytokine profiles in acute liver injury-Results from the US Drug-Induced Liver Injury Network (DILIN) and the Acute Liver Failure Study Group. PLoS One. 2019 Feb 11;14(2):e0212394. doi: 10.1371/journal.pone.0212394. Erratum for: PLoS One. 2018 Oct 25;13(10):e0206389. PMID: 30742679; PMCID: PMC6370229.

Bourdi M, Masubuchi Y, Reilly TP, Amouzadeh HR, Martin JL, George JW, Shah AG, Pohl LR. Protection against acetaminophen-induced liver injury and lethality by interleukin 10: role of inducible nitric oxide synthase. Hepatology. 2002 Feb;35(2):289-98. doi: 10.1053/jhep.2002.30956. PMID: 11826401.
Butterworth RF. Pathogenesis of hepatic encephalopathy and brain edema in acute liver failure. J Clin Exp Hepatol. 2015 Mar;5(Suppl 1):S96-S103. doi: 10.1016/j.jceh.2014.02.004. Epub 2014 Jul 9. PMID: 26041966; PMCID: PMC4442857.

Gao RY, Wang M, Liu Q, Feng D, Wen Y, Xia Y, Colgan SP, Eltzschig HK, Ju C. Hypoxia-Inducible Factor-2α Reprograms Liver Macrophages to Protect Against Acute Liver Injury Through the Production of Interleukin-6. Hepatology. 2020 Jun;71(6):2105-2117. doi: 10.1002/hep.30954. Epub 2020 Feb 4. PMID: 31529728; PMCID: PMC7075728.

Kim ND, Moon JO, Slitt AL, Copple BL. Early growth response factor-1 is critical for cholestatic liver injury. Toxicol Sci. 2006 Apr;90(2):586-95. doi: 10.1093/toxsci/kfj111. Epub 2006 Jan 19. PMID: 16423862.

Lee WM, Squires RH Jr, Nyberg SL, Doo E, Hoofnagle JH. Acute liver failure: Summary of a workshop. Hepatology. 2008 Apr;47(4):1401-15. doi: 10.1002/hep.22177. PMID: 18318440; PMCID: PMC3381946.

Mochizuki A, Pace A, Rockwell CE, Roth KJ, Chow A, O'Brien KM, Albee R, Kelly K, Towery K, Luyendyk JP, Copple BL. Hepatic stellate cells orchestrate clearance of necrotic cells in a hypoxia-inducible factor-1α-dependent manner by modulating macrophage phenotype in mice. J Immunol. 2014 Apr 15;192(8):3847-3857. doi: 10.4049/jimmunol.1303195. Epub 2014 Mar 17. PMID: 24639359; PMCID: PMC4538924.

Mossanen JC, Krenkel O, Ergen C, Govaere O, Liepelt A, Puengel T, Heymann F, Kalthoff S, Lefebvre E, Eulberg D, Luedde T, Marx G, Strassburg CP, Roskams T, Trautwein C, Tacke F. Chemokine (C-C motif) receptor 2-positive monocytes aggravate the early phase of acetaminophen-induced acute liver injury. Hepatology. 2016 Nov;64(5):1667-1682. doi: 10.1002/hep.28682. Epub 2016 Jul 22. PMID: 27302828.

Polycarpou A, Hricisák L, Iring A, Safar D, Ruisanchez É, Horváth B, Sándor P, Benyó Z. Adaptation of the cerebrocortical circulation to carotid artery occlusion involves blood flow redistribution between cortical regions and is independent of eNOS. Am J Physiol Heart Circ Physiol. 2016 Oct 1;311(4):H972-H980. doi: 10.1152/ajpheart.00197.2016. Epub 2016 Aug 5. PMID: 27496877.

Rama Rao KV, Verkman AS, Curtis KM, Norenberg MD. Aquaporin-4 deletion in mice reduces encephalopathy and brain edema in experimental acute liver failure. Neurobiol Dis. 2014 Mar;63:222-8. doi: 10.1016/j.nbd.2013.11.018. Epub 2013 Dec 7. PMID: 24321433; PMCID: PMC3982919.

Rolando N, Wade J, Davalos M, Wendon J, Philpott-Howard J, Williams R. The systemic inflammatory response syndrome in acute liver failure. Hepatology. 2000 Oct;32(4 Pt 1):734-9. doi: 10.1053/jhep.2000.17687. PMID: 11003617.

Roth K, Strickland J, Joshi N, Deng M, Kennedy RC, Rockwell CE, Luyendyk JP, Billiar TR, Copple BL. Dichotomous Role of Plasmin in Regulation of Macrophage Function after

Acetaminophen Overdose. Am J Pathol. 2019 Oct;189(10):1986-2001. doi: 10.1016/j.ajpath.2019.07.003. Epub 2019 Aug 2. PMID: 31381887; PMCID: PMC6892227.

Saito C, Zwingmann C, Jaeschke H. Novel mechanisms of protection against acetaminophen hepatotoxicity in mice by glutathione and N-acetylcysteine. Hepatology. 2010 Jan;51(1):246-54. doi: 10.1002/hep.23267. PMID: 19821517; PMCID: PMC2977522.

Smilkstein MJ, Knapp GL, Kulig KW, Rumack BH. Efficacy of oral N-acetylcysteine in the treatment of acetaminophen overdose. Analysis of the national multicenter study (1976 to 1985). N Engl J Med. 1988 Dec 15;319(24):1557-62. doi: 10.1056/NEJM198812153192401. PMID: 3059186.

Stravitz RT, Lee WM. Acute liver failure. Lancet. 2019 Sep 7;394(10201):869-881. doi: 10.1016/S0140-6736(19)31894-X. PMID: 31498101.

Triantafyllou E, Gudd CL, Mawhin MA, Husbyn HC, Trovato FM, Siggins MK, O'Connor T, Kudo H, Mukherjee SK, Wendon JA, Bernsmeier C, Goldin RD, Botto M, Khamri W, McPhail MJ, Possamai LA, Woollard KJ, Antoniades CG, Thursz MR. PD-1 blockade improves Kupffer cell bacterial clearance in acute liver injury. J Clin Invest. 2021 Feb 15;131(4):e140196. doi: 10.1172/JCI140196. PMID: 33320839; PMCID: PMC7880414.

Wendon JA, Harrison PM, Keays R, Williams R. Cerebral blood flow and metabolism in fulminant liver failure. Hepatology. 1994 Jun;19(6):1407-13. PMID: 8188170.

Yaseen MM, Abuharfeil NM, Darmani H, Daoud A. Mechanisms of immune suppression by myeloid-derived suppressor cells: the role of interleukin-10 as a key immunoregulatory cytokine. Open Biol. 2020 Sep;10(9):200111. doi: 10.1098/rsob.200111. Epub 2020 Sep 16. PMID: 32931721; PMCID: PMC7536076.

Zeng Y, Li Y, Xu Z, Gan W, Lu L, Huang X, Lin C. Myeloid-derived suppressor cells expansion is closely associated with disease severity and progression in HBV-related acute-on-chronic liver failure. J Med Virol. 2019 Aug;91(8):1510-1518. doi: 10.1002/jmv.25466. Epub 2019 Apr 4. PMID: 30905084.

Zigmond E, Samia-Grinberg S, Pasmanik-Chor M, Brazowski E, Shibolet O, Halpern Z, Varol C. Infiltrating monocyte-derived macrophages and resident kupffer cells display different ontogeny and functions in acute liver injury. J Immunol. 2014 Jul 1;193(1):344-53. doi: 10.4049/jimmunol.1400574. Epub 2014 Jun 2. PMID: 24890723.

CHAPTER 3

HEPATOPROTECTIVE ROLE OF AXL IN ACETAMINOPHEN INDUCED ACUTE LIVER FAILURE

3.1 Abstract

Acute liver failure (ALF) from acetaminophen (APAP) overdose remains a significant health burden with a high rate of mortality. After APAP-induced liver injury in mice, monocyte-derived macrophages (MDMs) infiltrate the liver and produce proinflammatory cytokines. As tissue injury resolves, these cells switch phenotype to pro-reparative macrophages—a process that terminates proinflammatory cytokine synthesis. The underlying mechanism by which these cells switch phenotype after APAP overdose remains to be fully characterized. Elucidation of this mechanism is important as clinical studies have revealed that macrophage dysfunction, leading to cytokine dysregulation, occurs in ALF patients with the poorest prognosis. In the present studies, we tested the hypothesis that TAM (Tyro3, Axl, and Mer) receptor signaling is critical for MDM phenotype switching after APAP overdose. To test this hypothesis, wild type (WT), $Axl^{-/-}$, and $Mer^{-/-}$ mice were treated with a dose of APAP associated with normal liver repair (300 mg/kg). Remarkably, by 48 hours after treatment, approximately 30% of $Axl^{-/-}$ mice had died. In the remaining mice, liver injury was substantially greater when compared to WT and $Mer^{-/-}$, and histopathological analysis revealed extensive hepatocellular necrosis and sinusoidal hemorrhaging in $Axl^{-/-}$. To by-pass the early impact on liver injury in $Axl^{-/-}$ mice, WT mice were treated with the Axl receptor inhibitor, LDC1267, or vehicle beginning at 24 hours after treatment with 300 mg/kg APAP. The area of necrosis was greater at 72 hours in mice treated with LDC1267 indicating impairment of MDM-dependent clearance of dead cells. Further, proinflammatory cytokine levels were higher in mice treated with LDC1267 and markers of pro-reparative macrophages were reduced. Collectively, these studies reveal that Axl protects the liver from injury early after APAP overdose. At later times, Axl mediates MDM-dependent clearance of dead cell debris and terminate proinflammatory cytokine synthesis. Further studies into the role of Axl in liver repair after APAP overdose could provide critical insight into the underlying cause of cytokine dysregulation in ALF patients.

3.2 Introduction

Acute liver failure (ALF) from acetaminophen (APAP) overdose remains a significant health burden in the United States, with a high rate of mortality. Several studies have shown that monocyte dysregulation is central to the pathogenesis of APAP-induced ALF, particularly in patients with the poorest prognosis (Antoniades 2008) (Triantafyllou et. al, 2018). In these patients, monocyte dysregulation causes sustained proinflammatory cytokine release that drives the development of life-threatening complications, including multi-organ failure (Triantafyllou et. al, 2018) (Antoniades 2008). The mechanistic basis for sustained cytokine synthesis in severe ALF remains largely unknown, although, it is conceivable that pathways which trigger resolution of inflammation are disrupted in these patients.

In mice treated with a moderately hepatotoxic dose of APAP (i.e., 300 mg/kg APAP), monocytes are rapidly recruited from the blood via the Ccl2/Ccr2 chemokine axis (Krenkel, Mossanen, Tacke, 2014) (Graubardt et al., 2017) (Dambach et al., 2002). These cells infiltrate the liver and produce proinflammatory cytokines that amplify inflammation (Graubardt et al., 2017). Fate tracing studies have revealed that the recruited proinflammatory monocytes, which are characterized as Ly6C^{hi}F4/80^{low}, ultimately switch phenotype and become Ly6C^{low}F4/80^{hi} pro-repair macrophages (Yona et al., 2014) (Girgis et al., 2014) (Sunderkotter et al., 2004) (Zigmond et al., 2014). This process terminates proinflammatory cytokine synthesis leading to the resolution of inflammation. (Graubardt et al., 2017). Although the mechanisms that stimulate proinflammatory monocytes to switch phenotype after APAP overdose are not fully known, it has been proposed that phagocytosis of dead cell debris is an important trigger for this process. In support of this, we showed previously that phagocytosis of necrotic hepatocytes by cultured Ly6C^{hi}F4/80^{low} cells decreases proinflammatory cytokine expression, while increasing expression of macrophage pro-repair markers (e.g., Arg-1, Cx3cr1, and Vsig4) (Roth et al., 2019). Interestingly, in a mouse model of true APAP-induced ALF, monocytes fail to clear dead cell debris from the liver, an effect that was associated with sustained proinflammatory cytokine

synthesis (Chapter 2). This suggested that impairment of monocyte phagocytosis may contribute to the failure to terminate cytokine production in ALF. The mechanistic basis for this, however, remains unknown. A better understanding of the processes regulating monocyte phagocytosis, however, are first needed before it can be determined how this process becomes disrupted in ALF.

The TAM (Tyro3, Axl, and Mer) family of receptor kinases has been shown to play vital role(s) in the resolution of inflammation. This family of receptors is activated by dead cells with phosphatidylserine exposed to the outer membrane leaflet. Activation of TAMs, which triggers phagocytosis and dampens the immune response, requires either Gas6 or Protein C, which form a bridge between the TAM receptor and the phosphatidylserine (Rothlin et al., 2015) (Lemke 2017). TAM knockout mice develop chronic inflammation that is associated with a reduction in the clearance of necrotic and apoptotic cells (Rothlin et al., 2015). Subsequent studies demonstrated that phagocytosis triggered by TAM receptors promotes macrophage polarization towards a reparative phenotype, which may explain the chronic inflammation that develops in TAM knockout mice (Myers, Amend, and Pienta, 2019). Interestingly, it was recently reported that Axl and the bridging ligand, Gas6, are upregulated in recruited proinflammatory monocytes purified from the livers of APAP treated mice (Graubardt et al., 2017). This suggested that Axl and Gas6 may contribute to the phagocytosis of dead cell debris after APAP overdose and may be critical for the switching of monocyte phenotype and termination of inflammation. To examine this further, we tested the hypotheses that Axl activation is critical for resolution of inflammation during normal liver repair and that impaired Axl signaling contributes to persistent cytokine production in APAP-induced ALF.

3.3 Materials and Methods

3.3.1 Animal Treatments. To determine which TAM receptor is important for regulating phagocytosis in APAP-induced ALI, WT (n=11 APAP; n=6 Saline), $Axl^{-/-}$ (n= 10 APAP; n=4 Saline), and $Mer^{-/-}$ (n= 6 APAP; n=3 Saline) mice were treated with either saline or 300 mg/kg APAP. TAM receptor knockout mice were graciously provided by Dr. Greg Lemke (Salk Institute). Generation of TAM mutant mouse lines has been described previously (Lemke 2013). All lines have been backcrossed for >9 generations to a C57BL/6 background. Mice were fasted in clean cages for 16 h (overnight) before injection the following morning. (Fasting is necessary to produce APAP-induced liver injury in mice). Mice were treated with 300 mg/kg APAP (10 µl/g) (Sigma-Aldrich Chemical Company) in sterile saline or sterile saline vehicle alone, by i.p. injection. Mice were monitored for general appearance, mobility, and survival at 12, 24, and 48 hours after treatment. Serum, liver sections, and RNA were collected at 48 hours from WT, $Mer^{-/-}$, and $Axl^{-/-}$ mice.

In addition to using Axl mutant mice, we conducted studies with the Axl receptor inhibitor, LDC1267. For these studies, mice were fasted in clean cages for 16 hours (overnight) before the injection the following morning. LDC1267 is a highly selective Axl inhibitor and 20 mg/kg i.p. daily has been shown to inhibit Axl receptor function (Paolino et al., 2014). LDC1267 was purchased from Cayman Chemical. For these experiments, 10-12-week-old male C57BL/6J wild-type mice were treated with 300 mg/kg APAP by i.p. injection and received either LDC1267 or DMSO vehicle 24 and 48 hours after APAP treatment. At 72 hours, serum, liver sections, and RNA were collected.

For treatment with recombinant Gas6, 10-12-week-old male C57BL/6J wild-type mice were fasted in clean cages for 12 hours before the injection the following morning. Two hours prior to the APAP injection, mice were pre-treated with recombinant Gas6 or vehicle. Full-length recombinant Gas6 was purchased from R&D Systems. Mice were then treated with 600 mg/kg

APAP. Liver, blood, and RNA were collected from the mice 24 hours following the APAP injection.

To examine the importance of Axl in KCs, KC-specific Axl mutant mice were generated by using Cre/Lox recombination. To accomplish this, Clec4f$^{em1(cre)Glass}$ (Jackson Laboratories) were crossed with Axl$^{flx/flx}$ mice. C-Type Lectin Domain Family 4 Member F, or Clec4f, is expressed selectively in KCs, and therefore, in Clec4f$^{em1(cre)Glass}$ mice, Cre expression is restricted to KCs in the liver. Axl$^{flx/flx}$ mice were generously provided by Dr. Carla Rothlin (Yale University). Mice were fasted in clean cages for 16 hours (overnight) before injection the following morning. Axl$^{flx/flx}$ Clec4f Cre+ mice and Axl$^{flx/flx}$ Clec4f Cre- mice were treated with 300 mg/kg APAP in sterile saline by i.p. injection. Liver, blood, and RNA were collected from the mice 24 hours following the APAP injection. All studies were approved by the Michigan State University Institutional Animal Care and Use Committee.

3.3.2 Sample Collection. Mice were anesthetized using Fatal-Plus Solution (Vortech Pharmaceuticals) or isoflurane. Blood was collected from the inferior vena cava and the livers were removed. A portion of each liver was fixed in 10% neutral-buffered formalin. The livers were embedded in paraffin, sectioned, and stained with hematoxylin and eosin. The area of necrosis was quantified as described by us previously (Mochizuki et al., 2014). Additional portions of the liver were homogenized in TRIzol Reagent (Thermo-Fisher Scientific) for RNA isolation or were snap-frozen in liquid nitrogen for sectioning and immunofluorescence staining.

3.3.3 Cell Isolation and Culture. KCs were isolated from livers of C57BL/6 mice and were perfused and digested with collagenase (Collagenase H; Sigma-Aldrich), as described previously (Roth et al., 2019). Briefly, following removal of hepatocytes by centrifugation, the nonparenchymal cells were centrifuged at 300xg for 10 minutes. Nonparenchymal cells were re-suspended in 180 µL of MACS Buffer (2.5 g bovine serum albumin, 0.416 g EDTA, and 500 mL phosphate-buffered saline) and 20 µL biotinylated anti-F4/80 antibody (Miltenyi Biotec, Bergisch Gladbach, Germany). The cell suspension was incubated for 10 minutes at 4°C and then

washed by adding 10 mL of MACS buffer and centrifugation (300×g for 10 minutes). The cell pellet was re-suspended in 180 µL of MACS Buffer and 20 µL streptavidin microbeads (Miltenyi Biotec). Cells were incubated at 4°C for 10 minutes and then washed by adding 10 mL of MACS buffer and centrifugation (300×g for 10 minutes). The pellet was resuspended with 500 µL MACS buffer and applied to MACS LS columns (Miltenyi Biotec). The column was rinsed three times with 3 mL MACS buffer. KCs were collected by removing the column from the midiMACS Separator (Miltenyi Biotec) and rinsing the column with 5 mL of MACS buffer.

For cell treatments, KCs were plated in 12 well tissue-culture treated plates in Williams E medium supplemented with FBS and Pen-Strep. Cells were allowed to attach for 2 hours. Following incubation, cells were switched to serum-free Williams E medium and treated with either ODN 1585 or ODN 1668. ODN 1585 and ODN 1688 are Tlr9 agonists.

3.3.4 Real-Time PCR. RNA was isolated from liver samples using TRIzol Reagent (Thermo-Fisher Scientific) or from cell culture samples by using the E.Z.N.A Total RNA Kit I (Omega Bio-Tek) according to manufacturer's instructions. Real-time PCR was performed as described by us previously (Kim, 2006). The following primer sequences were used: Tnf-α: Forward- 5'-AGGGTCTGGGCCATAGAACT-3', Reverse- 5'-CCACCACGCTCTTCTGTCTAC-3'; Ccl2 (MCP1): Forward- 5'-CCTGCTGTTCACAGTTGCC-3', Reverse- 5'-ATTGGGATCATCTTGCTGGT-3'; Il-10: Forward- 5'-TGTCAAATTCATTCATGGCCT-3', Reverse- 5'-ATCGATTTCTCCCCTGTGAA-3'; Rpl13a: Forward- 5'-GACCTCCTCCTTTCCCAGGC-3', Reverse- 5'-AAGTACCTGCTTGGCCACAA-3'; MMP12: Forward-5'-TTTGGATTATTGGAATGCTGC-3', Reverse-5'- ATGAGGCAGAAACGTGGACT-3'; Cd5l (AIM): Forward-5'-TTTGTTGGATCGTGTTTTTCAGA-3', Reverse-5'-CTTCACAGCGGTGGGCA-3'; Ccl5 (RANTES): Forward-5'- GTGCCCACGTCAAGGAGTAT-3', Reverse-5'- CCCACTTCTTCTCTGGGTTG-3'; Il1β: Forward-5'- CCTCTCCAGCCAAGCTTCC-3', Reverse-5'-CTCATCAGGACAGCCCAGGT-3'.

3.3.5 Flow Cytometry. To isolate non-parenchymal cells, mouse livers were perfused and digested with collagenase (Collagenase H, Sigma Chemical Company) as described previously(16). Hepatocytes were removed by centrifugation and non-parenchymal cells were collected after centrifugation at 300 *g* for 10 minutes. Non-parenchymal cells were washed and resuspended in FACs buffer (phosphate-buffered saline, 1% fetal bovine serum). The cells were then incubated with Fc blocking buffer (BD Biosciences; diluted 1:20) for 10 minutes at 4 °C, rinsed, and then pelleted by centrifugation at 300 *g* for 5 minutes. The cells were incubated with the following anti-bodies for 30 minutes at 4°C: anti-F4/80 conjugated to Alexa Fluor-488 and anti-Ly6C conjugated to phycoerythrin (PE), anti-Axl (PE), anti-CD45.1 (PE/Cyanine7), anti-F4/80 (Alexa Fluor-594), anti-Cx3cr1 (Alexa Fluor-700), anti-Ly6G (APC/Cyanine7), and anti-Cd11b (Brilliant Violet 605). All antibodies were purchased from Biolegend, except anti-Axl, which was purchased from Invitrogen. The fixable dye, Zombie Aqua, was used to determine cell viability. Following incubation, cells were washed twice and fixed in formalin (Sigma) for 15 minutes at 4°C. The fixed cells were washed twice and resuspended in FACs buffer. An Attune NxT flow cytometer (Life Technologies) was then used to measure fluorescence. Signal was quantified using Attune NxT software.

3.3.6 Soluble Axl. ELISA for measurement of sAxl (R&D Systems) was performed according to the manufacturer's instructions.

3.3.7 ALT Assay. ALT (TR71121) assay was from Thermo Fisher Scientific and was performed according to the manufacturer's instruction.

3.3.8 Processing of Liver Sections. Livers were removed and a portion was fixed in 10% neutral-buffered formalin. The tissues were embedded in paraffin, and sections of liver were stained with hematoxylin and eosin (H&E).

3.3.9 Immunofluorescence. Immunofluorescence was used to detect Axl, Mer, F4/80, CD31 and DAPI as described by Zagórska et al. (2020). The following antibodies were used for

immunostaining: Mer (DS5MMER; eBioscience), Axl (AF854; R&D Systems), CD31 (ab28364; Abcam), Caspase 3 (Asp175; Cell Signaling), MMP12 (MAF-32011; Invitrogen), CD68 (A1957F; Serotec), and F4/80 (MCA497; AbD Serotec).

Immunofluorescence was used to detect α-hemoglobin. Briefly, 8 μm sections were cut from frozen livers and fixed for 10 minutes in 4% formalin. The sections were then incubated in blocking buffer (10% goat serum) followed by incubation with hemoglobin alpha recombinant antibody (Invitrogen SN70-09) diluted 1:500. After washing, the sections were incubated with goat anti-rabbit secondary antibody conjugated to Alexa Fluor 488 (diluted 1:500, Thermo Fisher Scientific).

3.3.10 Statistical Analysis. Results are presented as the mean + SEM. Data were analyzed by a one-way or two-way Analysis of Variance (ANOVA) where appropriate. Data expressed as a percentage were transformed by arcsine square root prior to analysis. Comparisons among group means were made using the Student-Newman-Keuls test. The criterion for significance was $p < 0.05$ for all studies.

3.4 Results

3.4.1 Axl and Mer are Predominately Expressed in KCs in Mouse Liver Under Steady-State Conditions. Immunofluorescence was used to detect Axl and Mer in the adult mouse liver (Figure 3.1). Axl and Mer were detected on most KCs (Figure 3.1A and 3.1B) (Zagórska et al., 2020). Axl was detected on vascular endothelial cells but not on sinusoidal endothelial cells (Figure 3.1C). By contrast, Mer was detected on most CD31+ endothelial cells within the liver (Figure 3.1D).

3.4.2 Axl is activated in the Liver following APAP-Induced Liver Injury. Activation of the Axl tyrosine kinase triggers downstream metalloprotease cleavage of the Axl extracellular domain from the cell surface and the generation of soluble Axl (sAxl) (Lemke, 2013) (Zagórska et al, 2014) (Orme et al, 2016). Correspondingly, we measured elevation of circulating sAxl in serum 48 h after APAP treatment of WT mice (Figure 3.2E). Circulating sAxl was significantly elevated in APAP-treated mice compared to vehicle controls (Zagórska et al., 2020).

3.4.3 Role of Axl and Mer in Resolution of Hepatocellular Injury and Inflammation after APAP Overdose in Mice. To test the hypothesis that Axl and/or Mer are critical for resolution of inflammation after APAP overdose, WT, $Axl^{-/-}$, and $Mer^{-/-}$ mice were treated with 300 mg/kg APAP. Although resolution of inflammation occurs between 48 and 72 hours after APAP, we found that our studies of APAP-treated mice beyond 48 h after drug administration were precluded by the remarkably strong phenotype that we observed specifically in $Axl^{-/-}$ mice (Zagórska et al., 2020). In two independent experimental series, both WT and $Mertk^{-/-}$ mice were motile and superficially normal at 12, 24, and 48 h after APAP, but most $Axl^{-/-}$ mice were very sick and nonmotile across all of this period (Zagórska et al., 2020). Strikingly, 30% of Axl KO mice died by 48 hours after treatment with a dose of APAP (i.e., 300 mg/kg) that is typically nonlethal. Examination of the livers of APAP-treated mice at 48 hours after drug administration revealed massive hemorrhage specifically in the $Axl^{-/-}$ mice (Figure 3.2B) (Zagórska et al., 2020). A typical $Axl^{-/-}$ APAP-treated liver *in situ*, seen in 60% of treated mice, is shown in

Figure 3.2A. Histological staining of liver sections 48 h posttreatment revealed substantial congestion and hemorrhage within the $Axl^{-/-}$ but not WT or $Mertk^{-/-}$ liver parenchyma (Zagórska et al., 2020).

Serum levels of ALT were markedly elevated at 48 h after APAP, specifically in $Axl^{-/-}$ relative to WT and $Mertk^{-/-}$ mice (Figure 3.2C) (Zagórska et al., 2020). While APAP intoxication is primarily associated with necrosis, APAP-treated $Axl^{-/-}$ livers also displayed elevated numbers of cells with cleaved Caspase 3+ (cCasp3) compared to wild-type (Figure 3.2D) (Zagórska et al., 2020). We did not detect significant changes in the mRNA levels of either pro- or anti-inflammatory cytokines (i.e., Cd5l, Il10, Il1-β, Ccl2, Ccl5, or Tnf-α) in $Axl^{-/-}$ versus either WT or $Mertk^{-/-}$ livers, indicating that the enhanced liver injury in APAP-treated $Axl^{-/-}$ was not due to enhancement of inflammation (Figure 3.2F) (Zagórska et al., 2020).

3.4.4 Impaired Upregulation of MMP12 in the Livers of APAP-treated Axl Knockout Mice. A recent study by Kopec and colleagues documented increased hemorrhage and liver injury in $MMP12^{-/-}$ mice after APAP treatment mirroring histopathological changes occurring in $Axl^{-/-}$ mice (2017). This suggested that Axl activation may lead to upregulation of MMP12 after APAP overdose. Therefore, we quantified MMP12 mRNA levels to determine whether they were affected in APAP treated Axl knockout mice. As shown in Figure 3.2F, MMP12 was upregulated in the livers of WT and Mer knockout mice after APAP overdose. MMP12 levels, however, were substantially lower in $Axl^{-/-}$ mice treated with APAP (Figure 3.2F) (Zagórska et al., 2020).

3.4.5 MMP12 mRNA expression reduced in KC-specific $Axl^{-/-}$ mice. To determine if Axl activation on KCs mediates expression of MMP12 and is protective against hemorrhage, KC-specific Axl mutant mice were treated with 300 mg/kg APAP for 24 hours. We quantified MMP12 mRNA levels from livers isolated from these mice. As shown in Figure 3.7A, MMP12 mRNA expression is reduced in KC-specific $Axl^{-/-}$ mice. Interestingly, though, there was no difference in serum ALTs between KC-specific $Axl^{-/-}$ and control mice (Figure 3.7B).

Furthermore, examination of livers following treatment with 300 mg/kg APAP did not reveal the presence of hemorrhage in the KC-specific $Axl^{-/-}$ mice, indicating KC specific Axl activation may not protect against hemorrhage (data not shown). However, these studies are preliminary and need to be repeated.

3.4.6 Hepatic Expression of Axl and Mer in Mice with APAP-induced. We previously showed that recruited monocytes fail to clear dead cell debris from the livers of mice treated with a dose of APAP (i.e., 600 mg/kg) that recapitulates many of the pathological features of ALF in patients. Our findings above indicate that inhibition of Axl may reduce clearance of dead cells from the APAP injured liver resulting in sustained cytokine production. This suggests the possibility that impaired phagocytosis of dead cells by MDMs in mice with APAP-induced ALF may result from impaired Axl signaling. To examine this, we first quantified levels of Axl, and its primary ligand, Gas6, in mice treated with APAP. As shown in Figure 3.3, Axl mRNA was up-regulated 14-fold by 48 hours after treatment of mice with 300 mg/kg APAP. Interestingly, this represents a time when proinflammatory monocytes are accumulating in the liver. In these mice, Gas6 was upregulated in the liver and peaked at 24 hours (Figure 3.5A). In mice treated with 600 mg/kg APAP, Axl mRNA levels were increased compared to control mice, however, at 48 and 72 hours after treatment, Axl mRNA levels were markedly lower when compared to mice treated with 300 mg/kg APAP (Figure 3.3). Similarly, Gas6 mRNA levels were increased in mice treated with 600 mg/kg APAP at 24 hours after treatment, however, to a lesser extent when compared to mice treated with 300 mg/kg APAP (Figure 3.5A).

To identify the cells that express Axl, we isolated the non-parenchymal cell fraction from the livers of mice treated with either 300 mg/kg or 600 mg/kg APAP and labeled the cells with antibodies against F4/80, Ly6C, CD146, Cx3Cr1, Ly6G, Cd11b, CD11c, CD45, and Axl. We then analyzed the cells by flow cytometry (Supplementary Figure 1). As shown in Figure 3.4, Axl was expressed on F4/80+ cells (i.e., KCs), Ly6C+ cells (i.e., MDMs), Ly6G+ cells (i.e., neutrophils), Cx3Cr1+ cells, CD11b+ cells, and CD146+ cells (i.e., sinusoidal endothelial cells).

Interestingly, Axl expression on Ly6C+ cells, CD11b+ cells, and Cx3CR1+ cells was lower in mice treated with 600 mg/kg APAP when compared to mice treated with 300 mg/kg APAP (Figure 3.4). To our knowledge, our study is the first to report Axl on neutrophils.

3.4.7 Impact of Axl Inhibition on Late Phases of Repair in Mice Treated with APAP. To by-pass the early impact on liver injury in Axl KOs, WT mice were treated with the Axl receptor inhibitor, LDC1267, or vehicle beginning at 24 hours after treatment with 300 mg/kg APAP (Figure 3.8A). The area of liver necrosis at 48 hours after APAP treatment was not different between mice treated with vehicle or LDC1267 (Figure 3.8D). In mice treated with APAP and vehicle, the area of necrosis decreased from 48 to 72 hours indicating clearance of necrotic cells by MDMs (Figure 3.8D). In mice treated with APAP and LDC1267, however, the area of necrosis at 72 hours was not different from that at 48 hours suggesting impairment of dead cell clearance by MDMs (Figure 3.8D). The reduced clearance of dead cells was not the result of impaired recruitment of MDMs, as there was no difference in accumulation of CD68+ MDMs (Figure 3.9A and C). Further, proinflammatory cytokine mRNA levels (i.e., Ccl2 and TNFα) were higher in mice treated with APAP and LDC1267 at 72 hours, suggesting that termination of proinflammatory cytokine expression was disrupted in these mice (Figure 3.8E-F). We showed previously that as MDMs remove necrotic cells, they begin to express F4/80. In mice treated with APAP and vehicle, MDMs stained positive for F4/80 by 72 hours. By contrast, lower levels of F4/80 were observed in MDMs in mice treated with APAP and LDC1267 (Figure 3.9B and D).

3.4.8 Impact of Restoring Gas6 on MMP12 levels in APAP-induced ALF. Our studies above demonstrate that activation of Axl is important for upregulation of MMP12 after treatment of mice with 300 mg/kg APAP (Figure 3.2F). Interestingly, MMP12 levels are substantially lower in mice treated with 600 mg/kg APAP at 24 hours, a time where levels of the Axl ligand, Gas6 levels, are also reduced (Figure 3.3 B and 3.5A). Based upon these findings, we tested the hypothesis that reduced Gas6 levels contribute to the failure of MMP12

upregulation in mice with APAP-induced ALF and that this contributes to the substantial hemorrhage and congestion observed in the livers of these mice. To restore Gas6 levels, we treated mice that received APAP with recombinant Gas6 (rGas6). Importantly, restoration of Gas6 in these mice significantly increased MMP12 expression, suggesting the Gas6/Axl pathway is a critical regulator of MMP12 in this setting (Figure 3.5A).

3.4.9 Tlr9 Activation Suppresses Expression of Gas6 and Axl *In Vitro.* Tlr9 activation has been shown to suppress expression of Gas6 (Deng et al. 2012). To determine if activation of Tlr9 in KCs lead to decreased mRNA expression of Gas6 and Axl *in vitro*, KCs were isolated from wild-type mice. Treatment of KCs with two different Tlr9 agonists (ODN 1585 and ODN 1668; 5μM) led to decreased expression of Gas6 (Figure 3.10)

3.5 Discussion

Collectively, our results demonstrate that Axl alone plays a hepatoprotective role following APAP-induced acute liver injury. Our results in Mer mutant mice mirror what has been previously reported in APAP treated mice, where Mer mutants display only a ~1.4-fold increase in necrotic cells 24 hours after APAP administration (Triantafyllou et al, 2018). Similarly to Triantafyllou and colleagues, we show that Mer plays a modest role in hepatic repair following APAP-induced acute liver injury (Figure 3.2) (2018) (Zagórska et al., 2020). In our studies, liver injury in $Mer^{-/-}$ mice was comparable to wild-type APAP treated mice, with no statistical difference in ALTs (Zagórska et al., 2020). Histological assessment of $Mer^{-/-}$ mice revealed no signs of hemorrhage 48 hours following treatment with APAP (Zagórska et al., 2020). In stark contrast to $Mer^{-/-}$ mice, $Axl^{-/-}$ mice were at or near death 48 hours following treatment with a dose of APAP at which the liver should repair (Zagórska et al., 2020). Specifically, by 48 hours, 30% of $Axl^{-/-}$ mice had died. Histopathological analysis revealed extensive hepatocellular necrosis and sinusoidal congestion and hemorrhage in surviving $Axl^{-/-}$ mice (Figure 3.2B) (Zagórska et al., 2020). Strikingly, despite the presence of increased hepatic injury in surviving $Axl^{-/-}$ mice, there were no significant differences in cytokine mRNA levels (Zagórska et al., 2020). However, the higher death rate in $Axl^{-/-}$ mice complicates interpretation of this finding.

As noted above, approximately 30% of $Axl^{-/-}$ died before the 48 hour timepoint. This result was unexpected, as death rarely occurs following treatment with the 300 mg/kg APAP dose. However, the severity of injury that occurred in Axl mutant mice suggests Axl signaling plays a vital role in hepatic repair following acute liver injury, and that this role is not simply limited to macrophage polarization. Interestingly, surviving $Axl^{-/-}$ mice had significantly decreased mRNA expression of MMP12 as compared to wild-type mice treated with the same dose of APAP (Figure 3.2F) (Zagórska et al., 2020). Studies have shown MMP12 expression levels are increased in the liver following APAP-induced acute liver injury, and deletion of MMP12 in this setting is linked to increased sinusoidal congestion, hemorrhage, and

hepatocellular necrosis (Kopec et al, 2017). Importantly, several studies have shown that Axl regulates MMPs, including MMP 1, 2, 3, and 9 and over-expression of Axl in cancer cells has been shown to preferentially upregulate both MMP12 and MMP13 (Tai et al., 2009) (Divine et al., 2016) (Kimani et al., 2016). The mechanism by which MMP12 functions to maintain sinusoidal integrity in APAP-induced acute liver injury is not currently known; however, our studies suggest Axl is a critical regulator of MMP12. We hypothesized that Axl activation on KCs was protective in this setting and played a critical role in limiting sinusoidal destruction by increasing levels of MMP12 (Zagórska et al., 2020). To investigate whether Axl activation on KCs regulated expression of MMP12 during APAP-induced acute liver injury, we generated KC-specific Axl mutant mice. Following treatment with 300 mg/kg APAP, MMP12 mRNA expression was reduced in KC-specific Axl mutants (Figure 3.7A). However, upon examination of the livers of KC-specific Axl mutants, hemorrhage was not present (data not shown). MMP12 immunostaining of wild-type livers revealed MMP12 was present in multiple cell types in the liver following treatment with 300 mg/kg APAP, thus Axl regulation of MMP12 by another cell type may be important for limiting hemorrhage (Figure 3.7). However, these results are preliminary, and these studies need to be repeated to definitively rule whether Axl activation on KCs is hepatoprotective in this setting.

While the role of Mer had previously been investigated in the APAP model, no studies had investigated the role of Axl in APAP-induced ALF (Triantafyllou et al, 2018). However, studies in patients with acute-on-chronic liver failure have revealed decreased mRNA expression of Axl as compared to healthy individuals (Bernsmeier et al., 2017). To determine if suppression of Axl also occurs in APAP-induced ALF, we measured mRNA expression of Axl in both the APAP acute liver injury and APAP acute liver failure mice over a period of 72 hours. While mRNA expression was only slightly lower between the two doses at 24 hours, it was strikingly different at later time points. As shown in Figure 3.3, Axl mRNA is up-regulated 14-fold at 48 hours in mice treated with 300 mg/kg APAP. This upregulation failed to occur at the

600 mg/kg dose. Interestingly, these later timepoints coincide with the time when proinflammatory monocyte differentiation and phagocytosis are occurring under conditions of normal hepatic repair.

Studies have shown Axl signaling promotes both macrophage polarization and clearance of dead cells in inflammatory environments, thus decreased expression of Axl in the ALF mouse model could contribute to impaired phagocytosis and failed monocyte differentiation in these mice. The dramatic effects of APAP treatment in the $Axl^{-/-}$ mice precluded assessment of these endpoints in the knock-out mice. Thus, to investigate the role of Axl in these processes, we opted to by-pass the early impact on liver injury in $Axl^{-/-}$ mice by pharmacologically inhibiting Axl 24 hours after APAP treatment (Figure 3.8). Treatment of mice with an Axl inhibitor, LDC1267, both 24 and 48 hours following treatment with 300 mg/kg APAP led to increased necrosis, indicating impairment of bone marrow derived macrophage-dependent clearance of dead cells (Figure 3.8C-D). Additionally, proinflammatory cytokine levels were higher in mice treated with LDC1267 and markers of pro-reparative macrophages were reduced (Figure 3.8E-F). Thus, in addition to protecting the liver during the early phases of hepatic injury, Axl also plays a crucial role in repair at later timepoints where Axl signaling mediates bone marrow derived-macrophage dependent clearance of dead cell debris and terminates proinflammatory cytokine synthesis. Collectively, our results suggest Axl signaling is hepatoprotective during both the necro-inflammatory and resolution phases of APAP-induced acute liver injury.

As noted above, whole liver mRNA expression of Axl is suppressed at timepoints critical for hepatic repair in a mouse model of APAP-induced ALF. Furthermore, inhibition of Axl signaling recapitulated many key features of failed hepatic repair in APAP-induced ALF mice including failed clearance of necrosis and a persistent proinflammatory environment. Thus, restoration of Axl signaling may be beneficial in this setting. Axl activation relies not only on the presence of phosphatidyl serine, but also on the presence of its only known ligand, Gas6

(Lemke 2013). Thus, it is possible that the failed induction of Axl in APAP-induced ALF mice occurs directly as a result of suppression of Gas6. To determine if suppression of Gas6 occurs in APAP-induced ALF, we next measured whole-liver mRNA expression of Gas6 in both the APAP acute liver injury and APAP acute liver failure mice over a period of 72 hours. While mRNA expression of Gas6 was lower in ALF mice across all timepoints examined, it was dramatically different at 24 hours with mRNA expression of Gas6 being 15-fold higher in mice that received the lower dose of APAP.

Recently, a study using the LPS/D-GalN model of acute liver injury showed pre-treatment with recombinant Gas6 resulted in reduced neutrophil infiltration and prevented over-production of IL-6, TNF-α, and IL-10 (Wang, Zhao, and Zang, 2020). Like APAP-induced ALF, over-production of IL-6, TNF-α, and IL-10 are associated with a "sepsis-like" response in this model (Wang, Zhao, and Zang, 2020). To determine if restoration of Gas6 is similarly protective in APAP-induced ALF, we pre-treated high dose APAP mice with recombinant Gas6. As shown in Figure 3.5B, restoration of Gas6 in ALF mice recovered MMP12 expression. This important finding highlights the critical role of Gas6/Axl pathway activation in regulating MMP12 following APAP-induced ALF.

The underlying mechanism(s) of Gas6 suppression in this model are currently unknown; however, multiple factors may contribute to decreased Gas6. First, in the liver, Gas6 is primarily expressed by hepatic macrophages. In addition to being expressed on KCs, pro-inflammatory monocytes have been shown to significantly upregulate Gas6 following differentiation (Graubardt et al., 2017). As shown in Chapter 2 Figure 2.4G, flow cytometry analysis of non-parenchymal cell populations isolated from 300 mg/kg and 600 mg/kg APAP mice revealed fewer Ly6c$^+$ cells were present in the livers of the high dose mice at 24 hours. Additionally, these cells failed to change phenotype; thus, failed monocyte differentiation and a reduced hepatic macrophage pool may contribute fewer Gas6 expressing cells in APAP-induced ALF

mice. Secondly, several studies have shown Gas6 is secreted by endothelial cells (Tjwa et al., 2008) (Tutusaus et al., 2020). As indicated by flow cytometry in Figure 3.4C-D, there is a loss of sinusoidal endothelial cells in APAP-induced ALF. Twenty-four hours following APAP treatment, mice treated with the higher dose of APAP had significantly fewer sinusoidal endothelial cells ($CD146^{+}$) as compared to APAP-induced acute liver injury. This loss of sinusoidal endothelial cells in the high dose mice may result in less circulating Gas6, which could go on to activate Axl. Lastly, studies have shown activation of Tlr9 can lead to suppression of Gas6 (Deng et al. 2012). Activation of Tlr9 has been shown to occur in the mouse model of APAP-induced ALF (Imaeda et al., 2009). Specifically, endogenous DNA released from dead hepatocytes activates Tlr9 on sinusoidal endothelial cells (Imaeda et al., 2009). Thus, activation of Tlr9 in these cells may in turn lead to suppressed Gas6 secretion from sinusoidal endothelial cells. Intriguingly, histological analysis of livers from $Tlr9^{-/-}$ mice treated with 500 mg/kg APAP revealed reduced hemorrhage (Imaeda et al., 2009). This finding suggests a mechanism by which Tlr9 activation promotes the suppression of the Gas6/Axl signaling pathway leading to reduced expression and secretion of MMP12 by KCs, resulting in increased hemorrhage. Importantly, KC mRNA expression of Gas6 was reduced following treatment with a Tlr9 agonist *in vitro* (Figure 3.10).

Collectively, these studies reveal that Axl protects the liver from injury early after APAP overdose (Figure 3.6). During the necro-inflammatory phase of APAP-induced acute liver injury, the Axl/Gas6 signaling pathway regulates expression of MMP12, protecting the liver from sinusoidal destruction leading to hemorrhage. At later times, Axl mediates MDM-dependent clearance of dead cell debris and terminate proinflammatory cytokine synthesis (Figure 3.6). Future studies will further investigate the role of Axl in bone marrow derived proinflammatory monocyte populations following APAP-induced acute liver injury using a proinflammatory monocyte specific Axl mutant mouse. Given that Axl plays critical roles in multiple phases of APAP-induced acute liver injury and that expression of Axl is decreased in an experimental

model of APAP-induced ALF, full elucidation of mechanisms regulating Axl signaling following APAP overdose could provide critical insight into immune system dysfunction in ALF patients. Furthermore, our data suggests restoration of Axl signaling could prove to be therapeutically beneficial for ALF patients.

ACKNOWLEDGEMENTS

We thank Dr. Greg Lemke and Dr. Lidia Jimenez-Garcia (Salk Institute) for graciously providing TAM mutant mice and for their assistance in preforming APAP studies in TAM mutant mice. We thank Dr. Carla Rothlin (Yale University) for graciously providing $Axl^{flx/flx}$ mice.

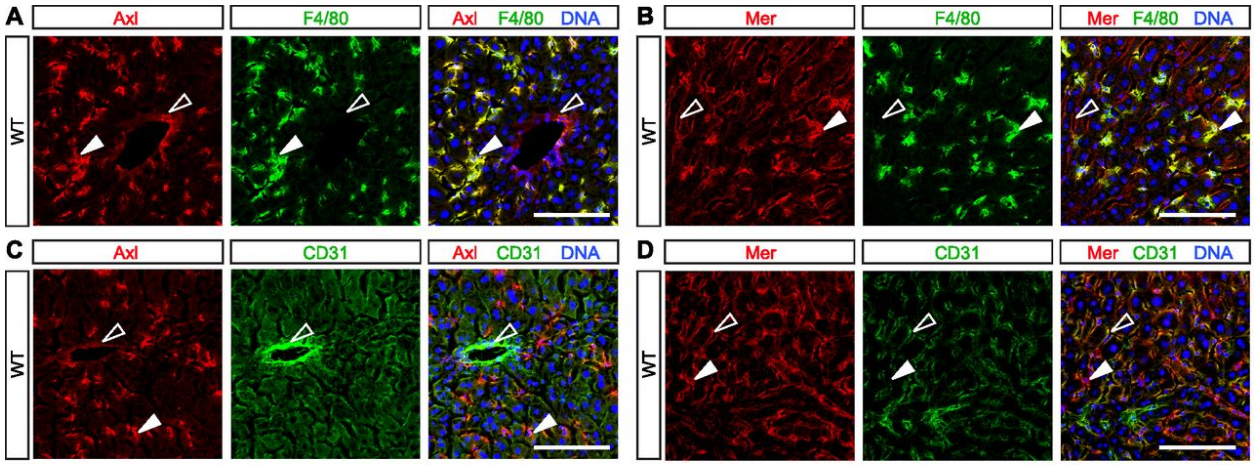

Figure 3.1: Basal TAM expression in normal liver. (A-G) Mouse liver immunohistochemistry (A,C,E) Axl is expressed by F4/80^{+} KCs (closed arrowheads) and strongly CD31^{+} blood-vessel-lining endothelial cells (open arrowheads) . (B,D,F) Mer is expressed by KCs (closed arrowheads), by weakly CD31^{+} sinus-lining endothelial cells (open arrowheads), and very weakly by perivascular macrophages (F, asterisk).

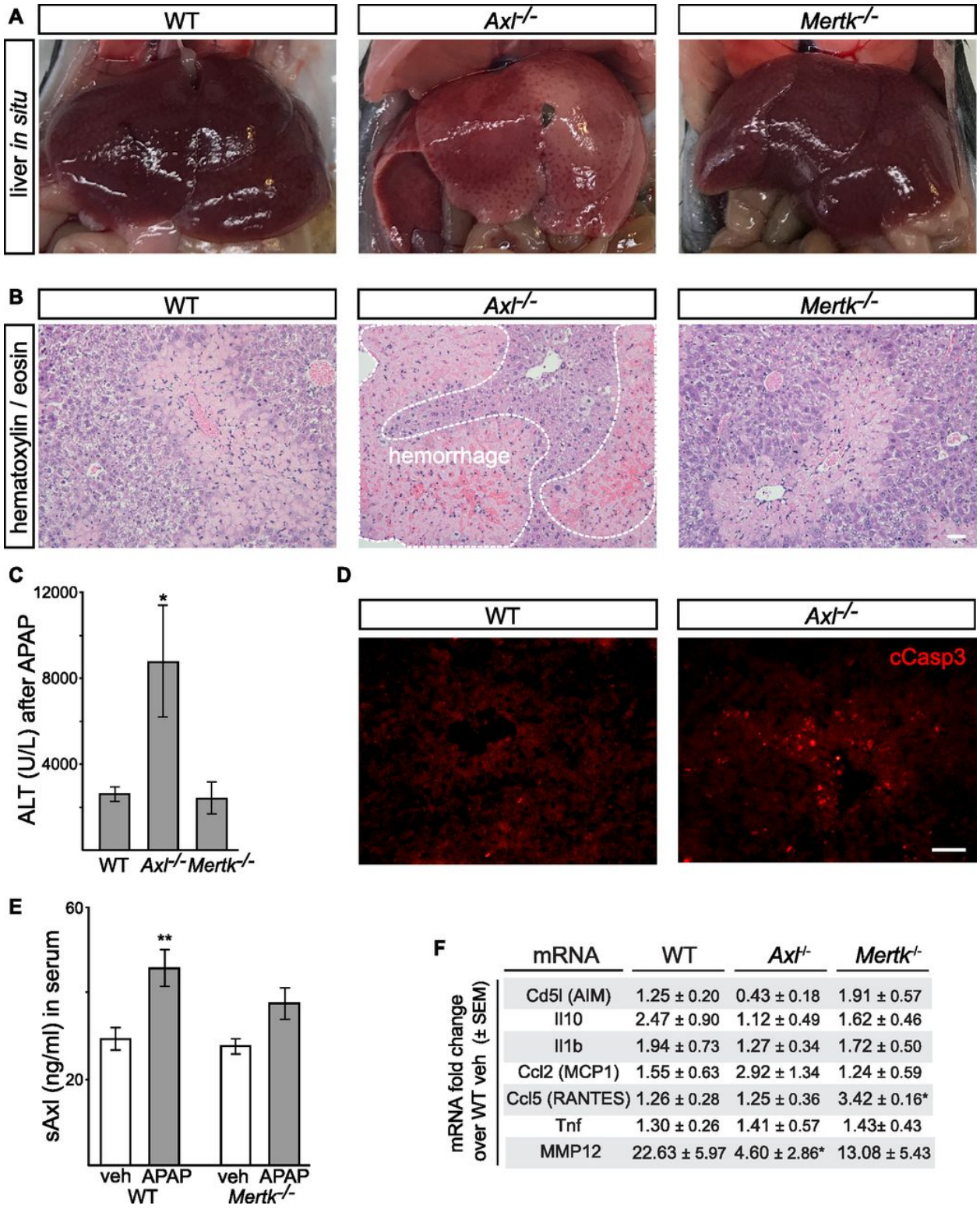

F

mRNA	WT	Axl-/-	Mertk-/-
mRNA fold change over WT veh (± SEM)			
Cd5l (AIM)	1.25 ± 0.20	0.43 ± 0.18	1.91 ± 0.57
Il10	2.47 ± 0.90	1.12 ± 0.49	1.62 ± 0.46
Il1b	1.94 ± 0.73	1.27 ± 0.34	1.72 ± 0.50
Ccl2 (MCP1)	1.55 ± 0.63	2.92 ± 1.34	1.24 ± 0.59
Ccl5 (RANTES)	1.26 ± 0.28	1.25 ± 0.36	3.42 ± 0.16*
Tnf	1.30 ± 0.26	1.41 ± 0.57	1.43± 0.43
MMP12	22.63 ± 5.97	4.60 ± 2.86*	13.08 ± 5.43

Figure 3.2: **Protective role of Axl in APAP intoxication**. (A) Representative images showing extensive hemorrhage and congestion of liver lobes 48 h after administration of acetaminophen

Figure 3.2 (cont'd) (APAP; 300 mg/kg) to Axl−/− but not WT or Mertk−/− mice. These in situ liver images are from non-perfused mice. (B) Representative liver sections from 48 h APAP-treated mice were analyzed by H&E staining. Markedly increased congestion and blood hemorrhage is observed in Axl−/− but not WT or Mertk−/− liver. Bar: 100 μm. (C) Measurement of circulating ALT (U/l, units per liter) 48 h after APAP administration in mice of the indicated genotypes. (D) Immunostaining for cleaved Casp3+ cells in liver sections of WT and Axl−/− mice at 48 h after APAP administration. Bar: 50 μm. (E) Induction of soluble Axl (sAxl) in WT and Mertk−/− mice 48 h after APAP. The trend toward sAxl induction in Mertk−/− mice is not statistically significant. As for all APAP treatments, mice were fasted for 16 h before drug administration. (F) Levels of the indicated mRNAs, isolated livers of the indicated genotypes 48 h after APAP treatment, and quantified by qRT-PCR. *P < 0.05; **P < 0.005. Two-way ANOVA (Bonferroni multiple comparison correction) (C, E); t test (F).

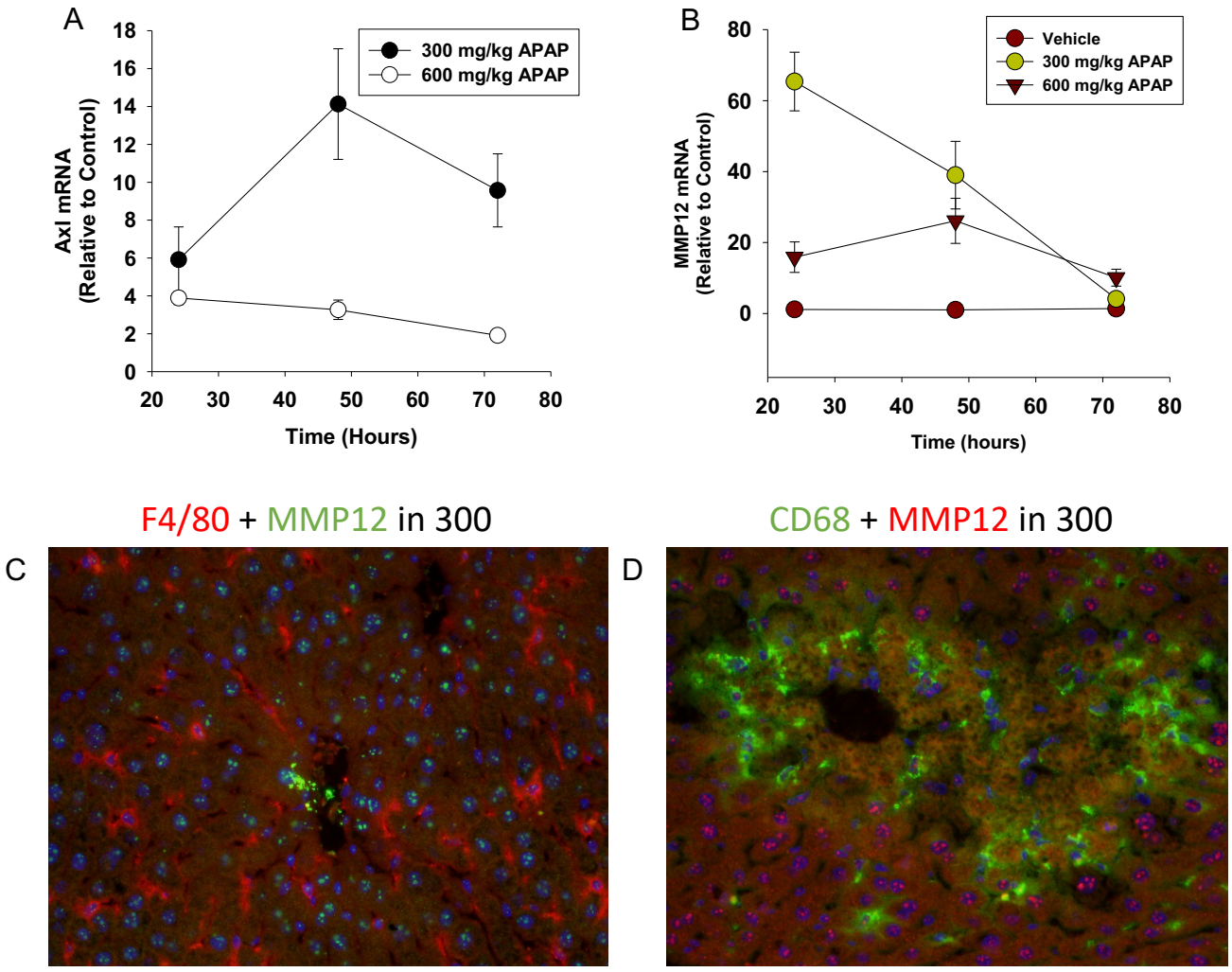

Figure 3.3: MMP12 and Axl expression in livers isolated from mice were treated with 300 or 600 mg/kg APAP. (A)Axl and (B)MMP12 mRNA levels were measured at 24, 48, and 72 hours after APAP treatment with the 300 mg/kg and 600 mg/kg dose. (C-D) Mice were treated with 300 mg/kg APAP for 24 hours. Mouse liver immunohistochemistry for (C) MMP12+F4/80 and (D) CD68+F4/80. Nuclei are stained with DAPI.

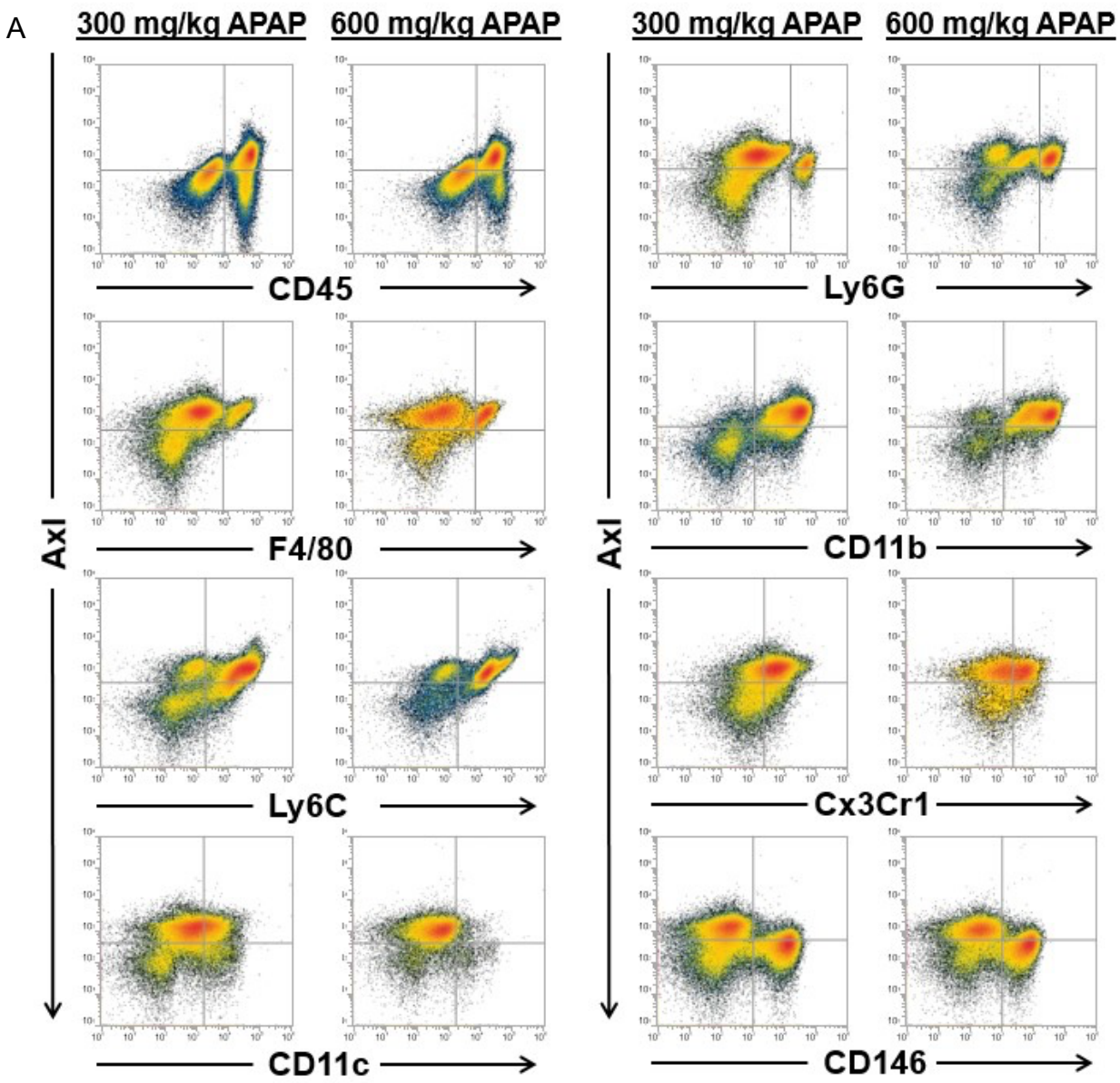
A
300 mg/kg APAP
600 mg/kg APAP
300 mg/kg APAP
600 mg/kg APAP
Axl
CD45
Ly6G
F4/80
CD11b
Ly6C
Cx3Cr1
CD11c
CD146
B
300 mg/kg APAP
600 mg/kg APAP
Cells/gram of Liver
1e+5
8e+4
6e+4
4e+4
2e+4
0
CD45
F4/80
Ly6C
CD11c
Ly6G
CD11b
Cx3Cr1
CD146

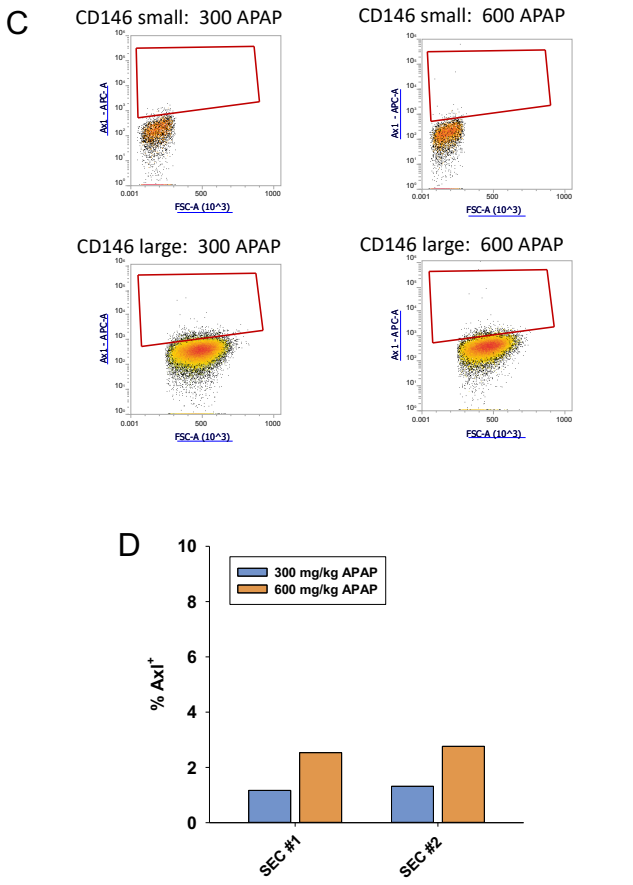

Figure 3.4: Quantification of Axl$^+$ cells present in the liver following APAP treatment. Mice were treated with either 300 mg/kg APAP or 600 mg/kg APAP. (A) At 24 hours after treatment, flow cytometry was used to detect CD45+, Cd11b+, Cd11c+, F4/80+, Ly6C+, Cx3cr1+, CD146+ and Ly6G+ cells in the liver. Boxes indicate the positive gate. (B) Quantification (percent Axl+) of the flow cytometry for each dose of APAP. (C) Flow cytometry was used to detect populations of CD146+ cells in the liver. (D) Quantification (percent Axl+) of the flow cytometry for each dose of APAP.

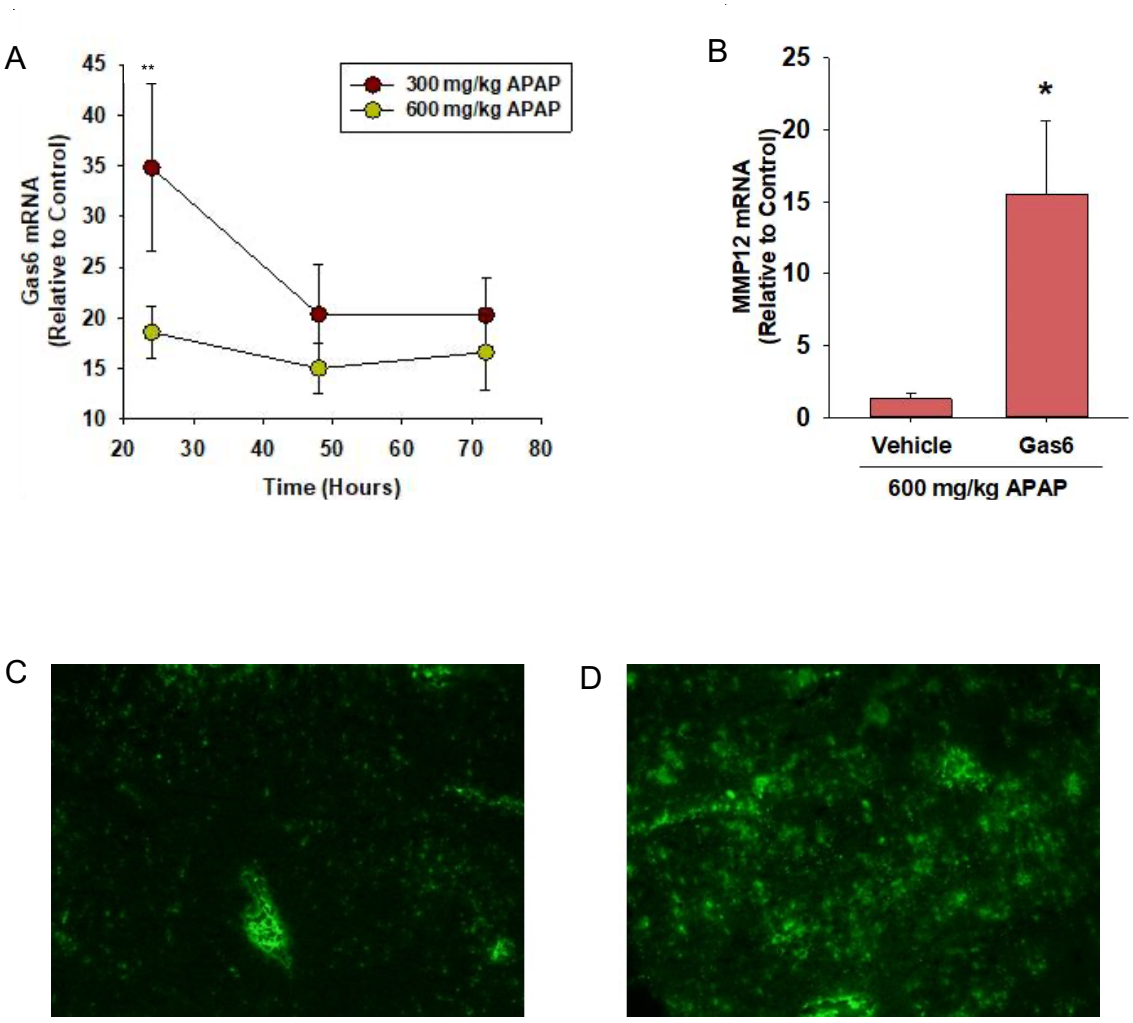

Figure 3.5: Restoration of Gas6 recovers MMP12 expression in mice treated with 600 mg/kg APAP. (A) Gas6 mRNA levels were measured at 24, 48, and 72 hours after APAP treatment. *Significantly different from vehicle-treated mice. **Significantly different from mice treated with 300 mg/kg at the same time point. (B) MMP12 mRNA expression were measured in livers collected from APAP-induced ALF mice treated with recombinant Gas6 or vehicle (saline). *Significantly different from vehicle-treated mice. (C) Immunostaining for α-hemoglobin in liver sections of mice treated with recombinant Gas6 and APAP for 24 hours (D) Immunostaining for α-hemoglobin in liver sections of mice treated with saline control and APAP for 24 hours.

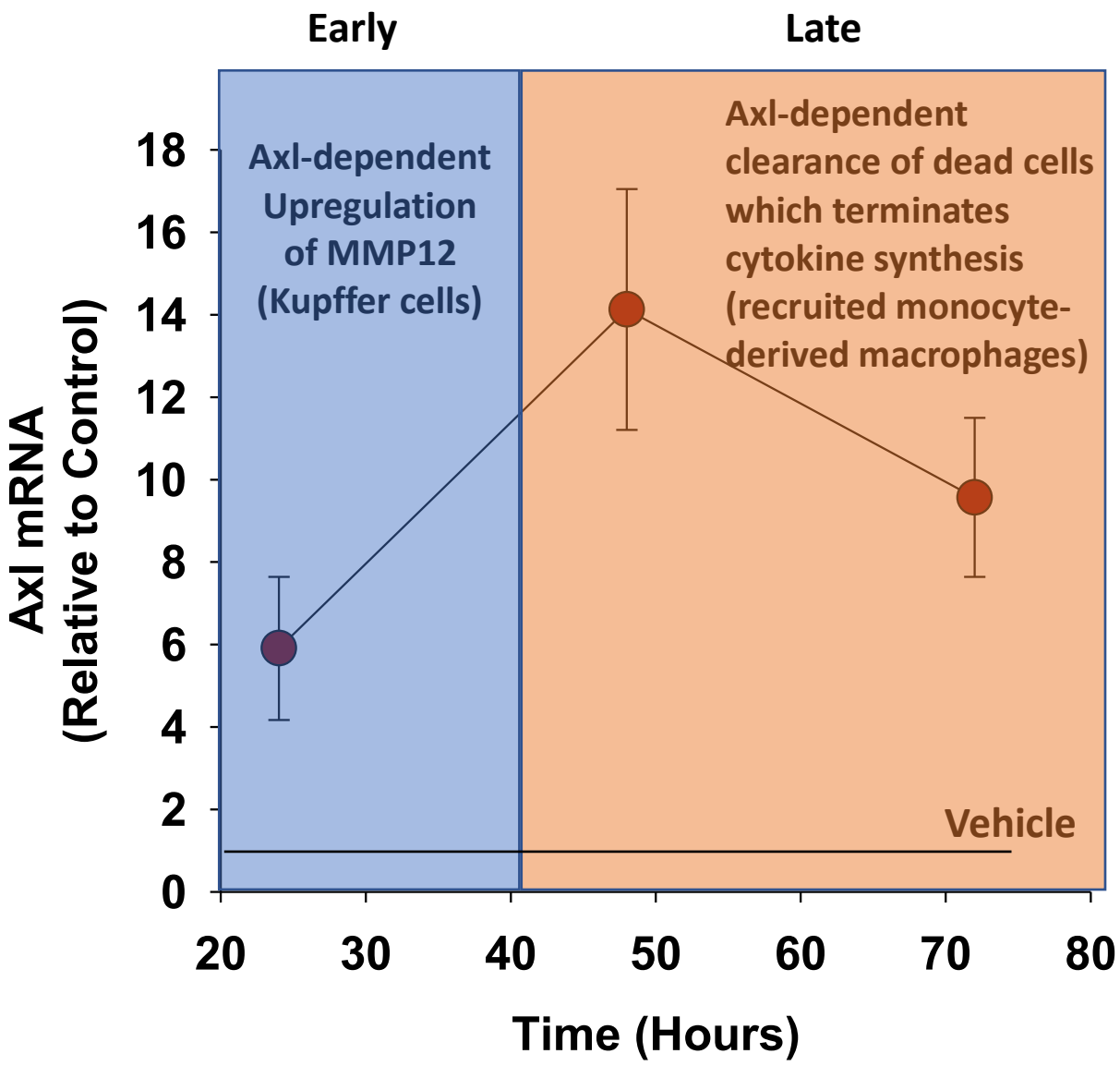

Figure 3.6: Axl is hepatoprotective during both early and late phases of liver injury following APAP overdose.

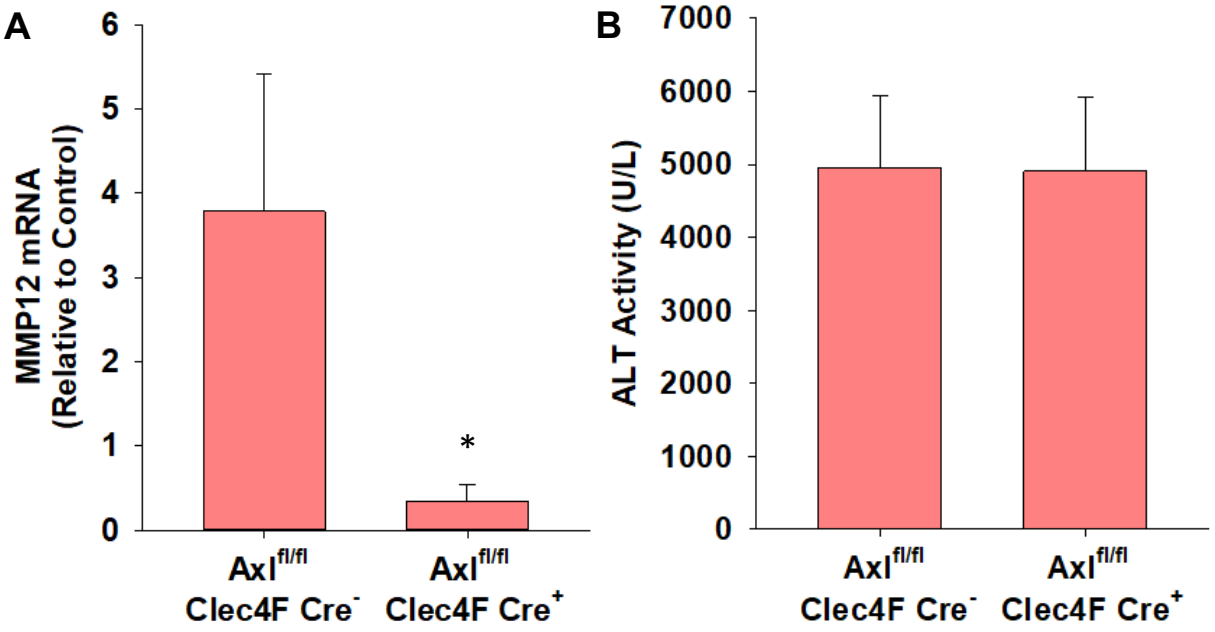

Figure 3.7: MMP12 expression reduced in KC-specific Axl mutant mice. Clec4F Cre^{-} Axl$^{fl/fl}$ and Clec4F Cre^{+} Axl$^{fl/fl}$ mice were treated with 300 mg/kg APAP for 24 hours. (A) MMP12 mRNA levels were measured. (B) Measurement of circulating ALT (U/l, units per liter) 24 h after APAP administration in mice of the indicated genotypes.

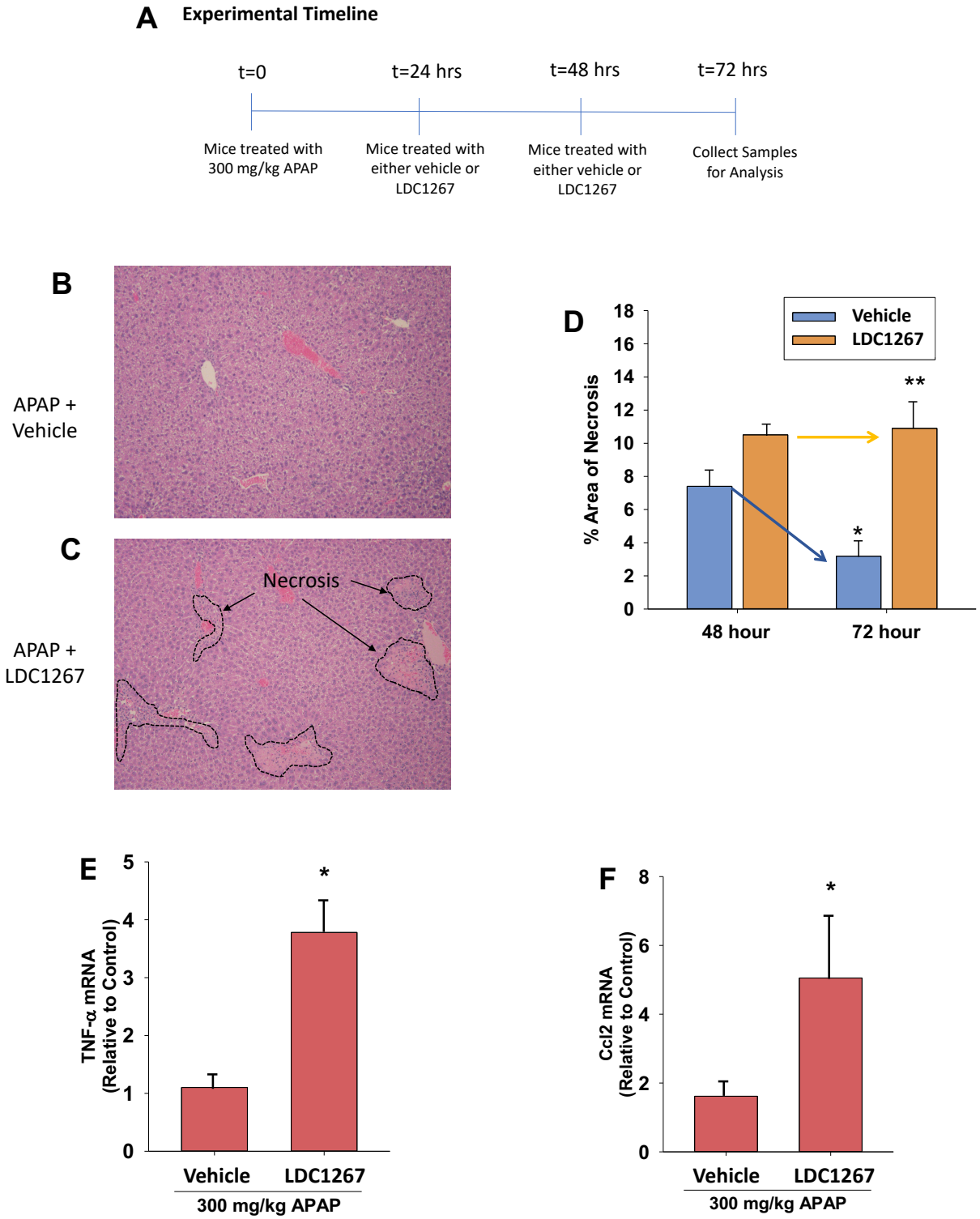

Figure 3.8: Axl inhibition delays late phases of hepatic repair following treatment 300 mg/kg APAP. (A) Experimental timeline of APAP-induced acute liver injury Axl inhibitor studies.

Figure 3.8 (cont'd) (B-C) Representative liver sections from mice treated with either APAP+vechicle or APAP+LDC1267 were analyzed by H&E staining. Areas of necrosis are indicated by the dashed line. (D) Quantification of area of necrosis following treatment with APAP+vechicle or APAP+LDC1267 for 48 and 72 hours. *Significantly different from vehicle-treated mice. (E-F) Ccl2 and TNFα mRNA expression were measured in livers collected from APAP-induced ALF mice treated with vehicle or LDC1267 at 72 hours. *Significantly different from vehicle-treated mice.

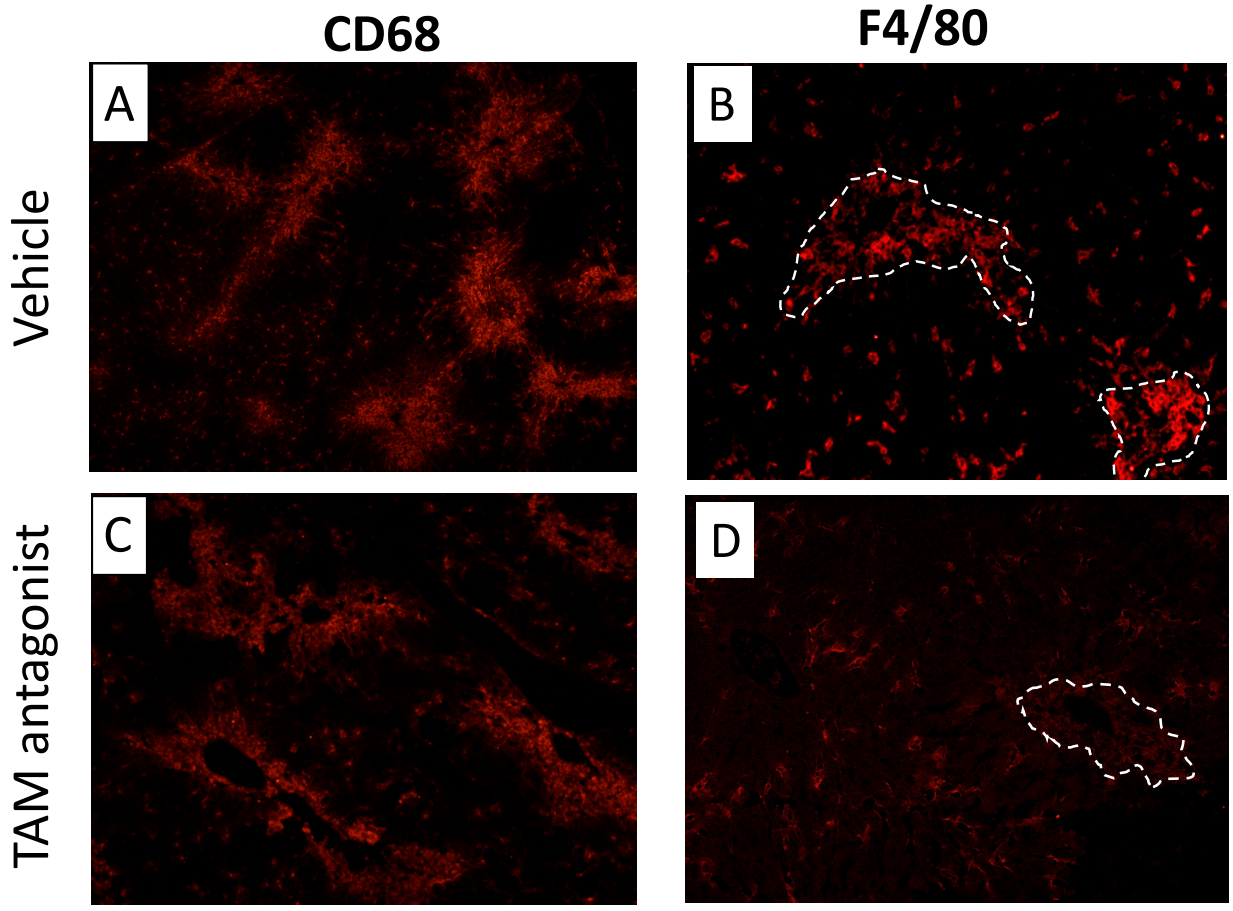

Figure 3.9: Axl inhibition prevents macrophage polarization following treatment 300 mg/kg APAP. Mice were treated with 300 mg/kg for 72 hours. LDC1267, an Axl inhibitor, of the was given 24 and 48 hours following APAP. Livers were isolated 72 hours following APAP treatment. CD68 (A and C) and F4/80 (B and D) were detected by immunofluorescence. Dashed line indicates area of necrosis.

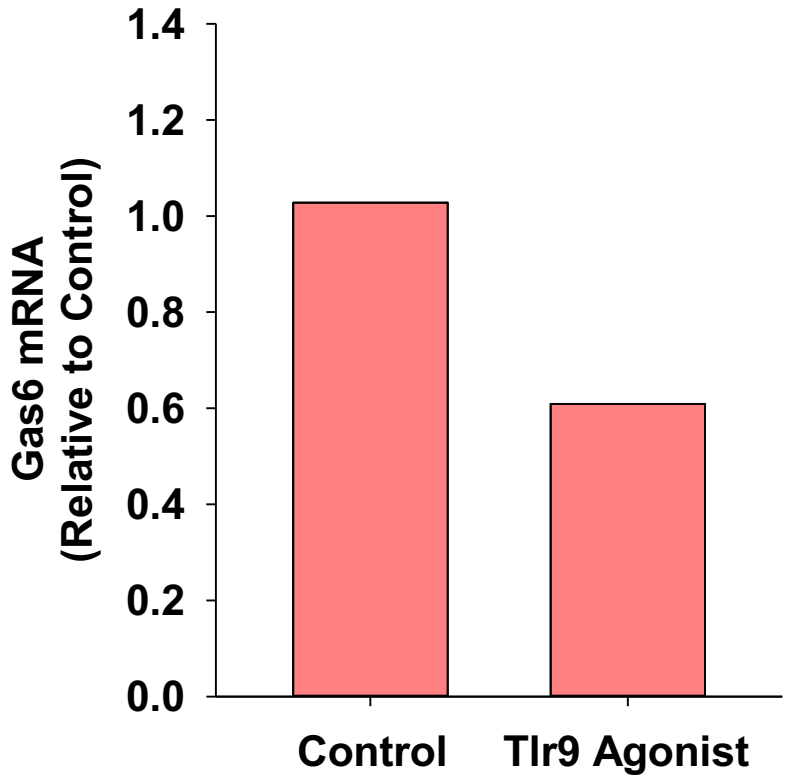

Figure 3.10: Treatment of Kupffer Cells with Tlr9 agonist decreases expression of Gas6.

KCs were isolated from untreated WT mice and treated with a Tlr9 agonist overnight. Gas6 mRNA levels were measured.

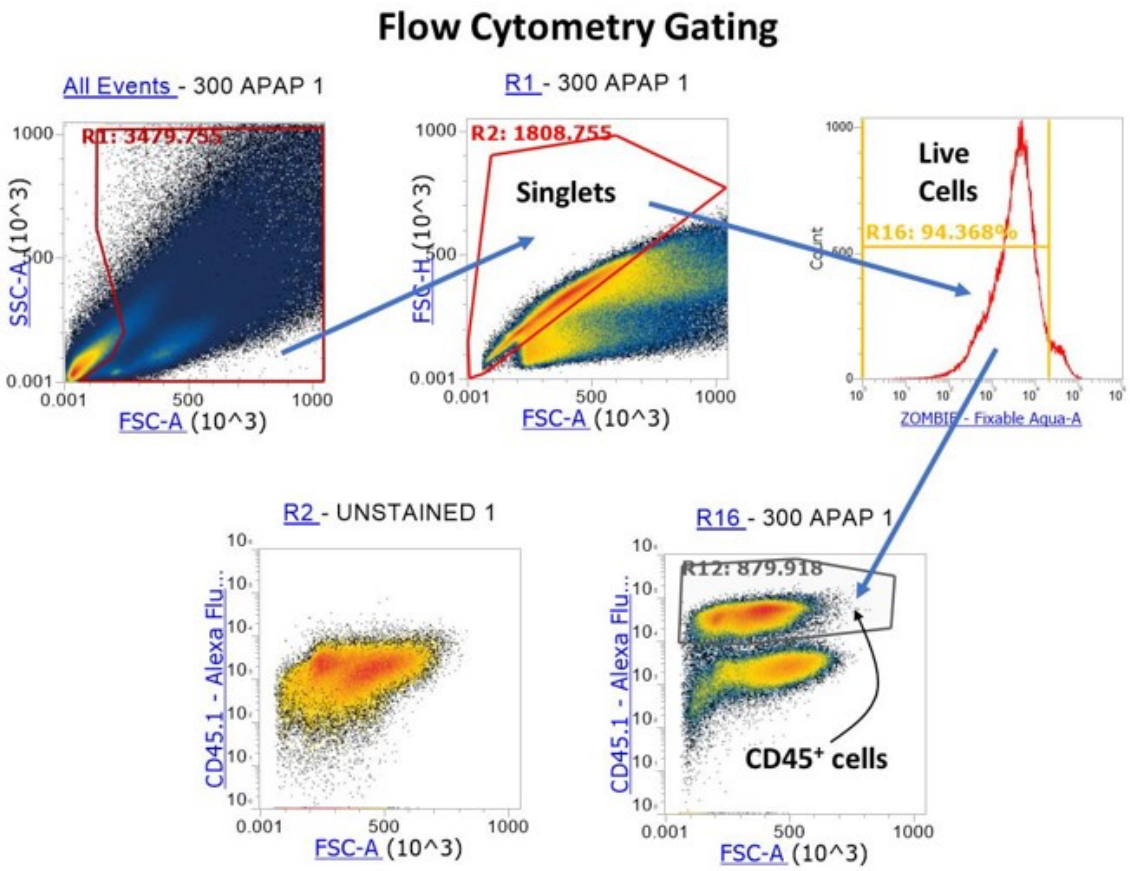

Supplementary Figure 3.1: Gating strategy for flow cytometry.

BIBLIOGRAPHY

Antoniades CG, Berry PA, Wendon JA, Vergani D. The importance of immune dysfunction in determining outcome in acute liver failure. J Hepatol. 2008 Nov;49(5):845-61. doi: 10.1016/j.jhep.2008.08.009. Epub 2008 Aug 21. PMID: 18801592.

Bárcena C, Stefanovic M, Tutusaus A, Joannas L, Menéndez A, García-Ruiz C, Sancho-Bru P, Marí M, Caballeria J, Rothlin CV, Fernández-Checa JC, de Frutos PG, Morales A. Gas6/Axl pathway is activated in chronic liver disease and its targeting reduces fibrosis via hepatic stellate cell inactivation. J Hepatol. 2015 Sep;63(3):670-8. doi: 10.1016/j.jhep.2015.04.013. Epub 2015 Apr 20. PMID: 25908269; PMCID: PMC4543529.

Bernsmeier C, Pop OT, Singanayagam A, Triantafyllou E, Patel VC, Weston CJ, Curbishley S, Sadiq F, Vergis N, Khamri W, Bernal W, Auzinger G, Heneghan M, Ma Y, Jassem W, Heaton ND, Adams DH, Quaglia A, Thursz MR, Wendon J, Antoniades CG. Patients with acute-on-chronic liver failure have increased numbers of regulatory immune cells expressing the receptor tyrosine kinase MERTK. Gastroenterology. 2015 Mar;148(3):603-615.e14. doi: 10.1053/j.gastro.2014.11.045. Epub 2014 Dec 3. PMID: 25479139.

Bernsmeier C, Triantafyllou E, Brenig R, Lebosse FJ, Singanayagam A, Patel VC, Pop OT, Khamri W, Nathwani R, Tidswell R, Weston CJ, Adams DH, Thursz MR, Wendon JA, Antoniades CG. CD14+ CD15- HLA-DR- myeloid-derived suppressor cells impair antimicrobial responses in patients with acute-on-chronic liver failure. Gut. 2018 Jun;67(6):1155-1167. doi: 10.1136/gutjnl-2017-314184. Epub 2017 Jun 7. PMID: 28592438; PMCID: PMC5969362.

Cai B, Dongiovanni P, Corey KE, Wang X, Shmarakov IO, Zheng Z, Kasikara C, Davra V, Meroni M, Chung RT, Rothlin CV, Schwabe RF, Blaner WS, Birge RB, Valenti L, Tabas I. Macrophage MerTK Promotes Liver Fibrosis in Nonalcoholic Steatohepatitis. Cell Metab. 2020 Feb 4;31(2):406-421.e7. doi: 10.1016/j.cmet.2019.11.013. Epub 2019 Dec 12. PMID: 31839486; PMCID: PMC7004886.

Dambach DM, Watson LM, Gray KR, Durham SK, Laskin DL. Role of CCR2 in macrophage migration into the liver during acetaminophen-induced hepatotoxicity in the mouse. Hepatology. 2002 May;35(5):1093-103. doi: 10.1053/jhep.2002.33162. PMID: 11981759.

Deng T, Zhang Y, Chen Q, Yan K, Han D. Toll-like receptor-mediated inhibition of Gas6 and ProS expression facilitates inflammatory cytokine production in mouse macrophages. Immunology. 2012 Jan;135(1):40-50. doi: 10.1111/j.1365-2567.2011.03511.x. PMID: 22043818; PMCID: PMC3246651.

Divine LM, Nguyen MR, Meller E, Desai RA, Arif B, Rankin EB, Bligard KH, Meyerson C, Hagemann IS, Massad M, Thaker PH, Hagemann AR, McCourt CK, Powell MA, Mutch DG, Fuh KC. AXL modulates extracellular matrix protein expression and is essential for invasion and metastasis in endometrial cancer. Oncotarget. 2016 Nov 22;7(47):77291-77305. doi: 10.18632/oncotarget.12637. PMID: 27764792; PMCID: PMC5340229.

Girgis NM, Gundra UM, Ward LN, Cabrera M, Frevert U, Loke P. Ly6C(high) monocytes become alternatively activated macrophages in schistosome granulomas with help from CD4+ cells. PLoS Pathog. 2014 Jun 26;10(6):e1004080. doi: 10.1371/journal.ppat.1004080. PMID: 24967715; PMCID: PMC4072804.

Graubardt N, Vugman M, Mouhadeb O, Caliari G, Pasmanik-Chor M, Reuveni D, Zigmond E, Brazowski E, David E, Chappell-Maor L, Jung S, Varol C. Ly6Chi Monocytes and Their Macrophage Descendants Regulate Neutrophil Function and Clearance in Acetaminophen-Induced Liver Injury. Front Immunol. 2017 Jun 1;8:626. doi: 10.3389/fimmu.2017.00626. PMID: 28620383; PMCID: PMC5451509.

Holstein E, Binder M, Mikulits W. Dynamics of Axl Receptor Shedding in Hepatocellular Carcinoma and Its Implication for Theranostics. Int J Mol Sci. 2018 Dec 18;19(12):4111. doi: 10.3390/ijms19124111. PMID: 30567378; PMCID: PMC6321118.

Huang JS, Cho CY, Hong CC, Yan MD, Hsieh MC, Lay JD, Lai GM, Cheng AL, Chuang SE. Oxidative stress enhances Axl-mediated cell migration through an Akt1/Rac1-dependent mechanism. Free Radic Biol Med. 2013 Dec;65:1246-1256. doi: 10.1016/j.freeradbiomed.2013.09.011. Epub 2013 Sep 21. Erratum in: Free Radic Biol Med. 2014 Feb;67:416. PMID: 24064382.

Imaeda AB, Watanabe A, Sohail MA, Mahmood S, Mohamadnejad M, Sutterwala FS, Flavell RA, Mehal WZ. Acetaminophen-induced hepatotoxicity in mice is dependent on Tlr9 and the Nalp3 inflammasome. J Clin Invest. 2009 Feb;119(2):305-14. doi: 10.1172/JCI35958. Epub 2009 Jan 26. PMID: 19164858; PMCID: PMC2631294.

Kim ND, Moon JO, Slitt AL, Copple BL. Early growth response factor-1 is critical for cholestatic liver injury. Toxicol Sci. 2006 Apr;90(2):586-95. doi: 10.1093/toxsci/kfj111. Epub 2006 Jan 19. PMID: 16423862.

Kimani SG, Kumar S, Davra V, Chang YJ, Kasikara C, Geng K, Tsou WI, Wang S, Hoque M, Boháč A, Lewis-Antes A, De Lorenzo MS, Kotenko SV, Birge RB. Normalization of TAM post-receptor signaling reveals a cell invasive signature for Axl tyrosine kinase. Cell Commun Signal. 2016 Sep 6;14(1):19. doi: 10.1186/s12964-016-0142-1. PMID: 27595981; PMCID: PMC5011882.

Konishi A, Aizawa T, Mohan A, Korshunov VA, Berk BC. Hydrogen peroxide activates the Gas6-Axl pathway in vascular smooth muscle cells. J Biol Chem. 2004 Jul 2;279(27):28766-70. doi: 10.1074/jbc.M401977200. Epub 2004 Apr 28. PMID: 15123721.

Kopec AK, Joshi N, Cline-Fedewa H, Wojcicki AV, Ray JL, Sullivan BP, Froehlich JE, Johnson BF, Flick MJ, Luyendyk JP. Fibrin(ogen) drives repair after acetaminophen-induced liver injury via leukocyte $\alpha_M\beta_2$ integrin-dependent upregulation of Mmp12. J Hepatol. 2017 Apr;66(4):787-797. doi: 10.1016/j.jhep.2016.12.004. Epub 2016 Dec 10. PMID: 27965156; PMCID: PMC5362307.

Krenkel O, Mossanen JC, Tacke F. Immune mechanisms in acetaminophen-induced acute liver failure. Hepatobiliary Surg Nutr. 2014 Dec;3(6):331-43. doi: 10.3978/j.issn.2304-3881.2014.11.01. PMID: 25568858; PMCID: PMC4273118.

Lemke G. Biology of the TAM receptors. Cold Spring Harb Perspect Biol. 2013 Nov 1;5(11):a009076. doi: 10.1101/cshperspect.a009076. PMID: 24186067; PMCID: PMC3809585.

Lemke G. Phosphatidylserine Is the Signal for TAM Receptors and Their Ligands. Trends Biochem Sci. 2017 Sep;42(9):738-748. doi: 10.1016/j.tibs.2017.06.004. Epub 2017 Jul 19. PMID: 28734578; PMCID: PMC5600686.

Mochizuki A, Pace A, Rockwell CE, Roth KJ, Chow A, O'Brien KM, Albee R, Kelly K, Towery K, Luyendyk JP, Copple BL. Hepatic stellate cells orchestrate clearance of necrotic cells in a hypoxia-inducible factor-1α-dependent manner by modulating macrophage phenotype in mice. J Immunol. 2014 Apr 15;192(8):3847-3857. doi: 10.4049/jimmunol.1303195. Epub 2014 Mar 17. PMID: 24639359; PMCID: PMC4538924.

Mukherjee SK, Wilhelm A, Antoniades CG. TAM receptor tyrosine kinase function and the immunopathology of liver disease. Am J Physiol Gastrointest Liver Physiol. 2016 Jun 1;310(11):G899-905. doi: 10.1152/ajpgi.00382.2015. Epub 2016 Feb 11. PMID: 26867565; PMCID: PMC4935487.

Myers KV, Amend SR, Pienta KJ. Targeting Tyro3, Axl and MerTK (TAM receptors): implications for macrophages in the tumor microenvironment. Mol Cancer. 2019 May 14;18(1):94. doi: 10.1186/s12943-019-1022-2. PMID: 31088471; PMCID: PMC6515593.

Orme JJ, Du Y, Vanarsa K, Mayeux J, Li L, Mutwally A, Arriens C, Min S, Hutcheson J, Davis LS, Chong BF, Satterthwaite AB, Wu T, Mohan C. Heightened cleavage of Axl receptor tyrosine kinase by ADAM metalloproteases may contribute to disease pathogenesis in SLE. Clin Immunol. 2016 Aug;169:58-68. doi: 10.1016/j.clim.2016.05.011. Epub 2016 May 27. PMID: 27237127; PMCID: PMC5193537.

Patin E, Kutalik Z, Guergnon J, Bibert S, Nalpas B, Jouanguy E, Munteanu M, Bousquet L, Argiro L, Halfon P, Boland A, Müllhaupt B, Semela D, Dufour JF, Heim MH, Moradpour D, Cerny A, Malinverni R, Hirsch H, Martinetti G, Suppiah V, Stewart G, Booth DR, George J, Casanova JL, Bréchot C, Rice CM, Talal AH, Jacobson IM, Bourlière M, Theodorou I, Poynard T, Negro F, Pol S, Bochud PY, Abel L; Swiss Hepatitis C Cohort Study Group, International Hepatitis C Genetics Consortium; French ANRS HC EP 26 Genoscan Study Group. Genome-wide association study identifies variants associated with progression of liver fibrosis from HCV infection. Gastroenterology. 2012 Nov;143(5):1244-1252.e12. doi: 10.1053/j.gastro.2012.07.097. Epub 2012 Jul 27. PMID: 22841784; PMCID: PMC3756935.

Roth K, Strickland J, Joshi N, Deng M, Kennedy RC, Rockwell CE, Luyendyk JP, Billiar TR, Copple BL. Dichotomous Role of Plasmin in Regulation of Macrophage Function after Acetaminophen Overdose. Am J Pathol. 2019 Oct;189(10):1986-2001. doi: 10.1016/j.ajpath.2019.07.003. Epub 2019 Aug 2. PMID: 31381887; PMCID: PMC6892227.

Rothlin CV, Carrera-Silva EA, Bosurgi L, Ghosh S. TAM receptor signaling in immune homeostasis. Annu Rev Immunol. 2015;33:355-91. doi: 10.1146/annurev-immunol-032414-112103. Epub 2015 Jan 14. PMID: 25594431; PMCID: PMC4491918.

Smirne C, Rigamonti C, De Benedittis C, Sainaghi PP, Bellan M, Burlone ME, Castello LM, Avanzi GC. Gas6/TAM Signaling Components as Novel Biomarkers of Liver Fibrosis. Dis

Markers. 2019 Sep 8;2019:2304931. doi: 10.1155/2019/2304931. PMID: 31583026; PMCID: PMC6754881.

Sunderkötter C, Nikolic T, Dillon MJ, Van Rooijen N, Stehling M, Drevets DA, Leenen PJ. Subpopulations of mouse blood monocytes differ in maturation stage and inflammatory response. J Immunol. 2004 Apr 1;172(7):4410-7. doi: 10.4049/jimmunol.172.7.4410. PMID: 15034056.

Tai KY, Shieh YS, Lee CS, Shiah SG, Wu CW. Axl promotes cell invasion by inducing MMP-9 activity through activation of NF-kappaB and Brg-1. Oncogene. 2008 Jul 3;27(29):4044-55. doi: 10.1038/onc.2008.57. Epub 2008 Mar 17. PMID: 18345028.

Tjwa M, Bellido-Martin L, Lin Y, Lutgens E, Plaisance S, Bono F, Delesque-Touchard N, Hervé C, Moura R, Billiau AD, Aparicio C, Levi M, Daemen M, Dewerchin M, Lupu F, Arnout J, Herbert JM, Waer M, García de Frutos P, Dahlbäck B, Carmeliet P, Hoylaerts MF, Moons L. Gas6 promotes inflammation by enhancing interactions between endothelial cells, platelets, and leukocytes. Blood. 2008 Apr 15;111(8):4096-105. doi: 10.1182/blood-2007-05-089565. Epub 2007 Dec 21. PMID: 18156494.

Triantafyllou E, Pop OT, Possamai LA, Wilhelm A, Liaskou E, Singanayagam A, Bernsmeier C, Khamri W, Petts G, Dargue R, Davies SP, Tickle J, Yuksel M, Patel VC, Abeles RD, Stamataki Z, Curbishley SM, Ma Y, Wilson ID, Coen M, Woollard KJ, Quaglia A, Wendon J, Thursz MR, Adams DH, Weston CJ, Antoniades CG. MerTK expressing hepatic macrophages promote the resolution of inflammation in acute liver failure. Gut. 2018 Feb;67(2):333-347. doi: 10.1136/gutjnl-2016-313615. Epub 2017 Apr 27. PMID: 28450389; PMCID: PMC5868289.

Tutusaus A, Marí M, Ortiz-Pérez JT, Nicolaes GAF, Morales A, García de Frutos P. Role of Vitamin K-Dependent Factors Protein S and GAS6 and TAM Receptors in SARS-CoV-2 Infection and COVID-19-Associated Immunothrombosis. Cells. 2020 Sep 28;9(10):2186. doi: 10.3390/cells9102186. PMID: 32998369; PMCID: PMC7601762.

Wang Q, Zhao Y, Zang B. Anti-inflammation and anti-apoptosis effects of growth arrest-specific protein 6 in acute liver injury induced by LPS/D-GalN in mice. Acta Cir Bras. 2020 Apr 9;35(2):e202000204. doi: 10.1590/s0102-865020200020000004. PMID: 32294688; PMCID: PMC7158606.

Yona S, Kim KW, Wolf Y, Mildner A, Varol D, Breker M, Strauss-Ayali D, Viukov S, Guilliams M, Misharin A, Hume DA, Perlman H, Malissen B, Zelzer E, Jung S. Fate mapping reveals origins and dynamics of monocytes and tissue macrophages under homeostasis. Immunity. 2013 Jan 24;38(1):79-91. doi: 10.1016/j.immuni.2012.12.001. Epub 2012 Dec 27. Erratum in: Immunity. 2013 May 23;38(5):1073-9. PMID: 23273845; PMCID: PMC3908543.

Zigmond E, Samia-Grinberg S, Pasmanik-Chor M, Brazowski E, Shibolet O, Halpern Z, Varol C. Infiltrating monocyte-derived macrophages and resident kupffer cells display different ontogeny and functions in acute liver injury. J Immunol. 2014 Jul 1;193(1):344-53. doi: 10.4049/jimmunol.1400574. Epub 2014 Jun 2. PMID: 24890723.

Zagórska A, Través PG, Lew ED, Dransfield I, Lemke G. Diversification of TAM receptor tyrosine kinase function. Nat Immunol. 2014 Oct;15(10):920-8. doi: 10.1038/ni.2986. Epub 2014 Sep 7. PMID: 25194421; PMCID: PMC4169336.

Zagórska A, Través PG, Jiménez-García L, Strickland JD, Oh J, Tapia FJ, Mayoral R, Burrola P, Copple BL, Lemke G. Differential regulation of hepatic physiology and injury by the TAM receptors Axl and Mer. Life Sci Alliance. 2020 Jun 22;3(8):e202000694. doi: 10.26508/lsa.202000694. PMID: 32571802; PMCID: PMC7335405.

Zhu C, Wei Y, Wei X. AXL receptor tyrosine kinase as a promising anti-cancer approach: functions, molecular mechanisms and clinical applications. Mol Cancer. 2019 Nov 4;18(1):153. doi: 10.1186/s12943-019-1090-3. PMID: 31684958; PMCID: PMC6827209.

CHAPTER 4

DEVELOPMENT OF A HIGH THROUGHPUT SCREENING ASSAY TO DETECT CHANGES IN MACROPHAGE POLARIZATION

4.1 Abstract

Chronic liver diseases, including fibrosis and cirrhosis, are leading causes of death worldwide. While studies have shown these diseases are reversible, antifibrotic therapies to treat these diseases are not currently available. Recently, recruited hepatic macrophage populations have been shown to play a key role in mediating fibrosis reversal. Specifically, differentiation of proinflammatory monocyte populations to pro-repair macrophages in this setting, has been linked to multiple facets of hepatic repair including MMP production, cessation of pro-inflammatory cytokine synthesis, and inactivation of hepatic stellate cells. Thus, development of macrophage targeted therapies has the potential to tremendously impact the treatment of these diseases. In the present studies, we developed a high-throughput screening assay that relies on the detection of F4/80 immunofluorescence, to identify compounds capable of shifting the polarization of pro-fibrotic macrophages towards pro-repair macrophages, an effect that increases the expression of F4/80. At present, we have screened over 2,500 compounds from the Glaxo-Smith-Kline (GSK) and National Center for Advancing Translational Sciences (NCATS) libraries available through the MSU Assay Development and Drug Repurposing Core (ADDRC). Hits were detected by determining the F4/80 mean fluorescence intensity in each well. The primary screen identified 145 compounds that increased F4/80, suggesting that they are potentially capable of shifting the polarization of pro-fibrotic macrophages (0.06% hit rate). Compounds identified as active included compounds known to suppress inflammation and regulate macrophage phenotype. Interestingly, analysis of hits also revealed multiple compounds with redundant signaling pathways including compounds that were inhibitors of: colony stimulating factor 1 receptor (CSF1R), Rho-associated coiled-coil containing protein kinase (ROCK), epidermal growth factor receptor (EGFR), protein kinase B (Akt), Janus kinases/signal transducer and activator of transcription proteins (JAK/STAT), vascular endothelial growth factor (VEGF), and discoidin domain receptor (DDR) signaling, suggesting multiple pathways that may be important targets for regulating macrophage

phenotype. Future studies will re-screen compounds identified as active to confirm hits and prioritize compounds for further testing. Upon completion of these studies, we expect to identify candidate drug(s) that change the polarization of fibrotic macrophages.

4.2 Introduction

Hepatic fibrosis represents a leading cause of death worldwide, and while studies have shown fibrosis is reversible, antifibrotic therapies to treat liver fibrosis and cirrhosis are not currently available (Ismail and Pinzani 2009) (Ramachandran and Iredale 2009). At present, treatments for fibrosis are limited to treating the underlying etiology, such as antivirals to eradicate hepatitis virus or cessation of alcohol consumption in alcoholic liver disease (Ismail and Pinzani 2009) (Ramachandran and Iredale 2009). However, in some patients, this treatment strategy is unsuccessful, and in the case of genetic disorders, it is not feasible. For these patients, supportive care and a liver transplant are the only remaining options. The demand for transplantable livers, however, far exceeds the available supply (Habka et al., 2015). Furthermore, the impeding epidemic of nonalcoholic steatohepatitis (NASH) is expected to exacerbate donor shortages with fewer high-quality organs available for transplantation (Habka et al., 2015) (Estes et al., 2018). Thus, novel therapeutics are urgently needed for the treatment of fibrosis and cirrhosis.

Similar to APAP-induced acute liver injury, studies have shown macrophage polarization from a proinflammatory to a pro-repair phenotype plays an important role in stimulating hepatic repair processes in an experimental setting of fibrosis (Figure 4.1) (Ramachandran et al., 2012). Importantly, the transition to pro-repair macrophages has been linked to several biological and pathological processes that promote the reversal of liver fibrosis (Figure 4.1) (Ramachandran et al., 2012). First, macrophage polarization has been shown to increase production of MMPs, which function to remove excess extracellular matrix (Figure 4.1) (Ramachandran et al., 2012). Loss of a proinflammatory phenotype also results in cessation of proinflammatory cytokine production. Prolonged proinflammatory cytokine production has been linked to the development of serious complications including multiorgan failure and hepatic encephalopathy (Ramachandran et al., 2012). Additionally, polarization to a pro-repair phenotype is linked to production of insulin-like growth factor-1 (Igf-1), which inactivates hepatic stellate cells, limiting

further production of extracellular matrix (Ramachandran et al., 2012). Furthermore, these studies revealed that reversal of liver fibrosis is prevented when pro-repair macrophage populations are depleted (Ramachandran et al., 2012). Thus, identification of drugs targeting macrophage differentiation in this setting could provide a novel therapeutic approach for the treatment of hepatic fibrosis. At present, no antifibrotic therapies exist, making this an area of acute need. Approaches aimed at identifying antifibrotics, such as high-throughput drug discovery, could lead to the repurposing of approved drugs for treatment of fibrosis or result in the identification of new chemical entities capable of stimulating reversal of this disease.

Over the last few decades, high-throughput screening (HTS) has gained popularity as a method to accelerate drug discovery, allowing for thousands of compounds to be assessed for drug activity in a relatively short period of time (Macarron et al., 2011) (Carnero 2006). In addition to allowing for rapid testing, HTS is highly controlled, relying on automated equipment, including robotics, with screening capabilities of up to 100,000 compounds per day (Szymański, Markowicz, and Mikiciuk-Olasik 2012). To date, HTS assays have been used for a vast range of endpoints including: inhibition of enzyme activity, increase cellular influx of calcium, inhibition of cell proliferation (Varma, Lo, and Stockwell 2011) (Szymański, Markowicz, and Mikiciuk-Olasik 2012). To date, no studies have used HTS to identify macrophage-targeted antifibrotics. However, several screens have been recently conducted to identify drugs that modify the phenotype of macrophages (Hu et al., 2021) (Rodell, Koch, and Weissleder, 2019). While these assays did not focus specifically on fibrosis, these approaches are amenable to screens aimed at identifying novel macrophage-targeted antifibrotics.

Typically, the development of a HTS assay involves a tiered screening paradigm beginning with a primary screen to identify possible active compounds. The primary assay allows for detection of compounds that have a pharmacological or biological activity of interest. Importantly, successful primary assays will be easy to preform, requiring minimal steps and reagents. Additionally, the assay readout must be robust in a microtiter plate format (Rodell,

Koch, and Weissleder 2019). Following the primary screen, active compounds, or hits, are re-screened for hit confirmation using the same format. Compounds that are confirmed as active are tested in a secondary assay, often using a different biological endpoint. After the secondary screen, compounds are selected for dose-response assessment using the secondary assay. Following this stage, compounds exhibiting acceptable inhibition curves (Hill Slope 0.5-2.0) and potencies (EC50 < 10 μM) are prioritized for further consideration. Lastly, these compounds are re-tested using fresh powder and re-analyzed using both the primary and secondary assay.

As noted above, development of a robust primary screening assay is essential to successful identification of biologically active compounds. High-content imaging is a HTS technique that involves the use of fluorescent endpoints (i.e. presence of cell markers) which can be coupled with changes in cell morphology, making it an intriguing platform for assessing compound-induced changes in macrophage polarization (Rodell, Koch, and Weissleder 2019). In addition to differences in distinctive cell surface markers, Ly6c and F4/80, studies have shown that pro-inflammatory monocytes are typically small and spherical, whereas pro-repair macrophages are large and elongated (Rodell, Koch, and Weissleder 2019). This notable difference in size and shape can be easily quantified on high content imaging platforms by measuring cell length-to-width ratios. The ability to combine cell surface marker expression and morphological analysis provides a rich data set that can be used to detect various macrophage phenotypes. Furthermore, this quantification can be automated by using a number of different software platforms, including some that are available as free, open-source software (e.g., CellProfiler).

In the present studies, we have developed a high-content imaging assay with the capability to detect compound-induced macrophage differentiation with the goal of identifying novel antifibrotic compounds. Specifically, our high-throughput assay utilizes immunocytochemistry to distinguish between proinflammatory monocytes that have undergone differentiation into pro-repair macrophages following incubation with a compound for 24 hours.

This high-throughput assay has been optimized for 384 well plates and F4/80 fluorescence can be detected in each well using a fluorescence plate reader. For the pilot screen we selected the Glaxo-Smith-Kline (GSK) Kinase Inhibitor Set and the National Center for Advancing Translational Sciences (NCATS) Mechanism Interrogation Plates (MIPE). These libraries are available through the Assay Development and Drug Repurposing Facility (ADDRC) at Michigan State University and contain compounds with known mechanism of action. Combined, these chemical libraries contain approximately 2,500 compounds that target multiple signaling networks. Individual compounds in these libraries inhibit mitogen-activated proteins kinases, tyrosine-kinase receptors, and components of NF-kB signaling, among many other pathways. Additionally, these libraries contain hundreds of approved and phase I-III investigational drugs, and 1,000 preclinical molecules with diverse and redundant mechanisms of action. Thus, using these libraries allows for the interrogation of multiple signaling networks, using an unbiased approach that will identify pathways that are critically involved in regulating macrophage phenotype. Importantly, active compounds identified from these libraries could be repurposed as antifibrotics and our results could lead to identification of signaling pathways that regulate macrophage phenotype.

4.3 Materials and Methods

4.3.1 Animal Treatments. 10-12-week-old male C57BL/6J mice (Jackson Laboratories) were used for all studies. Mice were housed in a 12-hour light/dark cycle under controlled temperature (18-21°C) and humidity. Food (Rodent Chow; Harlan-Teklad) and tap water were allowed ad libitum. Mice were treated twice weekly with 1 ml/kg of carbon tetrachloride (CCl_4) by intraperitoneal injection for a total of 6 weeks to induce liver fibrosis. All studies were approved by the Michigan State University Institutional Animal Care and Use Committee.

4.3.2 Cell Isolation. Liver digests collected at 24 hours after the final CCl_4 injection were used to isolate proinflammatory monocytes, whereas, liver digests collected at 96 hours after the final CCl_4 injection were used to isolate pro-repair macrophages (positive control for the drug screening assay). To isolate proinflammatory monocyte and pro-repair macrophage populations, mouse livers were perfused and digested with collagenase (Collagenase H, Sigma Chemical Company) as described previously (Roth et al., 2019). Briefly, hepatocytes were removed by centrifugation and non-parenchymal cells were collected after centrifugation at 300×g for 10 minutes. Non-parenchymal cells were washed with HBSS and resuspended in FACs buffer (phosphate-buffered saline (PBS), 1% fetal bovine serum). The cells were then incubated with Fc blocking buffer (BD Biosciences; diluted 1:20) for 10 minutes at 4°C, rinsed, and then pelleted by centrifugation at 300×g for 5 minutes. Next, immunomagnetic beads were used to purify the two macrophage types.

To isolate enriched populations of proinflammatory monocytes, nonparenchymal cells were re-suspended in 180 µL of MACS Buffer (2.5 g bovine serum albumin, 0.416 g EDTA, and 500 mL PBS) and 20 µL biotinylated anti-Ly6c antibody (Miltenyi Biotec, Bergisch Gladbach, Germany). The cell suspension was incubated for 10 minutes at 4°C and then washed by adding 10 mL of MACS buffer and centrifugation (300×g for 10 minutes). The cell pellet was re-suspended in 180 µL of MACS Buffer and 20 µL streptavidin microbeads (Miltenyi Biotec). Cells were incubated at 4°C for 10 minutes and then washed by adding 10 mL of MACS buffer and

centrifugation (300×g for 10 minutes). The pellet was resuspended with 500 µL MACS buffer and applied to MACS LS columns (Miltenyi Biotec). The column was rinsed three times with 3 mL MACS buffer. Proinflammatory monocytes were collected by removing the column from the midiMACS Separator (Miltenyi Biotec) and rinsing the column with 5 mL of MACS buffer.

To isolate pro-repair macrophages, we first performed a negative selection to remove any Ly6c+ cells. Briefly, nonparenchymal cells were re-suspended in 180 µL of MACS Buffer (2.5 g bovine serum albumin, 0.416 g EDTA, and 500 mL PBS) and 20 µL biotinylated anti-Ly6c antibody (Miltenyi Biotec, Bergisch Gladbach, Germany). The cell suspension was incubated for 10 minutes at 4°C and then washed by adding 10 mL of MACS buffer and centrifugation (300×g for 10 minutes). The cell pellet was re-suspended in 180 µL of MACS Buffer and 20 µL streptavidin microbeads (Miltenyi Biotec). Cells were incubated at 4°C for 10 minutes and then washed by adding 10 mL of MACS buffer and centrifugation (300×g for 10 minutes). The pellet was resuspended with 500 µL MACS buffer and applied to MACS LS columns (Miltenyi Biotec). The column was rinsed three times with 3 mL MACS buffer. The Ly6c+ cells collected in the column were discarded. The cells that flowed freely through the column during the negative selection were collected in a 50 mL tube. These cells were pelleted and re-suspended in 180 µL of MACS Buffer (2.5 g bovine serum albumin, 0.416 g EDTA, and 500 mL phosphate-buffered saline) and 20 µL biotinylated anti-Cx3cr1 antibody (Miltenyi Biotec, Bergisch Gladbach, Germany). This antibody was chosen because the resident macrophage population (i.e., Kupffer cells) also expresses F4/80. Mature Kupffer cells do not express CX3CR1; thus, eliminating the possibility that Kupffer cells may contaminate our purified pro-repair macrophage population. The cell suspension was incubated for 10 minutes at 4°C and then washed by adding 10 mL of MACS buffer and centrifugation (300×g for 10 minutes). The cell pellet was re-suspended in 180 µL of MACS Buffer and 20 µL streptavidin microbeads (Miltenyi Biotec). Cells were incubated at 4°C for 10 minutes and then washed by adding 10 mL of MACS buffer and centrifugation (300×g for 10 minutes). The pellet was resuspended with 500 µL MACS buffer

and applied to MACS LS columns (Miltenyi Biotec). The column was rinsed three times with 3 mL MACS buffer. Enriched populations of pro-repair macrophages were collected by removing the column from the midiMACS Separator (Miltenyi Biotec) and rinsing the column with 5 mL of MACS buffer.

4.3.3 Flow Cytometry. Proinflammatory monocyte and pro-repair macrophages were isolated as described above. Flow cytometry was used to verify isolated cell populations were enriched with proinflammatory monocytes ($Ly6c^{hi}F4/80^{low}$) or pro-repair macrophages ($Ly6c^{low}F4/80^{hi}$). Briefly, the cells were incubated with Fc blocking buffer (BD Biosciences; diluted 1:20) for 10 minutes at 4 °C, rinsed, and then pelleted by centrifugation at 300×g for 5 minutes. The cells were incubated with anti-F4/80 conjugated to Alexa Fluor-594 and anti-Ly6C conjugated to Alexa-488 for 30 minutes at 4°C. All antibodies were purchased from Biolegend. Following incubation, cells were washed twice and fixed using 4% formalin (Sigma) for 15 minutes at 4°C. The fixed cells were washed twice and resuspended in FACs buffer. An Attune NxT flow cytometer (Life Technologies) was then used to measure fluorescence, which was quantified using Attune NxT software.

4.3.4. Real-Time PCR. RNA was isolated from cell culture samples by using the E.Z.N.A Total RNA Kit I (Omega Bio-Tek) according to manufacturer's instructions. Real-time PCR was performed as described by us previously (Kim et al., 2006). The following primer sequences were used: Rpl13a: Forward- 5'-GACCTCCTCCTTTCCCAGGC-3', Reverse- 5'-AAGTACCTGCTTGGCCACAA-3', Clec4E: Forward-5'AAAAGAGGGCCAAGGATTCA-3', Reverse-5'-CCCGGAAATTTGAGAGCTGC-3', neutrophil (PMN) collagenase: Forward-5'-CCCAGTATCTGAACACCTGGA-3', Reverse-5'- AGACCGGAATTGATTGCTTG-3' , uPAR: Forward-5'- CCTGCAATGCCGCTATCCTA-3', Reverse-5'-GATGAGAGACGCCTCTTCGG-3', Tarm1: Forward-5'- GAGCCACCATGATCTCTAGGC-3', Reverse-5'-AGGTGTAGTGTCCGCCATCA-3', and iNOS: Forward-5'- GTCGATGTCACATGCAGCTT-3',

Reverse-5'- GAAGAAAACCCCTTGTGCTG-3'. Clec4E, PMN collagenase, uPAR, Tarm1 and iNOS are highly expressed in proinflammatory monocytes. The following primer sequences were used for genes highly expressed in pro-repair macrophage populations: Vsig4: Forward-5'-GTGCAGGGTTGTAGGTGCTT-3', Reverse-5'- GGCAGACTCCTGATGGAAAC-3', Cd5l: Forward-5'- AAAATCTATGGGCCTGGGGC-3', Reverse-5'- GAATGAGGGCCCACTGAACA-3', Gas6: Forward-5'- ATGAAGATCGCGGTAGCTGG-3', Reverse-5'-CCAACTCCTCATGCACCCAT-3', Igf-1: Forward-5'- CACTCATCCACAATGCCTGT-3', Reverse-5'- TGGATGCTCTTCAGTTCGTG-3', and MMP2: Forward-5'-CCAGCAAGTAGATGCTGCCT-3', Reverse-5'- GGGGTCCATTTTCTTCTTCA-3'.

4.3.5 Plating. Enriched cell populations were plated at 20,000 cells/well in black-walled Griner 384 well plates. Cells were plated using a Biomek automated cell dispenser. Proinflammatory monocytes were plated in Columns 1-22, while pro-repair macrophages were plated in Columns 23-24.

4.3.6 Dosing. Compound plates were obtained from the ADDRC at Michigan State University. The following compound libraries were screened: GSK Kinase Inhibitor Set (558 compounds) and the NCATS MIPE (1,910 compounds). All pipetting and treatments with compounds were done using the Biomek FX Laboratory Automation Workstation (liquid handling robotics). The compounds from the chemical libraries were added to a final concentration of 10 μM in DMSO.

4.3.7 Treatments. Following dosing with the GSK and NCATS libraries, plates were transferred to the incubator for 24 hours. Thirty-two wells (Columns 1 and 2) were treated with DMSO (vehicle) on each plate.

4.3.8 Immunostaining. At the end of the incubation, the cells were fixed with 4% formalin and F4/80 detected by immunofluorescence using the Alexa Flour 594 Tyramide Superboost Kit (Streptavidin; Catalog number: B40935) per the manufactures' instructions. Briefly, following fixation, cells were incubated at room temperature for 60 mins with a 3%

hydrogen peroxide solution to quench endogenous peroxidase activity. Cells were rinsed 3x with PBS. A biotin blocking kit was used to block endogenous biotin per the manufactures' instructions. Cells were washed 3x with PBS and then incubated for 60 minutes with blocking buffer (10% goat serum in PBS) at room temperature. Following the blocking step, cells were incubated with the primary antibody (Anti-Biotin F4/80) over-night in the cold room (4°C). The primary antibody was purchased from Miltenyi Biotec. Following incubation with the primary antibody, cells were washed 3x with PBS and incubated with the secondary antibody (HRP-conjugated streptavidin) for 60 minutes at room temperature. Following incubation with the secondary antibody, cells were rinsed 3x with PBS and the tyramide working solution was added to each well. Cells were incubated with tyramide working solution for 10 minutes at room temperature and stop reagent was applied. Cells were rinsed 3x with PBS and then counterstained with DAPI to detect nuclei.

4.3.9. Quantification of Immunostaining. The plates were scanned on a Cytation 3 Cell Imaging Multi-Mode Reader. To quantify this, images of each well were collected and analyzed using CellProfiler (www.cellprofiler.org). Nuclei were identified based on the fluorescent signal from DAPI. Secondary objects representing F4/80 were collected by propagation from the nuclei objects. For each object identified, measurements of the F4/80 mean intensity were taken (Figure 4.5B). F4/80 positive cells were defined as objects with an F4/80 mean intensity greater than the mean + 3SD of the control cells (proinflammatory monocytes). From this, the percentage of F4/80-positive cells per well was calculated (Figure 4.5C). To assess the quality of this assay, we next calculated the Z'.

4.4 Results

4.4.1 Verification of Enriched Cell Populations. Proinflammatory monocytes have been characterized as Ly6C^{hi} F4/80^{low} by flow cytometry, whereas pro-repair macrophages are characterized as Ly6C^{low} F4/80^{hi}. Thus, to confirm our cell isolation method yielded enriched populations of proinflammatory monocytes or pro-repair macrophages, we performed flow cytometry. As shown in Figure 4.3C, populations of pro-repair macrophages are approximately 87% enriched following magnetic bead separation, while populations of pro-inflammatory monocytes are approximately 93% enriched (Figure 4.3B). Thus, flow cytometry analysis (Figures 4.3) of purified populations of proinflammatory monocytes and pro-repair macrophages indicates immunomagnetic bead separation is an effective method for isolating these cell types from the livers of CCl_4 treated mice.

4.4.2. Quantification of mRNAs from Enriched Cell Populations. As a secondary measure to confirm cell phenotype, we performed real-time PCR to detect mRNA transcripts that are selective for each purified cell type. We confirmed that Clec4E, PMN collagenase, uPAR, Tarm1, and iNOS are highly expressed in proinflammatory monocytes, whereas, Vsig4, Cd5l, Gas6, Igf-1 and MMP2 are highly expressed on pro-repair macrophages (Figure 4.4) (Ramachandran et al., 2012). Importantly, these identified mRNAs could later be used as a secondary assay to confirm macrophage polarization has occurred following compound treatment.

4.4.3. Screening Assay Validation. For the primary screening assay, we aimed to develop a high-throughput assay that utilizes immunocytochemistry to detect the presence of F4/80. As noted above, proinflammatory monocyte populations do not express F4/80, thus this distinguishing marker will allow for identification of macrophages that have undergone compound-induced polarization to a pro-repair phenotype. Prior to screening compounds, the assay was optimized for 384 well plates so that screening could be performed in a high-throughput format. Briefly, proinflammatory and pro-repair macrophages were plated in a 384

well plate at a density of 20,000 cells per well. Half of the plate contained proinflammatory monocytes and half of the plate contained pro-repair macrophages. Half of these wells were treated with DMSO, the solvent used for compounds in the chemical libraries. All pipetting was done by using the Biomek FX Laboratory Automation Workstation. After treatment, the cells were incubated for 24 hours. The plates were scanned on a Cytation 3 Cell Imaging Multi-Mode Reader. As shown in Figure 4.5, there was a clear distinction in positive staining for F4/80 (red staining) between the proinflammatory monocytes (left panel) and the pro-repair macrophages (right panel). To quantify this, images of each well were collected and analyzed using CellProfiler (www.cellprofiler.org). Nuclei were identified based on the fluorescent signal from DAPI. Secondary objects representing F4/80 were collected by propagation from the nuclei objects. For each object identified, measurements of the F4/80 mean intensity were taken (Figure 4.5B-C). F4/80 positive cells were defined as objects with an F4/80 mean intensity greater than the mean + 3SD of the control cells (proinflammatory monocytes). From this, the percentage of F4/80-positive cells per well was calculated (Figure 4.5C). To assess the quality of this assay, the Z' was calculated. High-throughput screening assays are considered robust and high-quality for screening if the Z' > 0.5. As shown in Figure 4.5C, the Z' for this assay was 0.61 making it suitable for high-throughput screening.

4.4.4. Active Compounds in Primary Screen of NCATS and GSK Libraries.

Following confirmation that the primary assay was viable for screening, we next performed a pilot screen to identify chemicals that stimulate the transition of proinflammatory monocytes into pro-repair macrophages. The GSK Kinase Inhibitor Set and the NCATS MIPE were selected from the Michigan State University ADDRC chemical libraries for the primary screen. As noted, selection of these libraries permitted the interrogation of multiple signaling networks, allowing for identification of pathways that are critically involved in regulating macrophage phenotype.

Hits were identified by determining the F4/80 mean fluorescence intensity in each well using CellProfiler. A compound was deemed a hit if the F4/80 mean fluorescence intensity for

that well was greater than the mean + 3SD of the control cells (proinflammatory monocytes). An example of CellProfiler Output is shown in Figure 4.6. The primary screen of the NCATS and GSK libraries revealed 145 compounds that are potentially capable of regulating macrophage phenotype (0.06% hit rate). A complete list of these compounds is provided in Table 4.1. Importantly, several compounds with known anti-inflammatory properties and compounds known to modulate macrophage phenotype were identified as hits, confirming the robustness of the assay. For example, studies have shown MSU-40176, or Manoalide, is potent inhibitor of phospholipase A2 (PLA2) and has known anti-inflammatory properties.

Interestingly, analysis of hits revealed multiple compounds with redundant signaling pathways including compounds that were inhibitors of: colony stimulating factor 1 receptor (CSF1R), Rho-associated coiled-coil containing protein kinase (ROCK), epidermal growth factor receptor (EGFR), protein kinase B (Akt), Janus kinases/signal transducer and activator of transcription proteins (JAK/STAT), vascular endothelial growth factor (VEGF), and discoidin domain receptor (DDR) signaling (Table 4.2).

4.5 Discussion

Hepatic fibrosis is a leading cause of death worldwide, accounting for 1 million deaths annually (Asrani et al., 2019). Studies have revealed that recruited bone marrow derived macrophages are key mediators of fibrosis reversal, suggesting they may provide a novel therapeutic target for stimulating hepatic repair (Ramachandran et al., 2012). Currently, no antifibrotic therapies are available to treat liver fibrosis and cirrhosis, making this an area of acute need. In the present studies, we have developed a novel drug screening platform to identify compounds capable of stimulating differentiation of disease-causing, proinflammatory monocytes into disease-reversing, pro-repair macrophages (Figure 4.1).

The selection of a cell model that accurately reflects macrophage phenotype in a fibrotic microenvironment was an important consideration for development of our primary screening assay. Traditionally, macrophage polarization states were segregated into two functionally distinct subsets: classically activated (M1) or alternatively activated (M2) macrophages. However, recent studies have shown macrophage phenotypes are much more complex, and that an array activation states exists far beyond the traditional M1/M2 paradigm (Rodell, Koch, and Weissleder 2019). Thus, rather than rely on commercially available macrophage cell lines, we aimed to develop methods to purify proinflammatory macrophages from the livers of mice with fibrosis. This methodology can easily be applied to fibrosis mouse models, where pro-inflammatory monocyte populations express the unique cell surface marker, Ly6c (Ramachandran et al., 2012). Furthermore, use of these cells, which are the intended target of therapy, provides the best opportunity to identify drugs with the highest potential for efficacy *in vivo*.

Several experimental models have been used to successfully induce hepatic fibrosis in mice (Scholten et al., 2015). However, the most commonly used method relies on repeated administration of carbon tetrachloride (CCl_4) (Scholten et al., 2015). Mice treated with CCl_4 two times a week for a period of six weeks via intraperitoneal (IP) injection develop hepatic fibrosis

(Scholten et al., 2015). Lineage tracing studies have revealed that following treatment with CCl_4, proinflammatory monocyte populations are recruited to the liver from the bone-marrow (Ramachandran et al., 2012). During periods of fibrosis reversal, pro-inflammatory monocytes switch phenotype to pro-repair macrophages (Ramachandran et al., 2012). Thus, manipulation of this experimental model allows for isolation of enriched populations of both macrophage phenotypes, with pro-repair macrophages representing a model specific positive control. Following isolation, these cells can be subsequently used in high-throughput screening assays (Figure 4.2).

Prior to validating that our primary screening assay was suitable for HTS, we first verified that we could successfully isolate enriched populations of both proinflammatory and pro-repair macrophage populations from fibrotic mice. As shown in Figure 4.3, flow cytometry confirmed populations of pro-repair macrophages ($Ly6c^{low}F4/80^{hi}$) are approximately 87% enriched following magnetic bead separation, while populations of pro-inflammatory monocytes ($Ly6c^{hi}F480^{low}$) are approximately 93% enriched. RNA sequencing of proinflammatory monocytes and pro-repair macrophages isolated from the CCl_4-indcued fibrosis mouse model noted distinct gene expression patterns exist for each of these macrophage phenotypes (Ramachandran et al., 2012). Specifically, $Ly6c^{hi}F480^{low}$ populations expressed high levels of inflammatory genes including, Clec4E, PMN collagenase, uPAR, Tarm1, and iNOS (Ramachandran et al., 2012). Following polarization, pro-repair macrophage populations express low levels of inflammatory genes, and high levels of genes associated with phagocytosis, matrix degradation, and growth factors. These genes include Vsig4, Cd5l, Gas6, Igf-1 and MMP2 (Ramachandran et al., 2012). As an additional confirmation that enriched populations were phenotypically correlative to macrophages present in a fibrotic microenvironment, we measured mRNA expression of each set of genes identified above in enriched proinflammatory monocyte and pro-repair macrophage populations. RT-PCR confirmed Clec4E, PMN collagenase, uPAR, Tarm1, and iNOS are highly expressed in

proinflammatory monocytes, whereas, Vsig4, Cd5l, Gas6, Igf-1 and MMP2 are highly expressed on pro-repair macrophages (Figure 4.4).

Following the development of methods to isolate enriched cell populations, we next sought to develop a rapid and robust primary assay that could be used in a HTS drug screening platform to identify compounds capable of stimulating macrophage polarization. High-content imaging techniques frequently involve the use of fluorescently labeled antibodies to detect the presence of cell surface markers of interest. These techniques can be applied to either adherent cells in 384 or 1536 well plates, or to cells in suspension, and can allow for imaging of multiple cell surface markers at once (Rodell et al., 2019). Immunostaining protocols for macrophage phenotypic cell markers, including iNOS and Arg-1, have been developed and can be used to identify compounds stimulating macrophage maturation (Rodell et al., 2019). While Arginase 1, or Arg-1, has long been used to identify pro-resolution or M2 macrophages, it was recently shown Ly6c+ cells may also express detectable levels of Arg-1 (Arlauckas et al., 2018). Thus, use of Arg-1 as a phenotypic marker to identify pro-resolution macrophages must be used with caution, as Arg-1 expression could occur prior to full differentiation (Arlauckas et al., 2018). We propose immunostaining for F4/80 provides a more reliable method to detect compound induced macrophage polarization, as loss of Ly6c is highly correlated with increased expression of F4/80 in differentiated macrophages.

After selecting a phenotypic marker, we assessed quality and robustness of our assay to determine if it would be suitable for drug screening. High-throughput assays are regarded as high quality for screening if they have a Z-factor, or Z', greater than 0.5. The Z-factor represents a statistical measure of both the dynamic range of the signal of interest and variation in the data linked to the signal (Zhang, Chung, and Oldenburg 1999). To determine if our assays had a Z' suitable for HTS, we plated a 384 well plate with Ly6c and F4/80 enriched cell populations isolated from CCl_4-treated mice. Half of the plate contained proinflammatory monocytes, while the other half of the plate contained pro-repair macrophages. Proinflammatory monocytes were

treated with DMSO for 24 hours. DMSO is the solvent used for compounds in the MSU ADDRC chemical libraries. Following immunostaining with F4/80 there was a clear distinction in positive staining for F4/80 (red staining) between the proinflammatory macrophages (left panel) and the pro-resolution macrophages (right panel) (Figure 4.5). As shown in Figure 4.5, the Z' for this assay was 0.61. Importantly, in addition to indicating an appropriate Z', our preliminary studies demonstrated that our assay was highly reproducible, consistent across wells, required minimal pipetting (amenable to liquid handling robotics), and was inexpensive, making it suitable for HTS.

To determine if the primary assay could be used to identify compounds capable of stimulating macrophage polarization, we performed a small-scale pilot screen using ~2,500 compounds from the GSK Kinase Inhibitor Set and the NCATS MIPE (Figure 4.6). As noted above, these two compound libraries allow for the interrogation of multiple signaling networks, using an unbiased approach. In addition to identification of compounds capable of stimulating macrophage polarization, use of these libraries can identify pathways that are critically involved in regulating macrophage phenotype. Hits were identified by determining the F4/80 mean fluorescence intensity in each well using CellProfiler (Figure 4.7).

The primary screen of the NCATS and GSK libraries revealed 145 compounds that are potentially capable of regulating macrophage phenotype (0.06% hit rate). Notably, several compounds with known anti-inflammatory properties were identified as hits. For example, studies have shown MSU-40176, or Manoalide, is potent inhibitor of phospholipase A2 (PLA2) and has known anti-inflammatory properties (Mayer 1989). Another active compound, Leflunomide, is an immunosuppressive drug that is currently used to treat rheumatoid arthritis by reducing secretion of TNFα and IL-1β (Cutolo et al., 2003). Imatinib, a chemotherapeutic, also has potent anti-inflammatory effects and has been shown to modulate TNFα production in monocytes and macrophages (Wolf et al., 2005). Interestingly, treatment of mice with imatinib

was protective in two independent models of acute hepatitis (Con A and GalN/LPS), through inhibition of TNFα production by hepatic macrophages (Wolf et al., 2005). Cilostazol, an antiplatelet drug and a vasodilator, has been shown to suppress production of nitric oxide (NO), prostaglandin E2 (PGE2), interleukin-1 (IL-1), TNFα, and monocyte chemoattractant protein-1 (MCP-1), following LPS-stimulation of BV2 microglia *in vitro* (Jung et al., 2010). Additionally, lamotrigine, an anticonvulsant, has been shown to inhibit proinflammatory cytokines (L-6, TNF-α and IL-1β) secretion both *in vitro* and *in vivo* (Abu-Rish et al., 2018). While these compounds have not yet been specifically linked to macrophage polarization, their ability to modulate macrophage-mediated inflammatory responses makes them intriguing candidates for follow-up screening.

Compounds previously shown to modulate macrophage phenotype were also identified as hits. Niacin, or vitamin B3, has been shown to modulate macrophage polarization from a pro-inflammatory to a pro-repair phenotype in various settings including Parkinson's disease (Wakade et al., 2018) (Montserrat-de la Paz et al., 2016). Genistein, an isoflavone, has also been previously shown to skew macrophage polarization to a M2 phenotype in an experimental setting of colitis (Abron et al., 2018). Interestingly, analysis of hits revealed multiple compounds with redundant signaling pathways that have been implicated in regulating macrophage phenotype, including compounds that were inhibitors of: colony stimulating factor 1 receptor (CSF1R), Rho-associated coiled-coil containing protein kinase (ROCK), epidermal growth factor receptor (EGFR), protein kinase B (Akt), Janus kinases/signal transducer and activator of transcription proteins (JAK/STAT), vascular endothelial growth factor (VEGF), and discoidin domain receptor (DDR) signaling (Table 4.2) (Cannarile et al., 2017) (Liu et al., 2015) (Hardbower et al., 2021) (Vergadi et al., 2017) (Malyshev and Malyshev 2015) (Engel et al., 2019).

As noted, several compounds with known anti-inflammatory properties and compounds that have been previously shown to regulate macrophage phenotype were identified following the primary screen. Future studies will re-screen compounds identified as active to confirm hits. It is likely that some of these compounds are false positives. One pitfall of this assays is that compounds with fluorescent properties, that are phagocytosed by macrophages, may emit a fluorescent signal. For example, Rose Bengal, a fluorescein, was identified as an active compound. Thus, following hit confirmation, it will be vital to use a secondary endpoint, such as mRNA expression, to determine if compounds fully triggered a full phenotypic change. As shown in Figure 4.4, mRNA transcripts that are selective for each purified cell type have been previously identified. Thus, detection of these mRNAs could be used as a secondary screen using Nanostring technology. Following completion of the secondary assay, future studies, will test the *in vivo* efficacy of these compounds in animal models.

Importantly, we have developed novel drug screening platform to identify compounds capable of stimulating differentiation of proinflammatory macrophages into pro-resolving macrophages that reverse fibrosis. Following a small-scale pilot screen, we have identified active 145 compounds with the potential to modulate macrophage phenotype. Several compounds identified as hits have known anti-inflammatory properties and have been shown to modulate inflammatory responses in macrophages. Furthermore, compounds that have been previously shown to regulate macrophage phenotype were identified as hits in the primary screen. While active compounds will need to undergo rigorous conformation, these studies have the potential to lead to identification of novel antifibrotics, which could tremendously impact the treatment of liver fibrosis.

ACKNOWLEDGEMENTS

We thank Dr. Rick Neubig, Dr. Tom Dexheimer, and Behirda Karaj for their assistance with planning, designing and carrying out all aspects of the high-throughput screen.

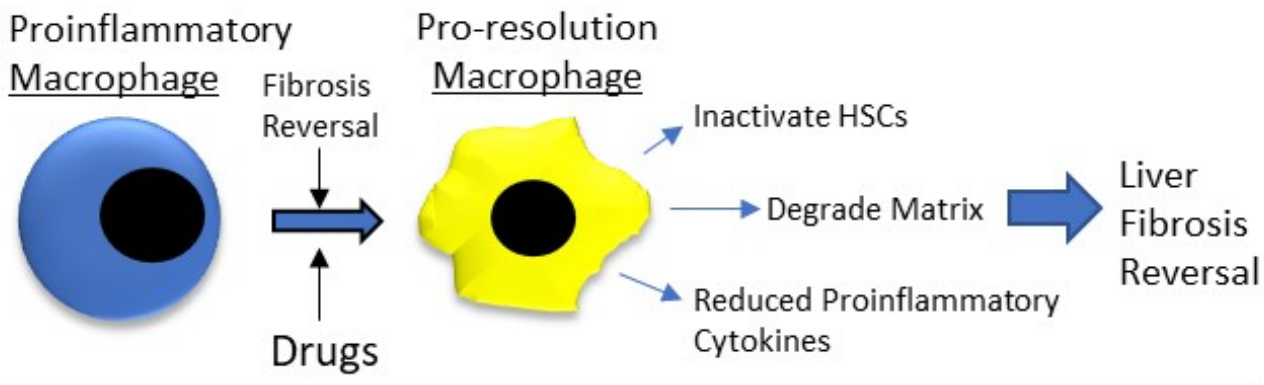

Figure 4.1: Diagram of macrophage polarization from a proinflammatory to a pro-repair phenotype. During liver fibrosis reversal, fibrosis-causing proinflammatory macrophages transition to pro-repair macrophages that produce mediators that inactivate matrix-producing HSCs, produce MMPs that degrade matrix, and terminate production of proinflammatory cytokines. Collectively, these events culminate in the reversal of liver fibrosis. The proposed studies will identify drugs that stimulate the transition of proinflammatory macrophages to pro-resolution macrophages for use as novel anti-fibrotic drugs.

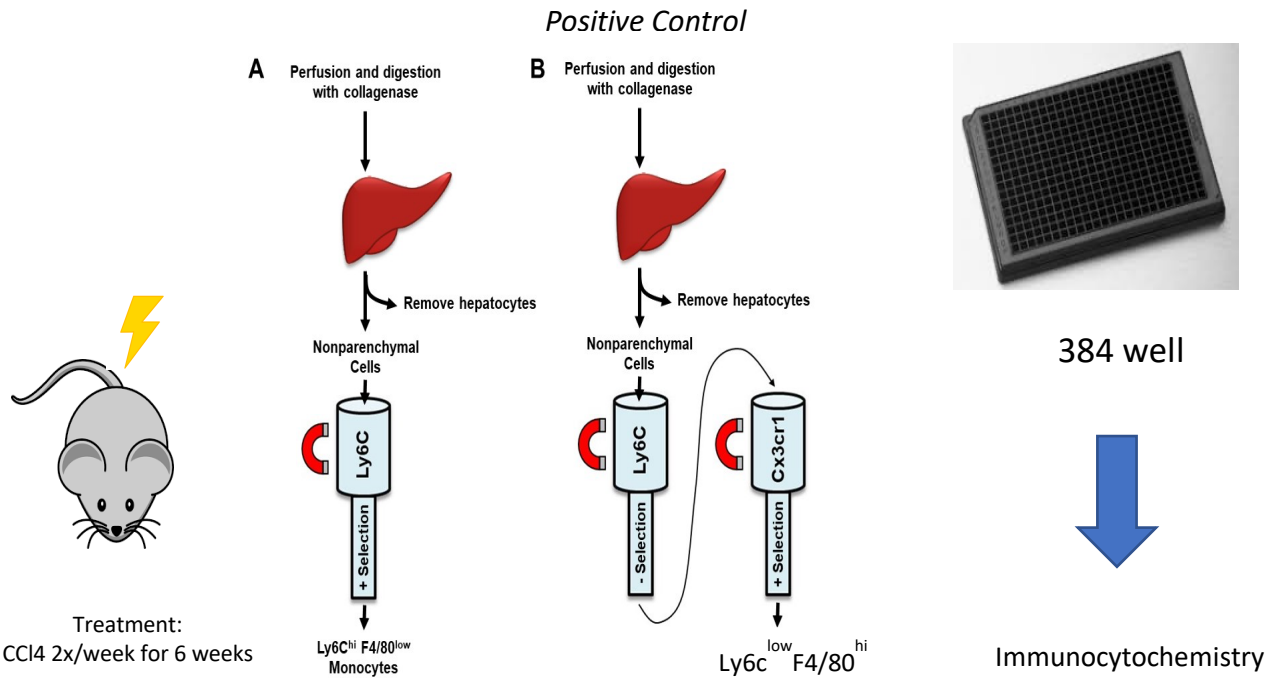

Figure 4.2: Experimental flow-through for high-throughput screen. Mice were treated with CCl_4 twice weekly for six weeks to induce fibrosis. (A) At 24 and (B) 96 hours, the livers were digested with collagenase and hepatocytes were removed by centrifugation. (A) $Ly6c^{hi}F4/80^{neg}$ cells were isolated from the nonparenchymal cells by using anti-Ly6C immunomagnetic beads. (B) $Ly6C^{neg}F4/80^{hi}$ cells were isolated from the nonparenchymal cells first by removing Ly6C positive cells using anti-Ly6C immunomagnetic beads. The $Ly6C^{neg}F4/80^{hi}$ were then purified by using anti-CX3CR1 immunomagnetic beads. (C) Cells were plated at 20,000 cells/well in 384 well plates and treated with compound for 24 hours. (D) Following incubation with compounds, cells were fixed, and F4/80 immunofluorescence was detected.

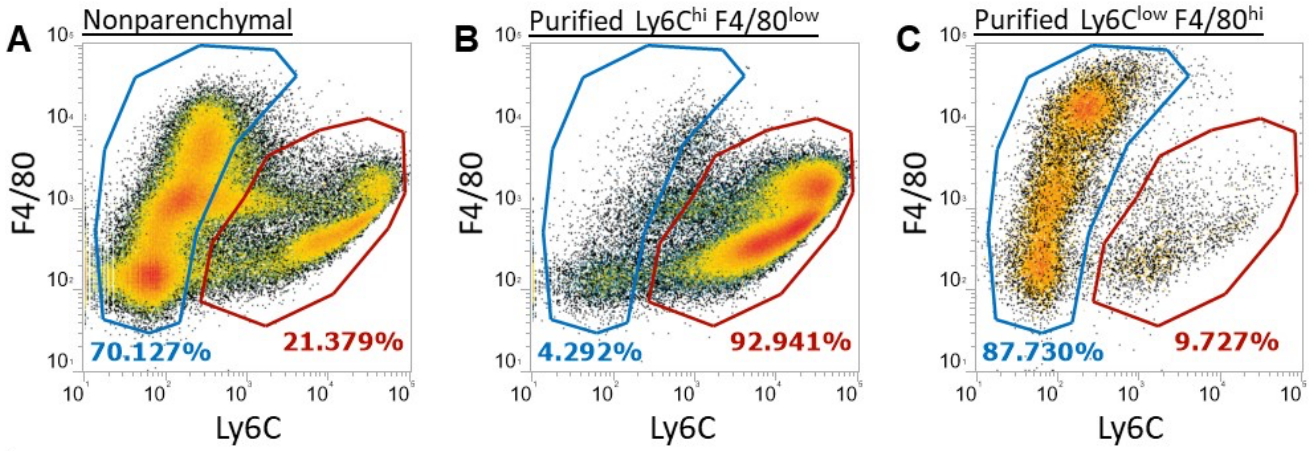

Figure 4.3: Verification of enriched cell populations using flow cytometry. Mice were treated with CCl4 as described. (A) Non-purified nonparenchymal cells, isolated 24 hours after the final CCl4 injection were stained for F4/80 and Ly6s. (B) Ly6c^{hi}F4/80^{low} (red circle) and (C) Ly6c^{low}F4/80^{hi} (blue circle) cells were purified, stained for Ly6c and F4/80, and analyzed by flow cytometry.

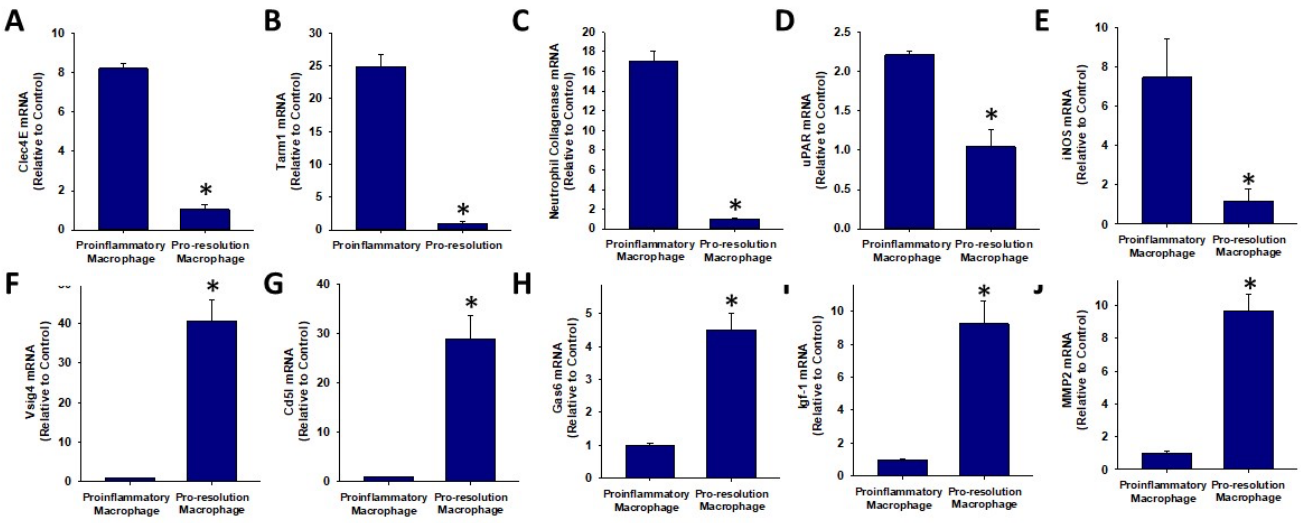

Figure 4.4: mRNAs highly expressed in proinflammatory monocytes and pro-repair macrophages. Ly6c^{hi}F4/80^{low} proinflammatory monocytes and Ly6c^{low}F4/80^{hi} pro-repair macrophages were isolated from CCl_4-treated mice. Real-time PCR was used to quantify the indicated mRNAs. *Significantly different from control.

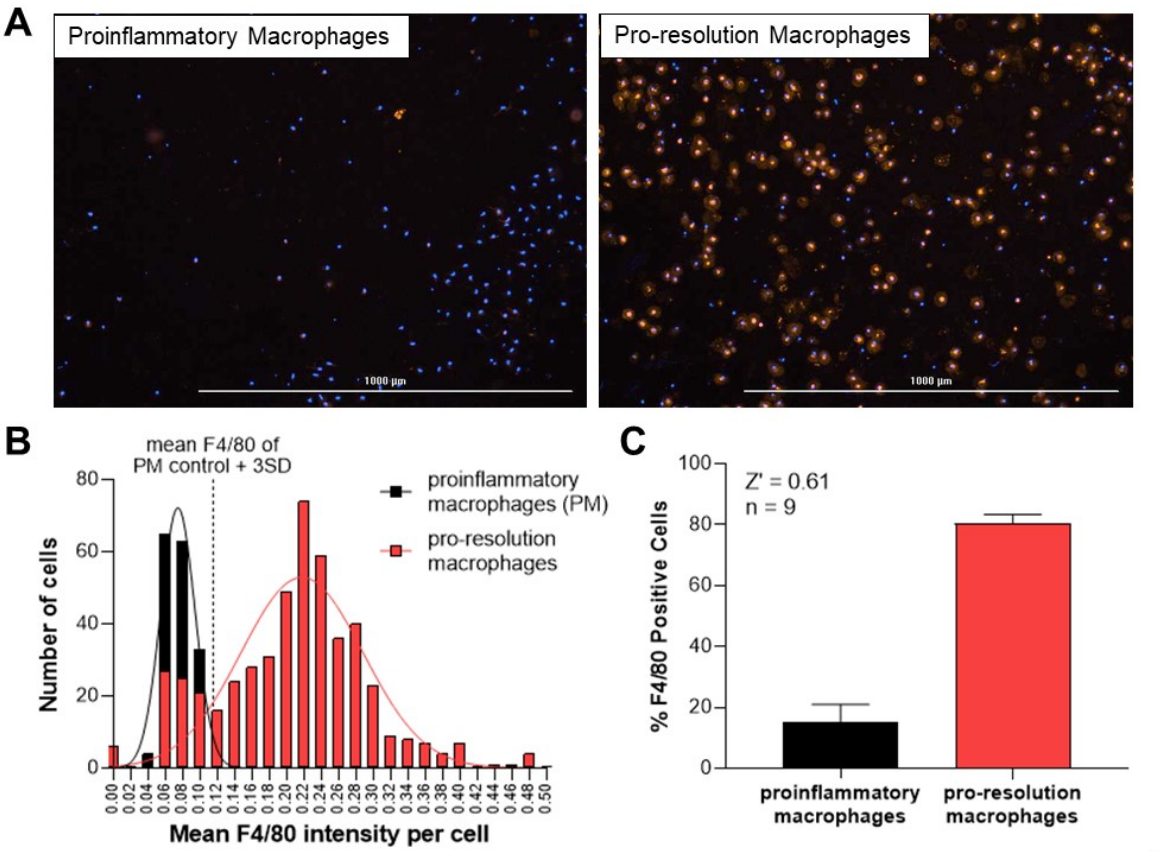

Figure 4.5: Validation of high-throughput screening assay. Proinflammatory and pro-resolution macrophages were isolated from mice. (A) Cells were stained for F4/80 (red) and DNA (DAPI, blue). Representative images. (B) The mean F4/80 intensity per cell was quantified in 2 individual wells containing either proinflammatory or pro-resolution macrophages. (C) The average percentage of F4/80 positive cells was calculated for each well and the Z' calculated.

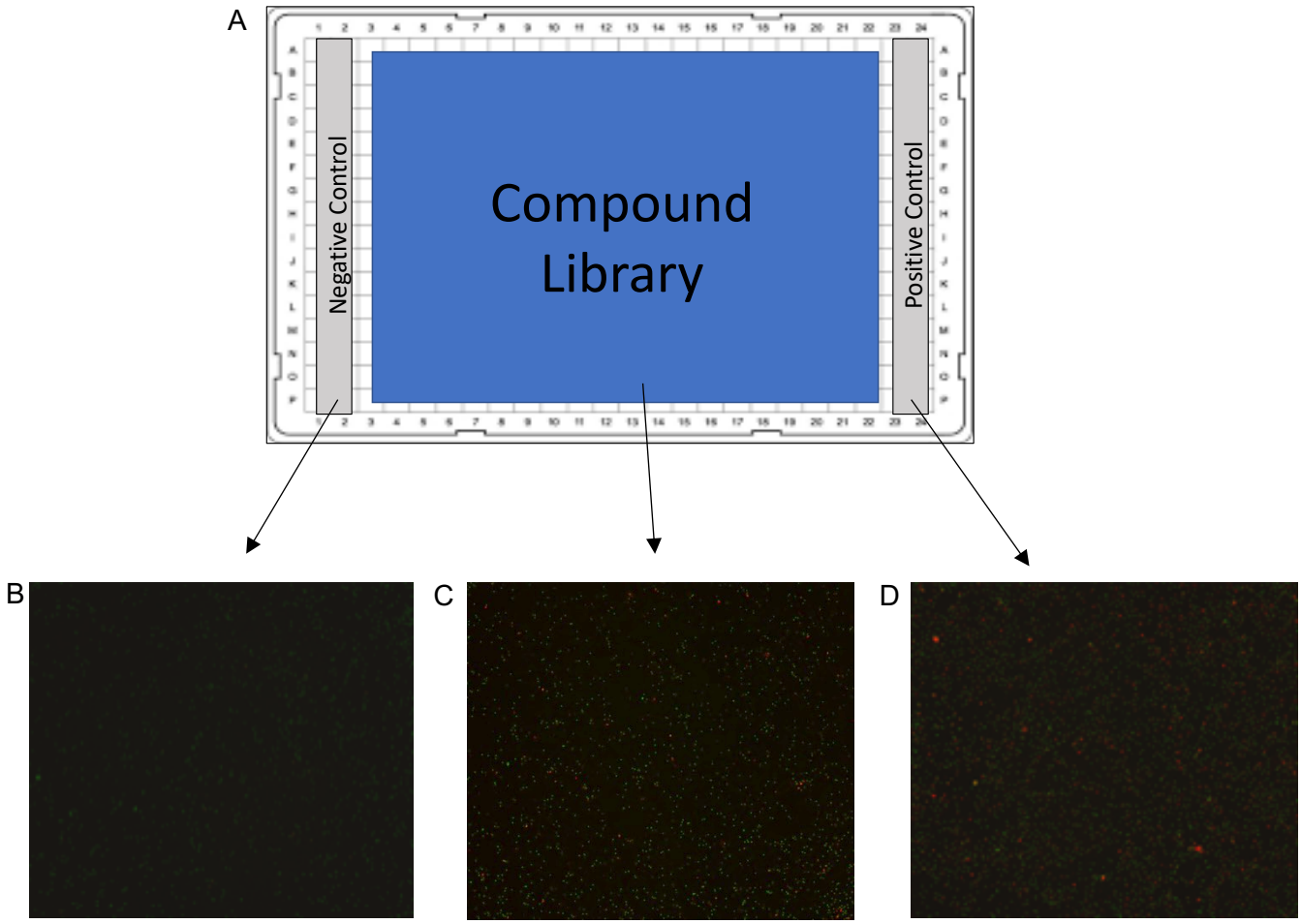

Figure. 4.6: High-throughput screening assay plate template with example negative control, positive control, and positive compound wells. (A) Enriched cell populations were isolated from CCL_4 treated mice and plated in 384 well cell culture plates as indicated. (B) Representative image of a negative control well. (C) Representative image of a positive compound well. (D) Representative image of a positive control well. Green staining represents DAPI and red staining indicates cells positive for F4/80.

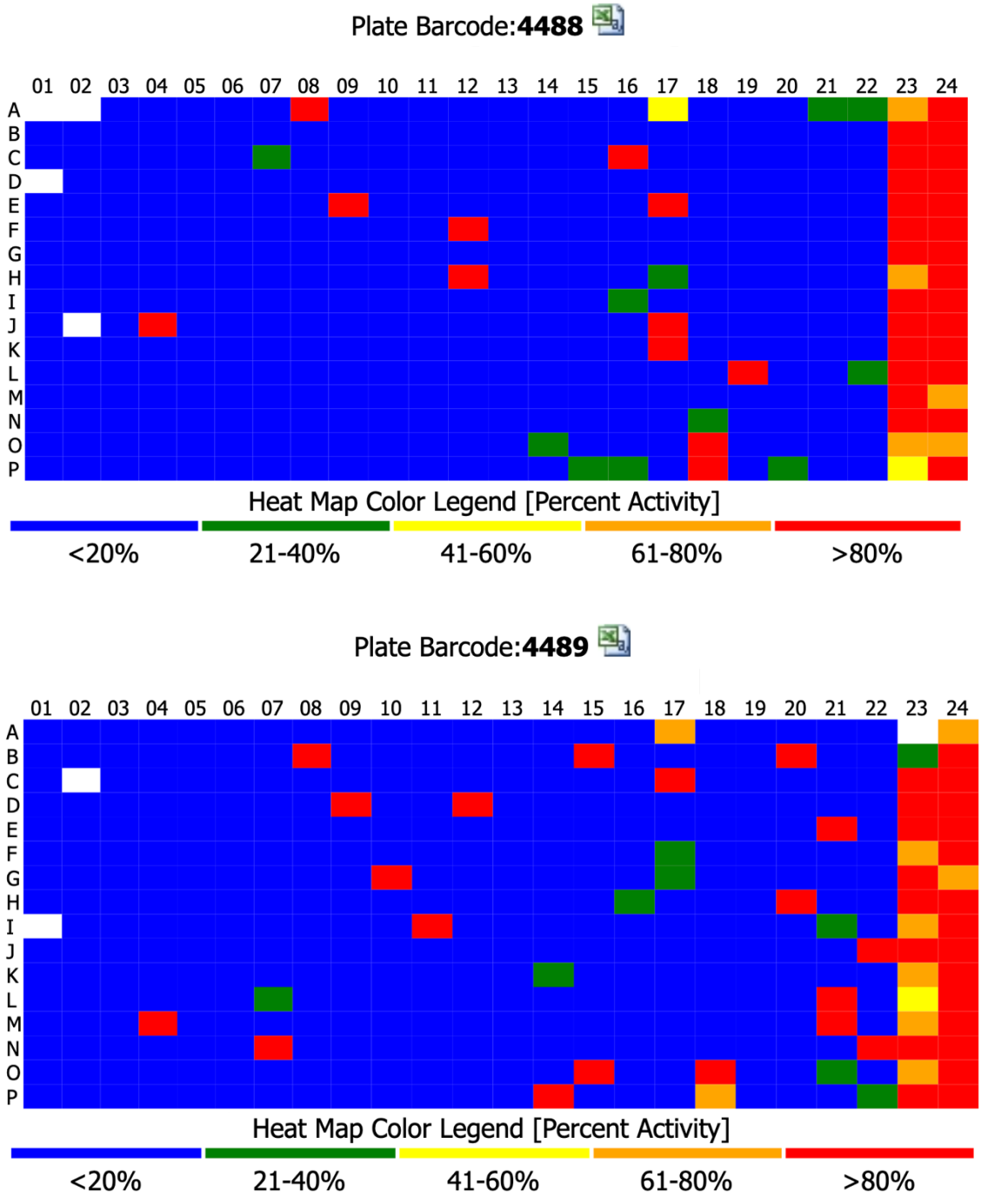

Figure 4.7: Example heat map color legends from green screen. Example of assay plate heatmaps for Plates 4488 and 4489 which were treated with compounds from the GSK library. The Heat Map Color Legend indicates the mean red fluorescence as determined using

Figure 4.7 (cont'd) CellProfiler analysis. Columns 1 and 2 were treated with DMSO. Positive control cells were plated in columns 23 and 24.

Compound ID	Library
Valspodar (P-Glycoprotein (MDR-1; ABCB1) Inhibitors)	NCATS
Rofecoxib (Cyclooxygenase-2 Inhibitor)	NCATS
Vancomycin hydrochloride (glycopeptide antibiotic)	NCATS
Merck-22-6 (AKT Inhibitor)	NCATS
PF-03716556 (H+/K+-ATPase Inhibitor)	NCATS
Genistin (Lipid lowering agents)	NCATS
Roxithromycin (Macrolide Antibiotic)	NCATS
KU-60019 (KU-60019)	NCATS
G?-6976 (G?-6976)	NCATS
Gandotinib (Jak2 inhibitor)	NCATS
Cisplatin (DNA Alkylating Agent)	NCATS
LY2109761 (TGF-bR1 (ALK5) and TGFbR2 inhibitor)	NCATS
ICRF-193 (DNA Topoisomerase II Inhibitors)	NCATS
Fluconazole (Antifungal Agent)	NCATS
Tivozanib (VEGFR-1/2/3 Inhibitor)	NCATS
Trazodone hydrochloride (alpha2-Adrenoceptor Antagonists)	NCATS
LRRK2-IN-1 (Leucine-Rich Repeat Kinase 2 (LRRK2) Inhibitors)	NCATS
Irestatin 9389 (IRE1alpha/XBP-1 inhibitor)	NCATS
BX-912 (Phosphoinositide Dependent Kinase (PDK) 1 Inhibitors)	NCATS
2',3'-Dideoxyinosine (Reverse Transcriptase Inhibitor)	NCATS
Histamine dihydrochloride (Histamine Receptor Agonist)	NCATS
Niacinamide (Vitamin)	NCATS
Mestranol (Estrogen Receptor (ER) Agonist)	NCATS
Kanamycin (30S Ribosomal Protein Inhibitors0	NCATS
A 804598 (P2X7 Receptor Antagonist)	NCATS
Lupeol (Steroid)	NCATS
Quinine (antimalarial agents; Cytochrome P450 CYP2D6 Inhibitors)	NCATS
Cortisone acetate (Glucocorticoid steroid)	NCATS
Prulifloxacin (Antibacterial)	NCATS
Chloroquine (antimalarial agents)	NCATS
Enzastaurin (PKCa, PKCb, PKCg inhbitor)	NCATS
MK-2461 (VEGFR-1 (Flt-1) Inhibitors)	NCATS
Propafenone hydrochloride (Propafenone hydrochloride)	NCATS

Table 4.1: Complete list of compounds identified as hits in the primary high-throughput screen.

Table 4.1 (cont'd)

Almotriptan (5-HT1B Agonist)	NCATS
Diclazuril (antiprotozoal agent)	NCATS
Tobramycin (30S Ribosomal Protein Inhibitors)	NCATS
Fenofibrate (PPARalpha Agonist)	NCATS
Ethisterone (Progestogen hormone)	NCATS
Rolofylline (Adenosine A1 Antagonist)	NCATS
GPLG-0634 (Jak1 Inhibitor)	NCATS
Imatinib (Bcr-Abl Inhibitor)	NCATS
Malotilate (Liver Protein Metabolism)	NCATS
Niraparib (PARP-1/PARP-2 Inhibitor)	NCATS
Manoalide (Calcium Channel Blocker)	NCATS
Lamotrigine (Sodium channel inhibitor)	NCATS
Eplerenone (Mineralocorticoid Receptor (MR) Antagonist)	NCATS
Gabapentin (Calcium Channels (Voltage-Gated) alpha2/delta-1/2 Subunit Ligand)	NCATS
NCGC00262331 (Flt3)	NCATS
BMS-345541 (IKK beta inhibitor)	NCATS
Testosterone propionate (Androgen Receptor Agonist)	NCATS
Lubiprostone (ClC-2 Channel Activators)	NCATS
Paclitaxel (Tubulin depolymerization inhibitor)	NCATS
Canertinib (EGFR (HER1; erbB1) inhibitor)	NCATS
Flurbiprofen (non-steroidal antiinflammatory)	NCATS
Thiazovivin (ROCK Inhibitor)	NCATS
Baricitinib (Jak2 inhibitor)	NCATS
Resistomycin (RNA Polymerase Inhibitor)	NCATS
S-Trityl-L-cysteine (Mitotic Kinesin Eg5 Inhibitor)	NCATS
Neomycin sulfate (30S Ribosomal Protein Inhibitors)	NCATS
Alibendol (treatments of indigestin, nausea)	NCATS
Pancuronium bromide (Steroid non-depolarizing blocker)	NCATS
GSK429286A (ROCK 1, ROCK 2 Inhibitor)	NCATS
Pepstatin (Aspartyl Protease Inhibitor)	NCATS
Rifampicin (DNA-Directed RNA Polymerase Inhibitor)	NCATS
Pravastatin sodium (HMG-CoA Reductase Inhibitor)	NCATS
A 839977 (P2X7 Receptor Antagonist0	NCATS
Etoposide (DNA Topoisomerase II Inhibitors)	NCATS
Artemisinin (antimalarial agents)	NCATS
HMSL10083 (CSF1R (c-FMS) Inhibitor)	NCATS
BIBR 1048 (Thrombin Inhibitors)	NCATS

Table 4.1 (cont'd)

Tie-2 kinase inhibitor	NCATS
Meglumine (amino sugar)	NCATS
HMSL10076 (discoidin domain receptor tyrosine kinase (DDR1))	NCATS
Dacomitinib (EGFR (HER1; erbB1) inhibitor)	NCATS
PF-431396 (Focal Adhesion Kinase (FAK) Inhibitor)	NCATS
Iloperidone (Dopamine D2 Antagonist)	NCATS
PNU-74654 (Wnt Signaling Inhibitor)	NCATS
Tempol (Free Radical Scavenger)	NCATS
Flupirtine maleate (Voltage-Gated K(V) 7 (KCNQ) Channel Activator)	NCATS
CP-724714 (HER2 (erbB2) Inhibitor)	NCATS
Orotic acid (metabolite)	NCATS
Ibutamoren mesilate (Growth Hormone Secretagogue)	NCATS
NSC-75503 (Hedgehog antagonist)	NCATS
GSK-1016790A (TRPV4 Agonist)	NCATS
Finasteride (Androgen Receptor Antagonist)	NCATS
GSK-2636771 (PI3Kbeta inhibitor)	NCATS
E-7010 (Tubulin polymerization inhibitor)	NCATS
Cefdinir (Cephalosporin antibiotic)	NCATS
ASR-isobudimer-SO2Ph-4-CH2OC(O)NMe2 (artemesinin analogue)	NCATS
BAY-41-8543 (Guanylate Cyclase Activator)	NCATS
Sulindac (non-steroidal antiinflammatory)	NCATS
Piraxostat (Xanthine Oxidase Inhibitor)	NCATS
Pentamidine isethionate (PRL Phosphatase Inhibitors)	NCATS
D-4476 (Casein Kinase I (CK1) Inhibitor)	NCATS
Rose Bengal disodium (Free radical formation)	NCATS
NVP-BVU-972 (HGFR (MET; c-Met) Inhibitor)	NCATS
TG-100115 (PI3K Inhibitor)	NCATS
Dorzolamide hydrochloride (Carbonic Anhydrase Type II Inhibitors)	NCATS
Leflunomide (Jak inhibitor)	NCATS
SU-6656 (Lyn Kinase Inhibitor)	NCATS
Antimycin A (Antifungal Agent)	NCATS
TPCK (Cysteine Protease Inhibitor)	NCATS
Esomeprazole magnesium (H+/K+-ATPase Inhibitor)	NCATS
HMSL10088 (Receptor-interacting serine/threonine-protein kinase 1 (RIPK1))	NCATS
Azelastine hydrochloride (Histamine H1 Receptor Antagonists)	NCATS
c-FMS inhibitor (CSF1R (c-FMS) Inhibitor)	NCATS
GSK837149A (Fatty acid synthase inhibitor)	NCATS

Table 4.1 (cont'd)

ADX-47273 (mgluR5 Antagonists)	NCATS
GNF-5837 (Tropomyosin Related Kinase A/B/C (TrkA/B/C) inhibitor)	NCATS
Odanacatib (Cathepsin K Inhibitors)	NCATS
CAL-101 (Idelalisib, GS-1101) (PI3Kdelta inhibitor)	NCATS
GSK1379762A	GSK
GW494702A	GSK
GSK323521A	GSK
SB-381891	GSK
GSK2593074A	GSK
GW835314X	GSK
GW552771X	GSK
SB-742352-AC	GSK
GSK2137462A	GSK
GW654607A	GSK
GW574783B (top three kinases: Mer Kinase; EGFR; ERBB4)	GSK
GW589961A (top three kinases: DDR2; KIT; PDGFRA)	GSK
GW607049A	GSK
GW694234A (top three kinases: DDR2; KIT; PDGFRA)	GSK
GW577921A (top three kinases: KIT; FLT3; FMS)	GSK
GW814408X (top three kinases: Mer Kinase; GSK3A; GSK3B)	GSK
GSK718429A (top three kinases: ERBB4; PIP5K1; MET)	GSK
GW831090X (top three kinases: KIT; CDK2/cyclinA; PIP5K1)	GSK
GW796921X (top three kinases: P38alpha; P38beta; PIP5K1)	GSK
Cyanein (Golgi-Specific Brefeldin A-Resistance Guanine Nucleotide Exchange Factor 1 (GBF1) Inhibitors)	NCATS
Teriflunomide (MMP-2, 9 Inhibitor)	NCATS
Obatoclax (Bcl-xL inhibitor)	NCATS
A-769662 (AMP-Activated Protein Kinase (AMPK) Activator)	NCATS
Compound 7 (Histone Deacetylase (HDAC) 6 Inhibitor)	NCATS
CAA0225 (Cathepsin L Inhibitors)	NCATS
Vidarabine (Adenosine Receptor Agonist; Anti-Herpes Simplex Virus Drug)	NCATS
Cilostazol (Phosphodiesterase III (PDE3) Inhibitor)	NCATS
ICI-D7288 (HCN [I(h)] Blockers)	NCATS
GSI-9 (g-Secretase Inhibitor)	NCATS
PD 0325901 (MEK inhibitor)	NCATS
TAK-715 (p38 MAPK Inhibitor0	NCATS
Diosmin (Aryl Hydrocarbon Receptor (AhR) Agonists)	NCATS

Table 4.1 (cont'd) The NCATS and GSK libraries were screen to identify compounds capable of stimulating macrophage polarization. The 145 compounds listed in Table 1 were identified as hits.

Active Compound	Target	Signaling Pathway
MSU-9017 (GW574783B)	top three kinases: Mer Kinase; EGFR; ERBB4	ErbB family of receptors
Canertinib	EGFR (HER1; erbB1) inhibitor	
Dacomitinib	EGFR (HER1; erbB1) inhibitor	
CP-724714	HER2 (erbB2) Inhibitor	
NVP-BVU-972	HGFR (MET; c-Met) Inhibitor	
GW574783B	top three kinases: Mer Kinase; EGFR; ERBB4	
MSU-40094 (HMSL10083)	CSF1R (c-FMS) Inhibitor	CSF-1 Receptor
HMSL10083	CSF1R (c-FMS) Inhibitor	
c-FMS inhibitor	CSF1R (c-FMS) Inhibitor	
GSK429286A	ROCK 1, ROCK 2 Inhibitor	Cytoskeleton and Actin Remodeling
Thiazovivin	ROCK Inhibitor	
GW831090X	top three kinases: KIT; CDK2/cyclinA; PIP5K1	
BX-912	Phosphoinositide Dependent Kinase (PDK) 1 Inhibitors	
GW796921X	top three kinases: P38alpha; P38beta; PIP5K1	
Merck-22-6	AKT Inhibitor	Akt Signaling
BX-912	Phosphoinositide Dependent Kinase (PDK) 1 Inhibitors	
GSK-2636771	PI3Kbeta inhibitor	
TG-100115	PI3K Inhibitor	
CAL-101	PI3Kdelta inhibitor	
GW831090X	top three kinases: KIT; CDK2/cyclinA; PIP5K1	
GW796921X	top three kinases: P38alpha; P38beta; PIP5K1	

Table 4.2: Redundant signaling pathways identified during analysis of hits from high-throughput screening assay.

Table 4.2 (cont'd)

GSK718429A	top three kinases: ERBB4; PIP5K1; MET	
A-769662	AMP-Activated Protein Kinase (AMPK) Activator	
Gandotinib	Jak2 inhibitor	Jak/Stat Signaling
GPLG-0634	Jak1 inhibitor	
Baricitinib	Jak2 inhibitor	
Leflunomide	Jak inhibitor	
Tivozanib	VEGFR-1/2/3 Inhibitor	VEGF Receptors
MK-2461	VEGFR-1 (Flt-1) Inhibitors	
Tie-2 kinase inhibitor	VEGFR-2/3 Inhibitor	
SU-6656	Lyn Kinase Inhibitor	DDR receptor signaling
GW589961A	top three kinases: DDR2; KIT; PDGFRA	
GW694234A	top three kinases: DDR2; KIT; PDGFRA	
HMSL10076	discoidin domain receptor tyrosine kinase (DDR1)	

Table 4.2 (cont'd) Analysis of hits revealed multiple compounds with redundant signaling pathways that have been implicated in regulating macrophage phenotype, including compounds that were inhibitors of: colony stimulating factor 1 receptor (CSF1R), Rho-associated coiled-coil containing protein kinase (ROCK), epidermal growth factor receptor (EGFR), protein kinase B (Akt), Janus kinases/signal transducer and activator of transcription proteins (JAK/STAT), vascular endothelial growth factor (VEGF), and discoidin domain receptor (DDR) signaling.

BIBLIOGRAPHY

Abron JD, Singh NP, Price RL, Nagarkatti M, Nagarkatti PS, Singh UP. Genistein induces macrophage polarization and systemic cytokine to ameliorate experimental colitis. PLoS One. 2018 Jul 19;13(7):e0199631. doi: 10.1371/journal.pone.0199631. PMID: 30024891; PMCID: PMC6053137.

Abu-Rish EY, Dahabiyeh LA, Bustanji Y, Mohamed YS, Browning MJ. Effect of lamotrigine on in vivo and in vitro cytokine secretion in murine model of inflammation. J Neuroimmunol. 2018 Sep 15;322:36-45. doi: 10.1016/j.jneuroim.2018.06.008. Epub 2018 Jun 11. PMID: 29937116.

Arlauckas SP, Garren SB, Garris CS, Kohler RH, Oh J, Pittet MJ, Weissleder R. Arg1 expression defines immunosuppressive subsets of tumor-associated macrophages. Theranostics. 2018 Nov 12;8(21):5842-5854. doi: 10.7150/thno.26888. PMID: 30613266; PMCID: PMC6299430.

Asrani SK, Devarbhavi H, Eaton J, Kamath PS. Burden of liver diseases in the world. J Hepatol. 2019 Jan;70(1):151-171. doi: 10.1016/j.jhep.2018.09.014. Epub 2018 Sep 26. PMID: 30266282.

Carnero A. High throughput screening in drug discovery. Clin Transl Oncol. 2006 Jul;8(7):482-90. doi: 10.1007/s12094-006-0048-2. PMID: 16870538.

Cannarile MA, Weisser M, Jacob W, Jegg AM, Ries CH, Rüttinger D. Colony-stimulating factor 1 receptor (CSF1R) inhibitors in cancer therapy. J Immunother Cancer. 2017 Jul 18;5(1):53. doi: 10.1186/s40425-017-0257-y. PMID: 28716061; PMCID: PMC5514481.

Cutolo M, Sulli A, Ghiorzo P, Pizzorni C, Craviotto C, Villaggio B. Anti-inflammatory effects of leflunomide on cultured synovial macrophages from patients with rheumatoid arthritis. Ann Rheum Dis. 2003 Apr;62(4):297-302. doi: 10.1136/ard.62.4.297. PMID: 12634225; PMCID: PMC1754507.

Engel JE, Williams E, Williams ML, Bidwell GL 3rd, Chade AR. Targeted VEGF (Vascular Endothelial Growth Factor) Therapy Induces Long-Term Renal Recovery in Chronic Kidney Disease via Macrophage Polarization. Hypertension. 2019 Nov;74(5):1113-1123. doi: 10.1161/HYPERTENSIONAHA.119.13469. Epub 2019 Sep 23. PMID: 31542966; PMCID: PMC6785403.

Estes C, Razavi H, Loomba R, Younossi Z, Sanyal AJ. Modeling the epidemic of nonalcoholic fatty liver disease demonstrates an exponential increase in burden of disease. Hepatology. 2018 Jan;67(1):123-133. doi: 10.1002/hep.29466. Epub 2017 Dec 1. PMID: 28802062; PMCID: PMC5767767.

Jung WK, Lee DY, Park C, Choi YH, Choi I, Park SG, Seo SK, Lee SW, Yea SS, Ahn SC, Lee CM, Park WS, Ko JH, Choi IW. Cilostazol is anti-inflammatory in BV2 microglial cells by inactivating nuclear factor-kappaB and inhibiting mitogen-activated protein kinases. Br J Pharmacol. 2010 Mar;159(6):1274-85. doi: 10.1111/j.1476-5381.2009.00615.x. Epub 2010 Jan 28. PMID: 20128801; PMCID: PMC2848931.

Habka D, Mann D, Landes R, Soto-Gutierrez A. Future Economics of Liver Transplantation: A 20-Year Cost Modeling Forecast and the Prospect of Bioengineering Autologous Liver Grafts. PLoS One. 2015 Jul 15;10(7):e0131764. doi: 10.1371/journal.pone.0131764. PMID: 26177505; PMCID: PMC4503760.
Hardbower DM, Singh K, Asim M, Verriere TG, Olivares-Villagómez D, Barry DP, Allaman MM, Washington MK, Peek RM Jr, Piazuelo MB, Wilson KT. EGFR regulates macrophage activation and function in bacterial infection. J Clin Invest. 2016 Sep 1;126(9):3296-312. doi: 10.1172/JCI83585. Epub 2016 Aug 2. PMID: 27482886; PMCID: PMC5004944.

Hu G, Su Y, Kang BH, Fan Z, Dong T, Brown DR, Cheah J, Wittrup KD, Chen J. High-throughput phenotypic screen and transcriptional analysis identify new compounds and targets for macrophage reprogramming. Nat Commun. 2021 Feb 3;12(1):773. doi: 10.1038/s41467-021-21066-x. PMID: 33536439; PMCID: PMC7858590.

Ismail MH, Pinzani M. Reversal of liver fibrosis. Saudi J Gastroenterol. 2009 Jan;15(1):72-9. doi: 10.4103/1319-3767.45072. PMID: 19568569; PMCID: PMC2702953.

Liu Y, Tejpal N, You J, Li XC, Ghobrial RM, Kloc M. ROCK inhibition impedes macrophage polarity and functions. Cell Immunol. 2016 Feb;300:54-62. doi: 10.1016/j.cellimm.2015.12.005. Epub 2015 Dec 17. PMID: 26711331.

Macarron R, Banks MN, Bojanic D, Burns DJ, Cirovic DA, Garyantes T, Green DV, Hertzberg RP, Janzen WP, Paslay JW, Schopfer U, Sittampalam GS. Impact of high-throughput screening in biomedical research. Nat Rev Drug Discov. 2011 Mar;10(3):188-95. doi: 10.1038/nrd3368. PMID: 21358738.

Malyshev I, Malyshev Y. Current Concept and Update of the Macrophage Plasticity Concept: Intracellular Mechanisms of Reprogramming and M3 Macrophage "Switch" Phenotype. Biomed Res Int. 2015;2015:341308. doi: 10.1155/2015/341308. Epub 2015 Aug 23. PMID: 26366410; PMCID: PMC4561113.

Mayer AM. Manoalide: un nuevo inhibidor de fosfolipasa A2 de origen marino con una potencial acción inmunorregulatoria [Manoalide: a new phospholipase A2 inhibitor of marine origin with potential immunoregulatory effect]. Medicina (B Aires). 1989;49(2):175-80. Spanish. PMID: 2640487.

Montserrat-de la Paz S, Naranjo MC, Lopez S, Abia R, Muriana FJG, Bermudez B. Niacin and its metabolites as master regulators of macrophage activation. J Nutr Biochem. 2017 Jan;39:40-47. doi: 10.1016/j.jnutbio.2016.09.008. Epub 2016 Oct 1. PMID: 27771381.

Ramachandran P, Iredale JP. Reversibility of liver fibrosis. Ann Hepatol. 2009 Oct-Dec;8(4):283-91. PMID: 20009126.

Ramachandran P, Pellicoro A, Vernon MA, Boulter L, Aucott RL, Ali A, Hartland SN, Snowdon VK, Cappon A, Gordon-Walker TT, Williams MJ, Dunbar DR, Manning JR, van Rooijen N, Fallowfield JA, Forbes SJ, Iredale JP. Differential Ly-6C expression identifies the recruited macrophage phenotype, which orchestrates the regression of murine liver fibrosis. Proc Natl Acad Sci U S A. 2012 Nov 13;109(46):E3186-95. doi: 10.1073/pnas.1119964109. Epub 2012 Oct 24. PMID: 23100531; PMCID: PMC3503234.

Rodell CB, Koch PD, Weissleder R. Screening for new macrophage therapeutics. Theranostics. 2019 Oct 15;9(25):7714-7729. doi: 10.7150/thno.34421. PMID: 31695796; PMCID: PMC6831478.

Roth K, Strickland J, Joshi N, Deng M, Kennedy RC, Rockwell CE, Luyendyk JP, Billiar TR, Copple BL. Dichotomous Role of Plasmin in Regulation of Macrophage Function after Acetaminophen Overdose. Am J Pathol. 2019 Oct;189(10):1986-2001. doi: 10.1016/j.ajpath.2019.07.003. Epub 2019 Aug 2. PMID: 31381887; PMCID: PMC6892227.

Scholten D, Trebicka J, Liedtke C, Weiskirchen R. The carbon tetrachloride model in mice. Lab Anim. 2015 Apr;49(1 Suppl):4-11. doi: 10.1177/0023677215571192. PMID: 25835733.

Szymański P, Markowicz M, Mikiciuk-Olasik E. Adaptation of high-throughput screening in drug discovery-toxicological screening tests. Int J Mol Sci. 2012;13(1):427-52. doi: 10.3390/ijms13010427. Epub 2011 Dec 29. PMID: 22312262; PMCID: PMC3269696.

Varma H, Lo DC, Stockwell BR. High-Throughput and High-Content Screening for Huntington's Disease Therapeutics. In: Lo DC, Hughes RE, editors. Neurobiology of Huntington's Disease: Applications to Drug Discovery. Boca Raton (FL): CRC Press/Taylor & Francis; 2011. Chapter 5. PMID: 21882410.

Vergadi E, Ieronymaki E, Lyroni K, Vaporidi K, Tsatsanis C. Akt Signaling Pathway in Macrophage Activation and M1/M2 Polarization. J Immunol. 2017 Feb 1;198(3):1006-1014. doi: 10.4049/jimmunol.1601515. PMID: 28115590.

Wakade C, Giri B, Malik A, Khodadadi H, Morgan JC, Chong RK, Baban B. Niacin modulates macrophage polarization in Parkinson's disease. J Neuroimmunol. 2018 Jul 15;320:76-79. doi: 10.1016/j.jneuroim.2018.05.002. Epub 2018 May 4. PMID: 29759143.

Wolf AM, Wolf D, Rumpold H, Ludwiczek S, Enrich B, Gastl G, Weiss G, Tilg H. The kinase inhibitor imatinib mesylate inhibits TNF-{alpha} production in vitro and prevents TNF-dependent acute hepatic inflammation. Proc Natl Acad Sci U S A. 2005 Sep 20;102(38):13622-7. doi: 10.1073/pnas.0501758102. Epub 2005 Sep 8. PMID: 16174751; PMCID: PMC1224614.

Zhang JH, Chung TD, Oldenburg KR. A Simple Statistical Parameter for Use in Evaluation and Validation of High Throughput Screening Assays. J Biomol Screen. 1999;4(2):67-73. doi: 10.1177/108705719900400206. PMID: 10838414.

CHAPTER 5

DISCUSSION

5.1 Summary and Significance

Acute liver failure (ALF) is a rare and life-threatening condition that occurs suddenly (<26 weeks in duration) in patients without pre-existing liver disease. The most common cause of ALF in the United States is acetaminophen (APAP) toxicity, which causes a potentially fatal, hepatic centrilobular necrosis. In patients that fail to recover from liver injury, through initiation of hepatic repair processes, a liver transplant is the only option for survival (Bernal et al., 2015). APAP-induced ALF patients with the poorest prognosis exhibit high systemic levels of the anti-inflammatory cytokine IL-10. The mechanistic basis for this counterintuitive connection is not known. It has been proposed that IL-10 levels may become elevated to counteract the pathologic effects of proinflammatory cytokines, which are also elevated in these patients. However, investigation into the function of IL-10 in murine models contradict this hypothesis as studies have shown liver injury and mortality are greatly increased in IL-10 knockout mice treated with APAP (Bourdi et al., 2002). The basis for these disparate findings was unknown. However, we show that this is related to the experimental paradigm used to investigate APAP-induced liver injury in mice. Typically, mice are treated with a dose of APAP (i.e., 300 mg/kg) that produces liver injury which is fully repaired without the need for additional therapeutic interventions. Because of this, many of the important features of APAP-induced ALF are not recapitulated, including failed liver repair and multiorgan dysfunction which contribute to the high mortality occurring in ALF patients. Higher doses of APAP (at or near 600 mg/kg), however, do recapitulate the many detrimental complications associated with ALF. Thus, as a part of this dissertation, we have investigated the role of IL-10 in a murine model of APAP-induced ALF.

In mice treated with 600 mg/kg APAP, macrophages failed to traffic into necrotic lesions (Figure 2.3C and 2.4A). Importantly, impairments in macrophage trafficking were associated with failed clearance of dead cells and sustained production of both proinflammatory (IL-6) and anti-inflammatory cytokines (IL-10). In mice treated with 300 mg/kg APAP, CD68+ macrophages filled the necrotic lesions by 48 hours (Figure 2.3C). This phenomenon has been

noted in ALF patient livers (Antoniades et al., 2008) (Antoniades et al., 2012). Treatment of ALF mice with an IL-10 neutralizing antibody restored macrophage trafficking into areas of necrosis (Figure 2.8E-F). Conversely, treatment of mice with recombinant IL-10, beginning at 24 hours after 300 mg/kg APAP, prevented intrahepatic macrophage trafficking into the necrotic lesions (Figure 2.8 H-I). These data suggest high levels of IL-10 negatively impact the ability of MDMs to migrate within the liver and contributes to failed repair.

Furthermore, our studies have identified Kupffer cells, the resident macrophages of the liver, are likely the primary source of IL-10 in APAP-induced ALF. In mice treated with 600 mg/kg APAP, these cells expressed several markers of MDSCs, including high-level expression of IL-10, PD-L1, CD11b, Axl and Cx3Cr1 (Figure 2.7) (Yaseen et al., 2020). MDSCs are highly immunosuppressive and are typically generated under pathological conditions (Yaseen et al., 2020). MDSCs have not been reported previously in ALF, however, previous studies have shown that these cells are increased in acute-on-chronic liver failure and associated with inflammatory diseases. Furthermore, our studies reveal, that high levels of IL-6, occurring under conditions of APAP-induced ALF, stimulates the formation of these cells, as neutralization of IL-6 reduced levels of both IL-10 and PD-L1 (Figure 2.10D-E).

Similarly to IL-10, high levels of IL-6 are also associated with a poor outcome in APAP-induced ALF patients (Bonkovsky et al., 2019). Thus, the studies presented in this dissertation provide potential insight into the mechanism by which IL-6 negatively impacts recovery in ALF patients. Intriguingly, neutralization of IL-6 also corresponded with decreased mortality in this setting (Figure 2.11A). Remarkably, mice treated with 600 mg/kg APAP and the IL-6 neutralizing antibody displayed decreased symptoms of HE and had increased cerebral blood flow compared to mice receiving 600 mg/kg APAP and control antibody (Figure 2.12). As noted in Chapter 1, the development of HE is a critical defining feature of ALF. Future studies are needed to determine the mechanistic link between this intriguing finding.

Another area of interest in this dissertation is the role of MDM dysfunction in APAP-induced ALF. Experimental studies have documented that MDM function is critical for repair of the APAP-injured liver (You et al., 2013). MDMs are characterized as Ly6C^{hi} F4/80^{-}, traffic into necrotic foci where they phagocytose dead cell debris (You et al., 2013) (Ju et al., 2016). During reparative phases of APAP-induced liver injury, this process is associated with a phenotypic shift from an M1-like proinflammatory macrophage towards an M2-like pro-reparative macrophage, a process that terminates proinflammatory cytokine synthesis and drives pathways central to cell proliferation and resolution of tissue necrosis (Zigmond et al., 2014). It has been proposed that blood levels of proinflammatory cytokines are high in patients with ALF because macrophages fail to switch phenotype (Antoniades et al., 2008).

To investigate whether proinflammatory monocytes fail to change phenotype in the murine model of APAP-induced ALF we challenged mice with either 300 mg/kg or 600 mg/kg APAP. Following treatment with both doses, a population of Ly6C^{+} F4/80^{-} macrophages accumulated in the injured liver (Figure 2.4C and E). By 72 hours, this population of cells was no longer detected in the livers of mice treated with 300 mg/kg APAP, indicating that they had switched to Ly6C^{-} F4/80^{+} pro-repair macrophages (Figure 2.4D). Consistent with this, F4/80^{+} macrophages were evident within repairing lesions of these mice at 72 hours after APAP, and levels of proinflammatory cytokines had returned to baseline (Figure 2.5). In stark contrast, hepatic Ly6C^{+} F4/80^{-} macrophages persisted in the livers of mice treated 72 hours earlier with 600 mg/kg APAP, indicating a failure of MDMs to switch phenotype (Figure 2.4D and F). Furthermore, F4/80^{+} macrophages were absent from the necrotic foci (Figure 2.4A), and levels of proinflammatory cytokines remained persistently elevated (Figure 2.5).

Collectively, the studies presented in this dissertation provide compelling experimental evidence suggesting that the unrestrained cytokine synthesis that occurs in APAP-induced ALF, results from a failure of MDMs to switch phenotype. The underlying cause remains to be determined. However, impaired phenotype switching may result, in part, from a failure of MDMs

to phagocytose dead cell debris in ALF. We recently reported that phagocytosis of necrotic hepatocytes by Ly6C^{hi} F4/80^{low} MDMs, purified from the livers of APAP-treated mice, decreased expression of several proinflammatory cytokines (Roth et al., 2019). This suggests that a failure of macrophages to phagocytose dead cell debris in ALF may prevent the phenotypic transition of these cells, leading to sustained cytokine synthesis and SIRS. Thus, therapeutic targeting of phagocytic pathways in this macrophage population may be a viable approach to terminate synthesis of proinflammatory cytokines.

The TAM family of receptor kinases are highly expressed on macrophages, and have been shown to play vital role(s) in the resolution of inflammation. Activation of this family of receptors has been shown to dampen the immune response through the phagocytosis of dead cells exposing phospotidylserine (PS) on their outer membrane leaflet (Rothlin et al., 2015) (Lemke 2017). Loss of TAMs has been shown to induce a proinflammatory state characterized by a reduction in clearance of necrotic and apoptotic cellular debris (Rothlin et al., 2015). Furthermore, studies have shown the TAM receptor Axl promotes macrophage polarization in inflammatory environments. Thus, we next investigated the role of TAM receptors in regulating monocyte differentiation in APAP-induced acute liver injury and APAP-induced ALF.

For these studies, we treated Axl and Mer mutant mice with 300 mg/kg APAP. The primary objective of these studies was to determine the role of TAM receptors in the resolution of inflammation following APAP overdose, which generally occurs between 48 and 72 hours after APAP administration. However, these analyses were precluded by the strong phenotype observed in Axl$^{-/-}$ mice. While wild-type and Mer$^{-/-}$ mice were motile and superficially normal at 12, 24, and 48 hours following treatment with APAP, 30% of Axl$^{-/-}$ mice had died by 48 hours. Surviving Axl$^{-/-}$ mice were nonmotile and at or near death at 48 hours. Not only was this result unexpected, but it also occurred following treatment with a dose off APAP at which liver injury is generally fully repaired without the need for additional therapeutic interventions by 72 hours (Bhushan et al., 2014). Histopathological analysis revealed extensive hepatocellular necrosis

and sinusoidal congestion and hemorrhage in surviving $Axl^{-/-}$ mice (Figure 3.2A and B) (Zagórska et al., 2020). Hemorrhage was not detected within the liver parenchyma of WT or $Mertk^{-/-}$ mice following treatment with APAP, suggesting $Axl^{-/-}$ mice were uniquely susceptible to APAP hepatotoxicity (Figure 3.2A and B). Surprisingly, despite increased hepatic injury in surviving $Axl^{-/-}$, there were no significant differences in cytokine/chemokine mRNA levels between TAM mutants and WT mice, indicating that the Axl-specific liver damage induced by APAP was not due to specific elevation of cytokine/chemokine mRNAs (Figure 3.2F) (Zagórska et al., 2020). However, interpretation of these findings is complicated given the increased mortality rate in Axl mutant mice.

Surviving $Axl^{-/-}$ mice did however have significantly decreased mRNA expression of MMP12 as compared to wild-type mice treated with the same dose of APAP (Figure 3.2F) (Zagórska et al., 2020). It has been previously reported that MMP12 expression is increased in the liver following APAP-induced acute liver injury (Kopec et al, 2017). Interestingly, deletion of MMP12 in this setting resembles liver injury in $Axl^{-/-}$ mice and is linked to increased sinusoidal congestion, hemorrhage, and hepatocellular necrosis (Kopec et al, 2017). Axl has been shown previously to regulate multiple MMPs, including MMP 1, 2, 3, and 9, and over-expression of Axl in cancer cells has been shown to preferentially upregulate both MMP12 and MMP13 (Tai et al., 2009) (Divine et al., 2016) (Kimani et al., 2016). The mechanism by which MMP12 functions to maintain sinusoidal integrity in APAP-induced acute liver injury is not currently known; however, our studies suggest Axl is a critical regulator of MMP12 in this setting. We hypothesize that Axl activation on KCs is protective in this setting and may play a critical role in limiting sinusoidal destruction by increasing levels of MMP12 (Zagórska et al., 2020) (Figure 3.6).

To investigate the role of Axl in APAP-induced ALF, we first measured mRNA expression of Axl in both the APAP acute liver injury and APAP ALF mice over a period of 72 hours to determine if Axl expression was suppressed in ALF mice. While mRNA expression

was only slightly lower in mice that received the high dose at 24 hours, it was strikingly different at later time points (Figure 3.3). Notably, these later timepoints coincide with the time when proinflammatory monocyte differentiation and phagocytosis are occurring under conditions of normal hepatic repair. These results suggest Axl may play an integral role in these processes. To investigate the role of Axl in repair at later time points, we opted to by-pass the early impact on liver injury in $Axl^{-/-}$ mice by pharmacologically inhibiting Axl 24 hours after APAP treatment (Figure 3.8). Treatment of mice with an Axl inhibitor, LDC1267, both 24 and 48 hours following treatment with 300 mg/kg APAP led to increased necrosis, indicating impairment of bone marrow derived macrophage-dependent clearance of dead cells (Figure 3.8). Additionally, proinflammatory cytokine levels were higher in mice treated with LDC1267 and markers of pro-reparative macrophages were reduced (Figure 3.8). Thus, in addition to protecting the liver during the early phases of hepatic injury, Axl also plays a crucial role in repair at later time points, where Axl signaling mediates bone marrow derived-macrophage dependent clearance of dead cell debris and terminates proinflammatory cytokine synthesis (Figure 3.6). Collectively, our results suggest Axl signaling is hepatoprotective during both the necro-inflammatory and resolution phases of APAP-induced acute liver injury.

At present, the only known agonist for Axl is Ga6. Thus, we next determined if failed induction of Axl in APAP-induced ALF mice occurs directly as a result of suppression of Gas6. While mRNA expression of Gas6 was lower in ALF mice across all timepoints examined, it was dramatically different at 24 hours with mRNA expression of Gas6 being 15-fold higher in mice that received the lower dose of APAP (Figure 3.5A). To determine if restoration of Gas6 is similarly protective in APAP-induced ALF, we pre-treated high dose APAP mice with recombinant Gas6. As shown in Figure 3.5, restoration of Gas6 in ALF mice recovered MMP12 expression. This important finding highlights the critical role of Gas6/Axl pathway activation in regulating MMP12 following APAP-induced ALF (Figure 5.1). The underlying mechanism(s) leading to suppression of Gas6 in this model are currently unknown; however, there are multiple

factors that may contribute to decreased Gas6. Thus, further investigation into the mechanism(s) contributing to the loss of Gas6 are needed. However, one possibility is that activation of Tlr9 may lead to suppressed Gas6 secretion. Activation of Tlr9 has been shown to occur in the mouse model of APAP-induced ALF (Imaeda et al., 2009). Furthermore, histological analysis of livers from $Tlr9^{-/-}$ mice treated with 500 mg/kg APAP revealed reduced hemorrhage (Imaeda et al., 2009). This finding suggests a mechanism by which Tlr9 activation promotes the suppression of the Gas6/Axl signaling pathway leading to reduced expression and secretion of MMP12 by KCs, resulting in increased hemorrhage (Figure 5.2).

Similarly to APAP-induced acute liver injury, studies have shown macrophage polarization from a proinflammatory to a pro-repair phenotype plays an important role in stimulating hepatic repair processes in an experimental setting of fibrosis (Figure 4.1) (Ramachandran et al., 2012). Importantly, the transition to pro-repair macrophages was linked to several biological and pathological processes that promote the reversal of liver fibrosis (Figure 4.1) (Ramachandran et al., 2012). Thus, there has been increasing interest in identifying drugs targeting macrophage differentiation, as they could provide a novel therapeutic approach for the treatment of hepatic fibrosis. At present, no antifibrotic therapies exist, making this an area of acute need. In the present studies, we have developed a novel high-throughput phenotypic assay capable of detecting compound induced macrophage polarization. Our assay relies on detection of F4/80, a cell marker specific to pro-repair macrophages (Figure 4.5). Furthermore, it utilizes pro-fibrotic macrophages, which are the intended target of therapy, providing the best opportunity to identify drugs with the highest potential for efficacy *in vivo*.

To determine whether our assay would be able to detect compound-induced macrophage polarization, we performed a small-scale pilot screen using ~2,500 compounds from the Glaxo-Smith-Kline (GSK) Kinase Inhibitor Set and the NCATS MIPE (Mechanism Interrogation Plates) (Figure 4.6). Hits were identified by determining the F4/80 mean fluorescence intensity in each well using CellProfiler (Figure 4.7). The primary screen of the

NCATS and GSK libraries identified 145 compounds that are potentially capable of stimulating macrophage differentiation (0.06% hit rate) (Table 4.1). Several compounds with known anti-inflammatory properties were identified as hits, including Manoalide, Leflunomide, Imatinib, Cilostazol, and Lamotrigine (Mayer 1989) (Cutolo et al., 2003) (Wolf et al., 2005) (Jung et al., 2010) (Abu-Rish et al., 2018). While these compounds still need to undergo additional testing to confirm they indeed triggered a full phenotypic change, their documented anti-inflammatory capabilities make intriguing. Furthermore, detection of these compounds highlights the robustness of our screening assay, indicating it is suitable for larger-scale screens.

Compounds previously shown to modulate macrophage phenotype were also identified as hits, including Niacin and Genistein (Wakade et al., 2018) (Montserrat-de la Paz et al., 2016) (Abron et al., 2018). Furthermore, analysis of hits revealed multiple compounds with redundant signaling pathways that have been implicated in regulating macrophage phenotype, including compounds that were inhibitors of: colony stimulating factor 1 receptor (CSF1R), Rho-associated coiled-coil containing protein kinase (ROCK), epidermal growth factor receptor (EGFR), protein kinase B (Akt), Janus kinases/signal transducer and activator of transcription proteins (JAK/STAT), vascular endothelial growth factor (VEGF), and discoidin domain receptor (DDR) signaling (Table 4.2) (Cannarile et al., 2017) (Liu et al., 2015). Future studies will re-screen compounds identified as active to confirm hits and consider additional endpoints that can be obtained from the primary screening assay, including determination of cell length-to-width ratios, as macrophage cell size has been shown to correlate to phenotype.

Importantly, as a part of this dissertation, we have developed novel drug screening platform to identify compounds capable of stimulating differentiation of proinflammatory macrophages into pro-resolving macrophages that reverse fibrosis. The success of the pilot screen highlights the suitability of using the assay for future larger scale screens of compounds from the MSU ADDRC libraires.

5.2 Future Directions

Collectively, our results indicate that exaggerated IL-10 expression disrupts intrahepatic macrophage trafficking and pro-repair polarization essential for liver repair. Interestingly, in this experimental setting, KCs exhibited many characteristics of MDSCs, including high-level expression of IL-10. Furthermore, our studies reveal, that high levels of IL-6, occurring under conditions of APAP-induced ALF, stimulates the formation of these cells, as neutralization of IL-6 reduced levels of both IL-10 and PD-L1. Intriguingly, neutralization of IL-6 also led to increased cerebral blood flow, indicating that high systemic levels of IL-6 in this setting may promote the development of HE. This finding is significant as HE represents a leading cause of death in patients who progress to APAP-induced ALF. The connection between IL-6 neutralization and protection from HE needs to be investigated further. Of particular interest would be determining the impacts of IL-6 neutralization on behavioral endpoints. Preliminary assessment of mouse behavior indicates mice that receive the IL-6 neutralizing antibody display increased motility and have higher activity levels as compared to mice receiving the control antibody. However, identification and development of methods to quantify behavioral endpoints need further development. One possibility for this analysis may be the use of DigiGait technology.

It has been previously reported that that macrophage function is critical for repair of the APAP-injured liver (You et al., 2013). Our studies provide the first experimental evidence that MDMs fail to change phenotype in a murine model of APAP-induced ALF. Importantly, our results suggest the TAM receptor, Axl, may play a critical role in regulating macrophage phenotype in this setting. Pharmacological inhibition of Axl signaling in mice treated with 300 mg/kg APAP, led to impaired phagocytosis of dead cells and sustained proinflammatory cytokine production. Future studies will use a MDM specific Axl mutant mouse to better characterize these findings. Importantly, the unexpected dramatic effects seen in Axl full-body knock-out mice following treatment with 300 mg/kg APAP suggested Axl plays multiple

protective roles following APAP-induced acute liver injury. Histopathological analysis revealed extensive hepatocellular necrosis and sinusoidal congestion and hemorrhage in surviving $Axl^{-/-}$ mice treated with 300 mg/kg APAP (Figure 3.2) (Zagórska et al., 2020). Our results indicate the Gas6/Axl signaling pathway plays an important role in regulating expression of MMP12. We propose that it is Axl activation on KCs that is protective in this setting playing a critical role in limiting sinusoidal destruction by increasing levels of MMP12 (Zagórska et al., 2020). A preliminary study in KC-specific Axl mutant mice supports this hypothesis, as MMP12 expression was reduced in the livers of these mice following APAP treatment. However, these studies need to be repeated.

Interestingly, whole liver mRNA expression of the Axl ligand, Gas6, was decreased in APAP-induced ALF mice across all timepoints. Pharmacological restoration of Gas6 signaling in this setting recovered expression of MMP12. However, the reasons for decreased Gas6 expression remain unclear and warrant further investigation. While it may be that Tlr9 activation leads to suppression of Gas6 during early phases of repair, it may be that monocyte dysfunction and a reduced hepatic macrophage pool contribute to Gas6 suppression at later timepoints. Furthermore, loss sinusoidal endothelial cells, which secrete Gas6, may result in less circulating Gas6, which could go on to activate Axl. Identification of factors contributing to decreased Gas6 will be important as restoration of Gas6 may provide therapeutic benefit in ALF patients.

Polarization of macrophage phenotype also plays an important role in hepatic repair in chronic liver diseases, including fibrosis and cirrhosis (Ramachandran et al., 2012). We have developed a novel high-throughput screening assay capable of detecting compound-induced macrophage maturation in enriched populations of profibrotic macrophages. At present, we have identified 145 compounds that potentially mediate macrophage polarization state. While these compounds will need to undergo rigorous conformation, these studies have the potential to lead to identification of novel antifibrotics, which could tremendously impact the treatment of liver fibrosis. Future studies include hit confirmation using the primary screening assay with a

dose response assessment. Compounds confirmed as active will be rescreened in a secondary assay using an additional biological endpoint (e.g., mRNA expression). Lastly, these compounds are re-tested using fresh powder and re-analyzed using both the primary and secondary assay.

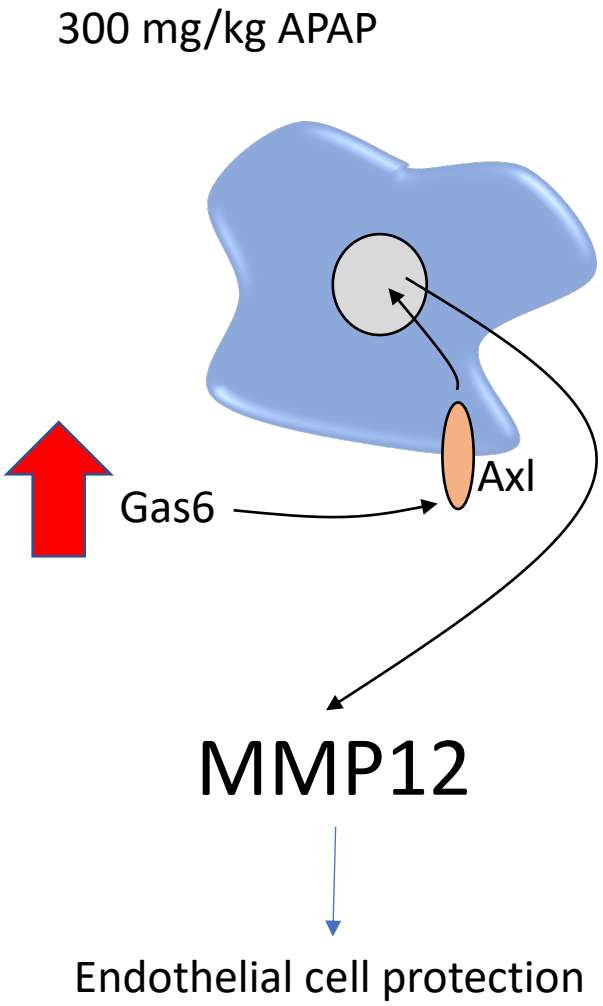

Figure 5.1: Working model of the protective role of Axl/Gas6 signaling during early phases of APAP-induced liver injury.

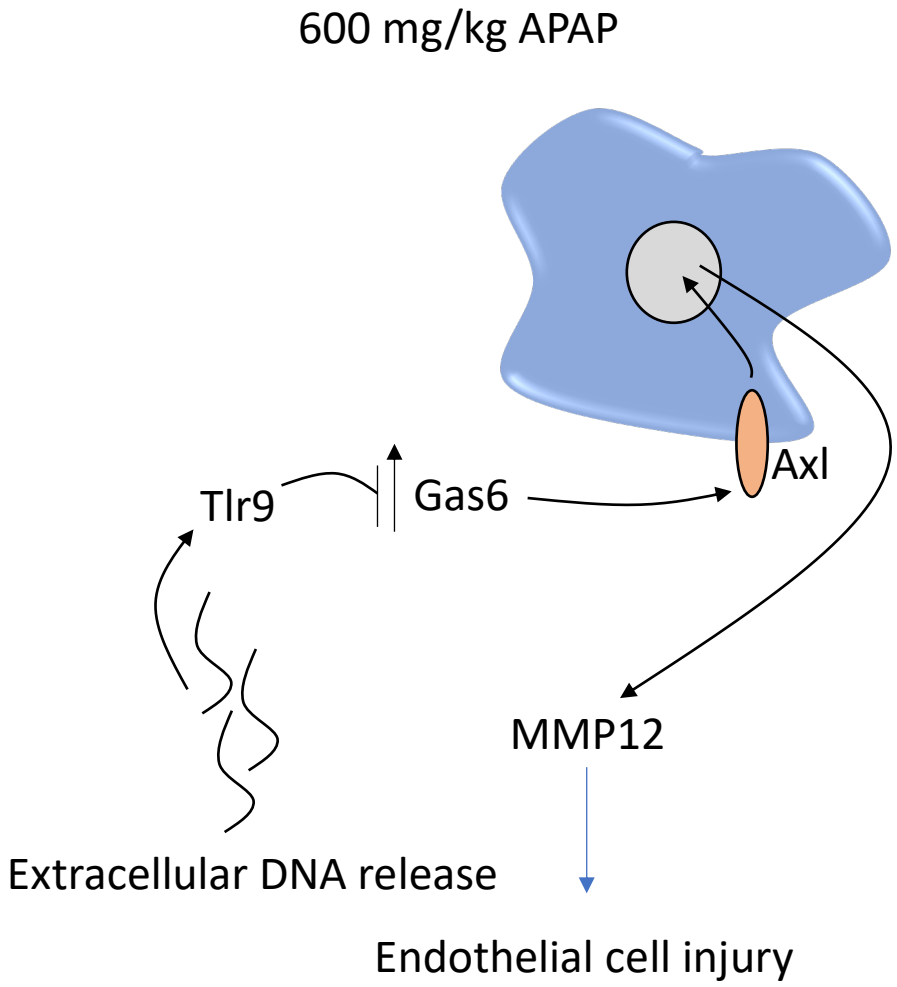

Figure 5.2: Working model for suppression of Gas6/Axl signaling in APAP-induced ALF.

BIBLIOGRAPHY

Abron JD, Singh NP, Price RL, Nagarkatti M, Nagarkatti PS, Singh UP. Genistein induces macrophage polarization and systemic cytokine to ameliorate experimental colitis. PLoS One. 2018 Jul 19;13(7):e0199631. doi: 10.1371/journal.pone.0199631. PMID: 30024891; PMCID: PMC6053137

Abu-Rish EY, Dahabiyeh LA, Bustanji Y, Mohamed YS, Browning MJ. Effect of lamotrigine on in vivo and in vitro cytokine secretion in murine model of inflammation. J Neuroimmunol. 2018 Sep 15;322:36-45. doi: 10.1016/j.jneuroim.2018.06.008. Epub 2018 Jun 11. PMID: 29937116.

Antoniades CG, Berry PA, Wendon JA, Vergani D. The importance of immune dysfunction in determining outcome in acute liver failure. J Hepatol. 2008 Nov;49(5):845-61. doi: 10.1016/j.jhep.2008.08.009. Epub 2008 Aug 21. PMID: 18801592.

Antoniades CG, Quaglia A, Taams LS, Mitry RR, Hussain M, Abeles R, Possamai LA, Bruce M, McPhail M, Starling C, Wagner B, Barnardo A, Pomplun S, Auzinger G, Bernal W, Heaton N, Vergani D, Thursz MR, Wendon J. Source and characterization of hepatic macrophages in acetaminophen-induced acute liver failure in humans. Hepatology. 2012 Aug;56(2):735-46. doi: 10.1002/hep.25657. Epub 2012 Jul 6. PMID: 22334567.

Bernal W, Wendon J. Acute liver failure. N Engl J Med. 2013 Dec 26;369(26):2525-34. doi: 10.1056/NEJMra1208937. PMID: 24369077.

Bonkovsky HL, Barnhart HX, Foureau DM, Steuerwald N, Lee WM, Gu J, Fontana RJ, Hayashi PH, Chalasani N, Navarro VM, Odin J, Stolz A, Watkins PB, Serrano J; US Drug-Induced Liver Injury Network and the Acute Liver Failure Study Group. Correction: Cytokine profiles in acute liver injury-Results from the US Drug-Induced Liver Injury Network (DILIN) and the Acute Liver Failure Study Group. PLoS One. 2019 Feb 11;14(2):e0212394. doi: 10.1371/journal.pone.0212394. Erratum for: PLoS One. 2018 Oct 25;13(10):e0206389. PMID: 30742679; PMCID: PMC6370229.

Bourdi M, Masubuchi Y, Reilly TP, Amouzadeh HR, Martin JL, George JW, Shah AG, Pohl LR. Protection against acetaminophen-induced liver injury and lethality by interleukin 10: role of inducible nitric oxide synthase. Hepatology. 2002 Feb;35(2):289-98. doi: 10.1053/jhep.2002.30956. PMID: 11826401.

Cannarile MA, Weisser M, Jacob W, Jegg AM, Ries CH, Rüttinger D. Colony-stimulating factor 1 receptor (CSF1R) inhibitors in cancer therapy. J Immunother Cancer. 2017 Jul 18;5(1):53. doi: 10.1186/s40425-017-0257-y. PMID: 28716061; PMCID: PMC5514481.

Cutolo M, Sulli A, Ghiorzo P, Pizzorni C, Craviotto C, Villaggio B. Anti-inflammatory effects of leflunomide on cultured synovial macrophages from patients with rheumatoid arthritis. Ann Rheum Dis. 2003 Apr;62(4):297-302. doi: 10.1136/ard.62.4.297. PMID: 12634225; PMCID: PMC1754507.

Divine LM, Nguyen MR, Meller E, Desai RA, Arif B, Rankin EB, Bligard KH, Meyerson C, Hagemann IS, Massad M, Thaker PH, Hagemann AR, McCourt CK, Powell MA, Mutch DG, Fuh KC. AXL modulates extracellular matrix protein expression and is essential for invasion and

metastasis in endometrial cancer. Oncotarget. 2016 Nov 22;7(47):77291-77305. doi: 10.18632/oncotarget.12637. PMID: 27764792; PMCID: PMC5340229.

Imaeda AB, Watanabe A, Sohail MA, Mahmood S, Mohamadnejad M, Sutterwala FS, Flavell RA, Mehal WZ. Acetaminophen-induced hepatotoxicity in mice is dependent on Tlr9 and the Nalp3 inflammasome. J Clin Invest. 2009 Feb;119(2):305-14. doi: 10.1172/JCI35958. Epub 2009 Jan 26. PMID: 19164858; PMCID: PMC2631294.

Ju C, Tacke F. Hepatic macrophages in homeostasis and liver diseases: from pathogenesis to novel therapeutic strategies. Cell Mol Immunol. 2016 May;13(3):316-27. doi: 10.1038/cmi.2015.104. Epub 2016 Feb 24. PMID: 26908374; PMCID: PMC4856798.

Jung WK, Lee DY, Park C, Choi YH, Choi I, Park SG, Seo SK, Lee SW, Yea SS, Ahn SC, Lee CM, Park WS, Ko JH, Choi IW. Cilostazol is anti-inflammatory in BV2 microglial cells by inactivating nuclear factor-kappaB and inhibiting mitogen-activated protein kinases. Br J Pharmacol. 2010 Mar;159(6):1274-85. doi: 10.1111/j.1476-5381.2009.00615.x. Epub 2010 Jan 28. PMID: 20128801; PMCID: PMC2848931.

Kimani SG, Kumar S, Davra V, Chang YJ, Kasikara C, Geng K, Tsou WI, Wang S, Hoque M, Boháč A, Lewis-Antes A, De Lorenzo MS, Kotenko SV, Birge RB. Normalization of TAM post-receptor signaling reveals a cell invasive signature for Axl tyrosine kinase. Cell Commun Signal. 2016 Sep 6;14(1):19. doi: 10.1186/s12964-016-0142-1. PMID: 27595981; PMCID: PMC5011882.

Kopec AK, Joshi N, Cline-Fedewa H, Wojcicki AV, Ray JL, Sullivan BP, Froehlich JE, Johnson BF, Flick MJ, Luyendyk JP. Fibrin(ogen) drives repair after acetaminophen-induced liver injury via leukocyte $\alpha_M\beta_2$ integrin-dependent upregulation of Mmp12. J Hepatol. 2017 Apr;66(4):787-797. doi: 10.1016/j.jhep.2016.12.004. Epub 2016 Dec 10. PMID: 27965156; PMCID: PMC5362307.

Lemke G. Phosphatidylserine Is the Signal for TAM Receptors and Their Ligands. Trends Biochem Sci. 2017 Sep;42(9):738-748. doi: 10.1016/j.tibs.2017.06.004. Epub 2017 Jul 19. PMID: 28734578; PMCID: PMC5600686.

Liu Y, Tejpal N, You J, Li XC, Ghobrial RM, Kloc M. ROCK inhibition impedes macrophage polarity and functions. Cell Immunol. 2016 Feb;300:54-62. doi: 10.1016/j.cellimm.2015.12.005. Epub 2015 Dec 17. PMID: 26711331.

Mayer AM. Manoalide: un nuevo inhibidor de fosfolipasa A2 de origen marino con una potencial acción inmunorregulatoria [Manoalide: a new phospholipase A2 inhibitor of marine origin with potential immunoregulatory effect]. Medicina (B Aires). 1989;49(2):175-80. Spanish. PMID: 2640487.

Montserrat-de la Paz S, Naranjo MC, Lopez S, Abia R, Muriana FJG, Bermudez B. Niacin and its metabolites as master regulators of macrophage activation. J Nutr Biochem. 2017 Jan;39:40-47. doi: 10.1016/j.jnutbio.2016.09.008. Epub 2016 Oct 1. PMID: 27771381.

Ramachandran P, Pellicoro A, Vernon MA, Boulter L, Aucott RL, Ali A, Hartland SN, Snowdon VK, Cappon A, Gordon-Walker TT, Williams MJ, Dunbar DR, Manning JR, van Rooijen N, Fallowfield JA, Forbes SJ, Iredale JP. Differential Ly-6C expression identifies the recruited macrophage phenotype, which orchestrates the regression of murine liver fibrosis. Proc Natl

Acad Sci U S A. 2012 Nov 13;109(46):E3186-95. doi: 10.1073/pnas.1119964109. Epub 2012 Oct 24. PMID: 23100531; PMCID: PMC3503234.
Rothlin CV, Carrera-Silva EA, Bosurgi L, Ghosh S. TAM receptor signaling in immune homeostasis. Annu Rev Immunol. 2015;33:355-91. doi: 10.1146/annurev-immunol-032414-112103. Epub 2015 Jan 14. PMID: 25594431; PMCID: PMC4491918.

Tai KY, Shieh YS, Lee CS, Shiah SG, Wu CW. Axl promotes cell invasion by inducing MMP-9 activity through activation of NF-kappaB and Brg-1. Oncogene. 2008 Jul 3;27(29):4044-55. doi: 10.1038/onc.2008.57. Epub 2008 Mar 17. PMID: 18345028.

Yaseen MM, Abuharfeil NM, Darmani H, Daoud A. Mechanisms of immune suppression by myeloid-derived suppressor cells: the role of interleukin-10 as a key immunoregulatory cytokine. Open Biol. 2020 Sep;10(9):200111. doi: 10.1098/rsob.200111. Epub 2020 Sep 16. PMID: 32931721; PMCID: PMC7536076.

You Q, Holt M, Yin H, Li G, Hu CJ, Ju C. Role of hepatic resident and infiltrating macrophages in liver repair after acute injury. Biochem Pharmacol. 2013 Sep 15;86(6):836-43. doi: 10.1016/j.bcp.2013.07.006. Epub 2013 Jul 19. PMID: 23876342; PMCID: PMC3863645.

Wakade C, Giri B, Malik A, Khodadadi H, Morgan JC, Chong RK, Baban B. Niacin modulates macrophage polarization in Parkinson's disease. J Neuroimmunol. 2018 Jul 15;320:76-79. doi: 10.1016/j.jneuroim.2018.05.002. Epub 2018 May 4. PMID: 29759143.

Wolf AM, Wolf D, Rumpold H, Ludwiczek S, Enrich B, Gastl G, Weiss G, Tilg H. The kinase inhibitor imatinib mesylate inhibits TNF-{alpha} production in vitro and prevents TNF-dependent acute hepatic inflammation. Proc Natl Acad Sci U S A. 2005 Sep 20;102(38):13622-7. doi: 10.1073/pnas.0501758102. Epub 2005 Sep 8. PMID: 16174751; PMCID: PMC1224614.

Zagórska A, Través PG, Jiménez-García L, Strickland JD, Oh J, Tapia FJ, Mayoral R, Burrola P, Copple BL, Lemke G. Differential regulation of hepatic physiology and injury by the TAM receptors Axl and Mer. Life Sci Alliance. 2020 Jun 22;3(8):e202000694. doi: 10.26508/lsa.202000694. PMID: 32571802; PMCID: PMC7335405.